12-2008

Development of a Computational Model to Predict the In Vivo Contact Mechanics of Modern Total Knee Arthroplasty

Adrija Sharma
University of Tennessee - Knoxville

To the Graduate Council:

I am submitting herewith a dissertation written by Adrija Sharma entitled "Development of a Computational Model to Predict the In Vivo Contact Mechanics of Modern Total Knee Arthroplasty." I have examined the final electronic copy of this dissertation for form and content and recommend that it be accepted in partial fulfillment of the requirements for the degree of Doctor of Philosophy, with a major in Biomedical Engineering.

Richard D. Komistek, Major Professor

We have read this dissertation and recommend its acceptance:

Mohamed R. Mahfouz, Phani K. Nukala, William R. Hamel, Kevin M. Kit

Accepted for the Council:

Carolyn R. Hodges

Vice Provost and Dean of the Graduate School

(Original signatures are on file with official student records.)

To The Graduate Council:

I am submitting herewith a dissertation written by Adrija Sharma entitled “Development of a computational model to predict the in vivo contact mechanics of modern total knee arthroplasty.” I have examined the final electronic copy of the dissertation for form and content and recommend that it be accepted in partial fulfillment of the requirements for the degree of Doctor of Philosophy, with a major in Biomedical Engineering.

Richard D. Komistek

Major Professor

We have read this dissertation and
recommend its acceptance:

Mohamed R. Mahfouz

Phani K. Nukala

William R. Hamel

Kevin M. Kit

Accepted for the Council:

Carolyn R. Hodges

Vice Provost and Dean of the
Graduate School and
Graduate Studies

(Original signatures are on file with official student records)

DEVELOPMENT OF A COMPUTATIONAL MODEL TO PREDICT THE IN VIVO CONTACT MECHANICS OF MODERN TOTAL KNEE ARTHROPLASTY

A Dissertation
Presented for the
Doctor of Philosophy Degree
The University of Tennessee, Knoxville

Adrija Sharma
December, 2008

To my grandparents

Acknowledgements

First and foremost I would like to express my gratitude to my advisor Dr. Richard D. Komistek, for being the source of knowledge, guidance, insight and support throughout my graduate life. His encouragement of my work and commitment to whatever project I undertook was inspiring and has made the time I have spent here enjoyable. I especially appreciate his recurring challenge to be engaged in work that is bold, innovative, and important. More than anyone else, his influence has contributed to my development as a scientist.

I am also very grateful to Dr Phani K. Nukala for being a mentor and friend and spending countless hours with me sharing his knowledge and expertise in computational mechanics. I deeply value his engagement with my work and his efforts to improve it. I am deeply indebted to Dr. Thomas Kane for his original ideas and encyclopedic knowledge in dynamics.

I would also like to thank Dr. Mohamed R Mahfouz, Dr. William R Hammel and Dr. Kevin M. Kit for serving on my committee and providing me with valuable insights and helpful feedbacks at various stages during the course of this dissertation. Special thanks

to Dr. Dennis, Dr. Cates, Dr. Ranawat and Dr. Scuderi who have enlarged my sphere of understanding of clinical orthopedic biomechanics with their immense expertise and fresh perspectives.

I would also like to show my appreciation to all my friends and colleagues for helpful discussions and invaluable comments without which this dissertation would not be possible. A special “thank you” to my roommates for excelling in culinary skills and providing me with sumptuous meals which kept me hale and hearty and gave me the much needed source of energy during the course of this dissertation.

Finally, I would never have embarked on this intellectual journey without the emotional support of my family. My parents have always encouraged and constantly motivated me throughout my life, but especially in attaining this degree. Their belief in me has helped me during times when I have doubted my own abilities. Thanks to my brother, for his unstinting support and encouragement and my wife and parents-in-law for their love and faith in me.

Abstract

This dissertation focuses on the development of a computationally efficient and fast method that incorporates the kinematics obtained from fluoroscopy and extends it to the prediction of the in-vivo contact mechanics at the femoro-tibial articulation in modern knee implants for the deep knee bend activity. In this endeavor, this dissertation deals with the use of an inverse dynamic rigid body model characterizing the slip and roll behavior observed in the femoro-polyethylene articulation and a coupled deformation model where the polyethylene in knee implants are modeled as hexahedral discrete element networks. The performance of this method is tested by comparing force predictions from a telemetric knee and finite element analysis. Finally, the method is applied to study the in vivo contact mechanics and mechanics of the quadriceps mechanism in six popular knee designs. During the deep knee bend activity, the contact force generally increased with flexion. However, the medial lateral forces were not equally distributed and the medial lateral force distribution generally varied from 60%-40% at full extension to as high as 75%-25% at full flexion in some patients. Also, the magnitude of axial force in the superior-inferior direction was the highest and was found to contribute around 98%-99% of the total load acting at the femorotibial joint. The forces in the medio-lateral and antero-posterior directions were low and the maximum

magnitude observed was around 0.5BW. The contact areas and contact pressures were much more sensitive to the geometries involved and the in vivo kinematics. Though no definite pattern was observed for the variation of the contact areas throughout flexion, the contact pressures increased in both condyles with increasing flexion. Also, the contact pressures on the medial condyle were higher than the contact pressures observed in the lateral condyle. The patellofemoral and the quadriceps force ratio increased with the increase in flexion while the patellar ligament and the quadriceps force ratio decreased with increasing flexion. In some patients at high flexion, the quadriceps force and as a result the patellofemoral, patellar ligament and the knee contact forces were found to decrease due to the wrapping of the quadriceps coupled with posterior movement of the femoral condyles leading to the increase in the quadriceps moment arm.

Index

List of Tables

APPENDIX D IN VIVO TKA MECHANICS DATA

List of Figures

CHAPTER 5 ERROR ANALYSIS

Abbreviations and Acronyms

ACL	=	Anterior Cruciate Ligament
PCL	=	Posterior Cruciate Ligament
TKA	=	Total Knee Arthroplasty
TKAs	=	Total Knee Arthroplasties
BW	=	Body Weight
AP	=	Antero-Posterior
ML	=	Medio-Lateral
SI	=	Superior-Inferior
CR	=	Cruciate Retaining
PCR	=	PCL Retaining
PCS	=	PCL Sacrificing
PS	=	Posterior Stabilized
RSA	=	Roentgen Stereophotogrammetric Analysis
FEA	=	Finite Element Analysis
UHMWPE	=	Ultra High Molecular Weight Polyethylene

Chapter 1

Background

The knee is the largest joint in the human body, serving as the connection between the upper and the lower leg and controlling the relative motion between the two structures. It consists of bicondylar articulation between the femur (thigh bone) and the tibia (shin bone) and the articulation of the patella in the trochlear grove of the femur. In the normal knee, direct bone to bone contact is prevented by the presence of soft cushioning viscoelastic cartilage and meniscal layers. It is a diarthrodial or synovial joint, i.e. a freely moving joint, lubricated by synovial fluid and the whole structure is enclosed in a joint capsule.

According to the Arthritis Foundation, arthritis-related problems are second only to heart disease as the leading cause of work disability. Mechanical loading, especially dynamic loading, is believed to play a major role in the degenerative process, where the cushioning layers are damaged and create bone to bone contact. Osteoarthritis can be

extremely disabling, leading to discomfort and often excruciating pain. Therefore artificial orthopedic implants are designed so as to replace these damaged articulating surfaces and provide pain relief and allow a subject with severe osteoarthritis to return to a normal daily life.

Since the knee carries a high amount of load, it is highly susceptible to osteoarthritis. The first attempt to design knee arthroplasty occurred approximately 80 years ago. With more research focusing in this area and with greater knowledge about normal knee kinematics, these knee arthroplasty designs have transformed from highly constrained hinged type and highly conforming designs to moderately conforming designs. Modern knee arthroplasty designs can largely be classified as unicondylar or total (bicondylar). While in total knee arthroplasty (TKA), the complete femorotibial and patellofemoral articulation is reconstructed, unicondylar knee arthroplasty (UKA) is utilized in minor osteoarthritis damage, when only one condyle of the femorotibial articulation has to be reconstructed.

A modern TKA design consists of at least three components. (Figure 1-1). Two components, attached separately to the femur and the tibia, are made of high strength, wear resistant and biocompatible titanium or cobalt chromium alloys. The other component is made of biocompatible crosslinked ultra high molecular weight polyethylene and acts a bearing material between the femoral and tibial components.

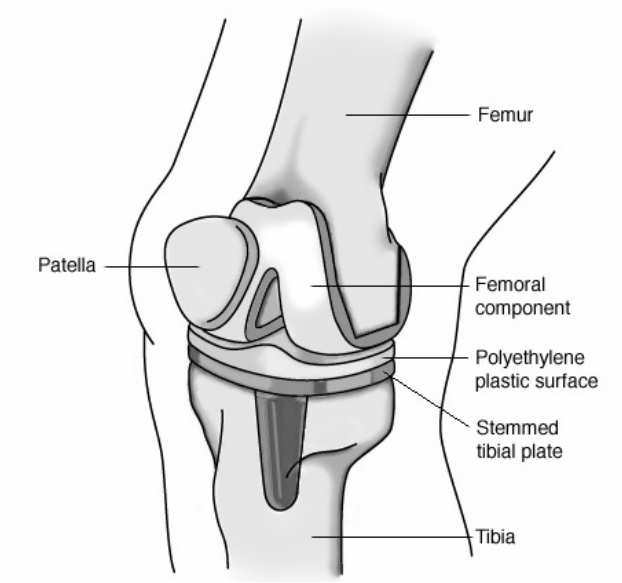

Figure 1-1: Simplified image of TKA.

The contact surface between the polyethylene insert and the tibial component is generally flat with modifications pertaining to fixation mechanisms between them. The articulation between the femoral condyles and the polyethylene bearing is characterized by elliptical surfaces having single or multiple radii both in the sagittal and the coronal planes. There can be a fourth component, a dome shaped insert made of polyethylene, fitted to the patella bone, to aid in the patellofemoral articulation. However, the use of this component is a subject of much debate. While some surgeons routinely resurface the patella and fit this insert others are skeptical towards its use. Nonetheless, the original or resurfaced patella articulates in a reconstructed grove made on the anterior aspect of the femoral

component and resembles the articulation of the patella on the trochlear grove in the femur of the normal knee.

In a normal knee, with the increase in flexion (bending of the knee), the femoral condyles roll with slip in the posterior direction (known as rollback) on the tibial plateau. Since the medial condyle radius in the normal knee is different compared to the lateral condyle, such a posterior motion is also accompanied by an external axial rotation of the femur with respect to the tibia. In general, throughout most flexion angles, both the femoral condyles remain in contact with the tibia. However, at extreme, very high flexion angles (> 140º), there can be a condition when only one femoral condyle stays in contact. This happens mainly due to two reasons: (1) Extreme roll back in the knee causing the lateral condyle to lose contact with the tibial surface in the posterior direction. (2) Generation of an abduction/adduction moment that causes one of the condyles to lift off the tibial surface. The patellar always remains in contact with the femur and with increasing flexion travels upward on the trochlear grove of the femur and rotates towards the femur. The incidence of normal axial rotation of the femur on the tibia has been found to affect patellofemoral tracking significantly.

Various approaches are used by surgeons in order to cut through the skin in order to reach the bones during a TKA. Also, in order to make space for the implant components, a sufficient amount of bone has to be cut off and necessary soft-tissue structures released

and resected to ensure proper fit, correct alignment and balancing of the installed components. Since the normal soft tissue constraints present in the normal knee are modified after TKA implantation, the TKA kinematics have been found to be different than normal knee kinematics. Some of the abnormalities include:

(1) The incidence of paradoxical anterior slide of the femur on the tibia with increasing knee flexion. This results in the impingement of the femoral condyles on the polyethylene bearing, resulting in a loss of flexion.
(2) Opposite axial rotation patterns, where the femur rotates internally relative to the tibial component with increasing knee flexion and can occur throughout flexion or at various increment of flexion.
(3) Incidence of condylar lift-off, throughout normal ranges of flexion causing higher stresses to be generated in the polyethylene bearing surface.
(4) Incidence of patellar separation (patella losing contact with femur), patellar dislocation and abnormal patellar tracking that causes pain and discomfort and is one of the leading causes of revision surgery.

Armed with the knowledge of the drawbacks of current designs and with the focus of attaining normal knee kinematics in TKAs, the design of knee implants have continuously evolved and there are various types of knee implants in the market. Modern TKA designs can be broadly classified into the following groups:

(1) Cemented, non-cemented or hybrid: This classification is based on the attachment of the components on the respective bones. The femoral, tibial and patellar components can be attached to the bone with the use of bone cement, or can be fixated without cement, using the concept of interference fit. The non-cemented designs use a porous coating on the surface for the bone to grow into the metallic components leading to a more secure fixation. A hybrid approach, utilizing some cemented and some non-cemented components can also be used.

(2) Fixed or mobile bearing: This classification is based on the attachment of the polyethylene insert on the tibial component. Fixed bearings rigidly fix the two components with grooves, notches and other locking mechanisms. In this case, the femoro-polyethylene is much less constrained in order to account for the multiaxial rotational nature of the femoral motion. Mobile bearings, however, allow relative motion between the tibial and polyethylene articulation. Such designs aim to separate the translational and rotational nature of the femoral-polyethylene articulation and therefore can employ higher constrained designs. Mobile bearing designs can be of the more successful rotating type (where only rotational motion of the polyethylene insert is allowed) or the less popular meniscal type (where the polyethylene insert can rotate and translate on the tibial component).

(3) Cruciate retaining, cruciate sacrificing or cruciate substituting: This classification is based on the surgical procedure that is adopted during TKA for the cruciate

ligaments (the main anterior-posterior stabilizers in the normal knee). Though some TKAs are designed to retain the anterior cruciate ligament (ACL), in most designs the ACL is resected to facilitate in the fitting of the implant. With respect to the posterior cruciate ligament (PCL), TKAs can be PCL retaining (PCR), PCL sacrificing (PCS) or PCL substituting, also known as posterior stabilized (PS). PS designs differ from the PCR designs by having an additional cam-spine (also called post-cam) mechanism between the femoral component and the polyethylene insert in order to initiate posterior femoral rollback, the primary role of the PCL. The spine (post) is located on the polyethylene insert and the cam is provided on the femoral component in between the two condyles. PCR designs do not have this mechanism as the PCL in these designs is not resected. The PCS designs resect the PCL and do not provide for any substitution. In modern PCS designs, stability is achieved by incorporating spherical femoro-polyethylene contact surfaces in the medial condyle to facilitate "pivotal motion" in that condyle.

(4) Symmetrical or asymmetrical condyles: This classification is based on the design differences between the two femoral condyles and their corresponding articulating surfaces on the polyethylene insert. The newer, asymmetrical designs are motivated by the asymmetrical nature of the femoral condyles in the normal knee which is believed to be a main cause for normal axial rotation. In, these designs, the medial condylar radii are smaller than the lateral condylar radii, just as in the

normal knee. Therefore, for same amount of flexion, the distance traveled by the medial condyle is lesser than the distance traveled by the lateral condyle causing a normal axial rotation pattern. Some newer designs also incorporate different heights of the medial and lateral condyles when measured in the superior-inferior direction. The symmetrical designs are characterized by identical radii in both the medial and lateral condyles.

With more successful designs in the market, advancement of technology and higher patient expectations, newer generation knee implants are aiming for higher performance goals and some of the current trends driving new knee designs are as follows:

(1) High Flexion: These types of designs are intended to provide patients with the capability of experiencing activities that require very high flexion range (>120º) such as kneeling, squatting, gardening, etc. New TKAs accommodating for as high as 160º of flexion are available today. These high flexion designs incorporates subtle changes in the femoro-polyethylene articulation radii so as provide extra articulating surface and reduce the chance of the femoral component falling of the polyethylene surface. They also employ a deeper anterior groove on the polyethylene insert in order to prevent the impingement of the patellar tendon during high flexion.

(2) Gender knees: Compared to males, females have a wider pelvis, a higher antero-posterior (AP) to medio-lateral (ML) length ratio and a greater Q-angle. Today, modern TKAs are designed so as to better fit both the female and the male knee geometry. In order to reduce overhang of the bone and the fitted implant components some designs incorporate modified AP/ML ratios while other designs provide a wider range of available component sizes to choose from. Also, the trochlear groves in these designs are more anatomical and are adjusted so as to account for the varying Q-angle between men and women.

(3) Resurfacing: Aimed at a much younger, active population who have good bone quality, these designs are thinner and resects much less bone than normal TKA implant. These designs aim at replacing only the damaged contact surfaces rather than provide for a complete reconstruction of the entire knee joint.

Chapter 2

Literature Review

The disparities in the in-vivo performance of a TKA compared to the normal knee and the nature of its failure have been the main driving force behind the evolution and development of TKAs. Since cadaveric studies fail to simulate in-vivo conditions adequately (Komistek 2005) and experimental studies are difficult and restrictive in humans due to their invasive nature, researchers have strived for new and unique methods for indirect measurements.

Modern day TKAs have been found to have survival rates of more than 90% at ten years and 84% at fifteen years (Godest 2000; Rand 2003) and have been found to be very successful in treating severe osteoarthritis. However, failure, especially in the form of polyethylene wear limits its longevity (Howling 2001; Currier 2005). Efforts to address this issue have concentrated on improving the manufacturing process and the material properties. Some of these efforts include improvement of the sterilization techniques to

reduce oxidation and therefore reduce fatigue related delamination and pitting of the polyethylene (Li 1994; Williams 1998), development of highly crosslinked polyethylene (Marathon™, Depuy; Longevity™ and Durasul™, Zimmer; Crossfire™ and X3™, Stryker) and scratch resistant femoral components (Oxinium™, Smith and Nephew, Ceramics) to reduce abrasive wear mechanisms (Wroblewski 1999; Heimke 2002).

Methods to study wear behavior in ultra high molecular weight polyethylene (UHMWPE) have been limited to the use of simulators or retrieval studies (Hood 1983; Wasielewski 1994, 1997; DesJardins 2000; Currier 2005). Simulators work under in-vitro conditions for a prescribed, often assumed, motion pattern and truly do not reflect the in-vivo patient specific patterns. A comparison between wear generated by simulators and that obtained from retrieval studies, for the same bearing designs and for similar cycles, have indicated greater amount of wear in the retrieved inserts (Harman 2001). However, physical wear testing is essential and recent knee simulator designs are becoming more and more successful in simulating wear patterns observed in retrievals (Walker 1997; Bei 2003) However, high costs and the time required in using a physical simulator limit their mass scale applicability. Retrieval studies, on the other hand, involve a backward approach and can only give us an idea about what 'might have caused' such wear rather than pinpointing as to 'this is the cause'. Also, revision and post-mortem retrievals are difficult to obtain and can take significant time before they are available (Harman 2001; Bei 2003).

A computational wear model is therefore an attractive solution to these limitations (Sathasivam 1998; Bei 2003; Fregly 2005). Wear is a complicated surface/sub-surface phenomenon which is ideally a function of kinematics, contact kinetics and material properties (Wimmer 1997; Sathasivam 2001). Interestingly enough, all the various types of TKA available today use similar material types but have wide differences in the design and the dimension of the components. With new designs being created and with modern TKA designs aiming at higher degree of flexion, which generates higher forces (Komistek 2005), and TKAs being implanted in younger and more active patients, analyses of their kinematics and contact mechanics quickly and efficiently become increasingly important (Walker 1999).

Previous methods to study in vivo TKA kinematics have produced invasive techniques like fracture fixation devices (Cappozzo 1993), bone pins (LaFortune 1992; Benoit 2006) and Roentgen Stereophotogrammetric Analysis (RSA) (Karrholm 1989; Nilsson 1995) and non invasive techniques like skin markers (Antonsson 1989; Benedetti 1994; Andriacchi 2000), externally worn goniometric devices (Chao 1980; Holden 1997), single plane and biplanar fluoroscopic techniques (Banks 1996; Hoff 1998; Komistek 2003; Tashman 2003) and non-invasive RSA technique (Valstar 2001). Due to high amount of out of plane rotational and translational error between skin markers and the underlying osseous structures (Murphy 1990; Holden 1997), skin marker technology using suitable correction measures like artifact assessment, point cluster technique and

optimization using minimization (Lucchetti 1998; Andriacchi 2000; Alexander 2001) are used extensively when multi body movements need to be tracked. However, for the analysis of in vivo kinematics of individual joints, use of video fluoroscopy along with two dimensional (2D) to three dimensional (3D) registration technique (Mahfouz 2003) has become the golden standard due to the low amount of error associated with the process.

In order to estimate in vivo joint loads telemetric implants are being developed. Studies using telemetry utilize force sensors, fitted to the prosthetic components, which are implanted directly inside the human body. This method does generate the most accurate results because it directly derives in vivo measurements. Previous attempts to incorporate telemetry for the knee have either used special femoral prosthesis (non TKA) fitted with strain gauges (Taylor 1998, 2001; Burny 2000) or have used a modified tibial tray of the TKA fitted with load cells (Kauffman 1996; Morris 2001). While the first set of studies has generated in vivo data for weight bearing conditions, the second set was tested in-vitro. Telemetry is a developing art and recently a few telemetric TKAs has been designed (D'Lima 2005; D'Lima 2007; Grachien 2007) and implanted which have provided valuable insight into knee forces and moments. Nonetheless, telemetry is restricted in its use because of the high amount of costs involved in developing a telemetric implant, making it unsuitable for mass scale production and use. Also, being invasive in nature, this method is not feasible for non-implanted natural joints.

In order to estimate contact areas and pressures, in vitro experimental methods are extensively used mainly due to their ability to quickly generate data. Some experimental techniques used previously include stereophotogrammetric methods (Ateshian 1994), dye injection methods (Greenwald 1971; Black 1981), silicone rubber methods (Kurosawa 1980), 3S technique (Yao 1991), Fuji pressure sensitive film (Stewart 1995), resistive ink sensors (K-Scan^{TM}) (Ochoa 1993), ultrasound (Zdero 2001), piezoelectric transducers (Mikosz 1988; Buechel 1991) and micro-indentation transducers (Ahmed 1983). All of these experimental methods, however, are in vitro techniques that either assumes the contact forces and/or the orientation of the implanted components. Also, the differences between these various techniques and loading conditions make direct data comparisons difficult.

The key, therefore, lies in the development of a non-invasive approach for measuring in vivo joint loading and their contact mechanics. As a result, computational modeling and simulations have been extensively used to develop predictions. Since muscle co-contractions increase joint compressive forces, multibody dynamic musculoskeletal models have been used previously to provide the estimated muscle forces (Delp 1998; Anderson 1999; Neptune 2000; Davoodi 2003). Due to a large number of muscles and soft tissues, the number of unknowns in the human body is large and is mathematically indeterminate in nature. Therefore mathematical modeling of the human body is a challenging task and relies on two techniques – optimization and reduction, to resolve

this issue. In the optimization technique, the number of unknowns is greater than the number of equations that can be generated for the solution (Komistek 2005). Therefore, the process deals with the solution generated by the minimization of a suitably chosen objective function (Seireg 1973; Brand 1982; Anderson 2001; Piazza 2001). However, there still lacks a consensus as to which objective function is physiologically most suitable (Komistek 2005). The reduction technique, however, uses simplifying assumptions to reduce the complexity of the system. In this case the system is always kept determinate i.e. the number of unknowns is always made equal to the number of equations that can be generated to solve them (Paul 1965, 1976; Wimmer 1997; Lu 1997, 1998; Komistek 1998, 2005; Sharma 2007, 2008). This method therefore generates a faster solution when compared to optimization, but only a certain number of values can be calculated.

The knee is one of the most investigated joints in the human bodies. Therefore, there exists a wide range of knee models. Though, the earlier knee models were two dimensional (2D), it is now widely accepted that three dimensional (3D) anatomical models produces muscle force estimates that are more consistent with experimental EMG data (e.g. antagonistic muscle activity) than estimates from 2D models (Li 1999; Bei 2003). 3D knee models have progressed from quasi-static to dynamic, from rigid body to deformable body and from simple surface geometry to complex surface geometry. Wismans et al. (Wismans 1980) was one of the first studies to develop a quasi-static

three-dimensional natural knee model using rigid body contact. Pandy et al. (Pandy 1997) presented a quasi-static natural knee model using deformable contact with idealized (i.e., planes and polynomials) surfaces. Abdel-Rahman and Hefzy (Abdel-Rahman 1998) used similar idealized surfaces with rigid body contact to create a dynamic model of a natural knee. Piazza and Delp (Pizza 2001) extended this work by applying rigid body contact to an artificial knee within a full-body dynamic simulation. Sharma et. al. (Sharma 2007, 2008) developed a rigid body knee model to predict separate medial and lateral condyle contact forces. Blankevoort et al. (Blankevoort 1991), Cohen et al. (Cohen 2001, 2003), Kwak et al. (Kwak 2000), and Elias et al. (Elias 2004) reported quasi-static natural knee models with deformable contact, where subject-specific contact surfaces were generated from medical imaging data. Bei (Bei 2003) and Fregly et al. (Fregly 2003, 2005) developed dynamic models of artificial knees using deformable contact.

Significant rigid body computational tools already exist for modeling and simulating of human movement (Delp 1995; Komistek 1998, 2005; Davoodi 2001, 2003). Rigid body contact analyses using multibody simulation methods have been successfully used to predict knee motion and contact forces (Godest 2000; Piazza 2001; Komistek 2005; Sharma 2007, 2008) build on subject-specific models. However, this method cannot predict the contact pressures occurring at the joint interfaces. Therefore, deformable body contact analyses become important. One of the first used methods in this regard was in the use of Hertzian contact analysis (Hertz 1881) to calculate the stresses in polyethylene

insert (Bartel 1985; Walker 1988; Jin 1995). However, the accuracy of this method is limited due to the simplifying assumptions on which the theory is based (Lewis 1998). The most accurate and widely used method today is finite element analysis (FEA) (Lewis 1998). FEA has been used to study knee joint contact mechanics under static loading conditions (Bartel 1986, 1995; Bendjaballah 1997; Sathasivam 1998, 1999; Périé 1998; D'Lima 2001; Otto 2001; Rawlinson 2002; Machan 2004). Dynamic FEA has recently been applied to simulations of knee implant components under well-defined loading conditions (Giddings 2001; Godest 2002; Halloran 2005). Apart from a significant amount of preprocessing required, one major drawback of these analyses is their intensive use of CPU time especially during nonlinear analysis which requires repeated updates of the stiffness matrix. This makes them impractical for incorporation into larger multi-dynamic musculoskeletal models. Furthermore, detailed stress analyses carried out by FEA are unimportant in gross movement simulations (Fregly 2005).

Therefore, in order to be applicable to multibody dynamic simulations, the best method would be to use one that has comparable accuracy as FEA and is also computationally not very intensive and fast. A feasible solution might be in the use of discrete element analysis (DEA). Discrete spring networks (mostly 2D) also known as lattice models are used extensively to model atomic level interactions where the continuum theory does not hold good. Lattice models are used in the field of molecular dynamics, micromechanics, statistical and computational mechanics to study behavioral characteristics and failure

nature in various types of materials – crystalline solids, granular, amorphous, composite, polymers, etc (Alexander 1998, Burda 1998, Roberts 2002, Bolander 2005). Discrete networks can also be used to model continuum where the lattice is much coarser than the true atomic one. This coarse lattice idea obviates the need to work with enormously large degrees of freedom required in a true lattice and allows a very modest number of nodes per heterogeneity. As a result, discrete networks are a close relative of the much more widespread finite element method (Starzewski 2002). For both these methods the solution technique is discrete, however, finite element method is based on the principles of continuum while discrete networks do not assume continuum.

With the development of computational speed and power, the branch of computer animations is a highly researched field where the challenge has been to constantly improve animations of deformable objects that appear realistic and closer to the real world physics. Various methods ranging from non-physical to continuum mechanics based have been explored. Some of them include elastic theory method (Debunne 1999), tensor mass model (Cotin 1997; Picibono 2002), hybrid elasticity model (Cotin 1999; Tseng 2000), method of finite spheres (De 2001; Kim 2002), boundary element method (James 2001), long element method (Costa 2001) and volume distribution method (Sundaraj 2004). The two most widely used approaches for modeling soft tissues are

discrete spring networks (Walters 1987; Terzopoulos 1990; Brown 2001) and modified FEA (Dimaio 2002; Menzoda 2003).

Spring systems have been widely used in 2D and 3D (tetrahedral) facial animation. Terzopoulos et. al. (Terzopoulos 1990) used a three-layer mesh of mass points associated to three anatomically distinct layers of facial tissue (dermis, subcutaneous fatty tissue, and muscle). To improve realism, Lee et. al. (Lee 1995) added further constraints to prevent penetrations between soft tissues and bone. In biomechanical modeling, mass-spring systems were used by Nedel et. al. (Nedel 1998) to simulate muscle deformation. Muscles were represented at two levels: action lines and muscle shape. This shape was deformed using a spring mesh. Aubel et. al. (Aubel 2001) used a similar approach with a multi-layered model based on physiological and anatomical considerations. Bourguignon et. al. (Bourguignon 2000) proposed a model offering control of the isotropy or anisotropy of elastic material. Mass spring systems have also been used for cloth motion (Baraff 1998) and surgical simulation (Brown 2001).

Spring networks are therefore very versatile. They have been used in atomic scale modeling where the focus is on correct solution and less on computational speed. The goal in the field of animations is entirely opposite – achieve fast computational speeds as long as the solutions look realistic. Moreover, they are easy to construct as they do not

have stringent mesh requirements, and can handle both large displacements and large deformations (Maciel 2003).

With respect to TKA mechanics, previous studies have concentrated on a simpler version of the spring network systems known as the elastic foundation contact model (Blankevoort 1991; Li 1997; Pandy 1997; Nuño 2001). In this method the polyethylene is modeled as a bed of discrete non-connected springs. Fregly et. al (Fregly 2005) has also extended this method in the prediction of wear. The greatest advantage of using this method is that a pressure over closure relationship can be analytically obtained. Thus the contact pressures can be easily calculated based on the amount of interpenetration of the femoral component on the polyethylene. This makes this method computationally very efficient. However, this method is restrictive as the deformation in this case is essentially one-dimensional (ID) with no capability to reflect the Poisson's ratio of the material, in other words deformations in other dimensions. Also, the deformation of one spring does not affect the others. Thus, in essence the contact area prediction in this case is analogous to an interference area of the femur with polyethylene leading to higher values being calculated (Gonzalez 2008). Due to these drawbacks, some studies have concentrated on using optimized parameters while using this method (Fregly 2005; Halloran 2005; Gonzalez 2008). However, these suggested correction parameters are non physiological and different values must be used for different thickness of the deformation layer.

Chapter 3

Research Aims

The primary goal of this dissertation is to introduce the use of discrete element models in the study of TKA mechanics. In this endeavor, this dissertation focuses on the development of a computationally efficient and fast method that incorporates the kinematics obtained from fluoroscopy (the golden standard in joint kinematics) and extends it to the prediction of the in-vivo contact mechanics (contact forces, contact areas and contact pressures) at the femoro-tibial articulation in modern knee implants. This methodology is not only fast and accurate but also works with minimal amount of human interaction with a minimum amount of preprocessing so that it can be easily automated.

In the fluoroscopic process dynamic X-ray video is discretized into individual frames. 3D CAD models are overlaid on the 2D images based on their silhouette to generate the transformation matrices that defines the assembly of the components (Figure 3-1).

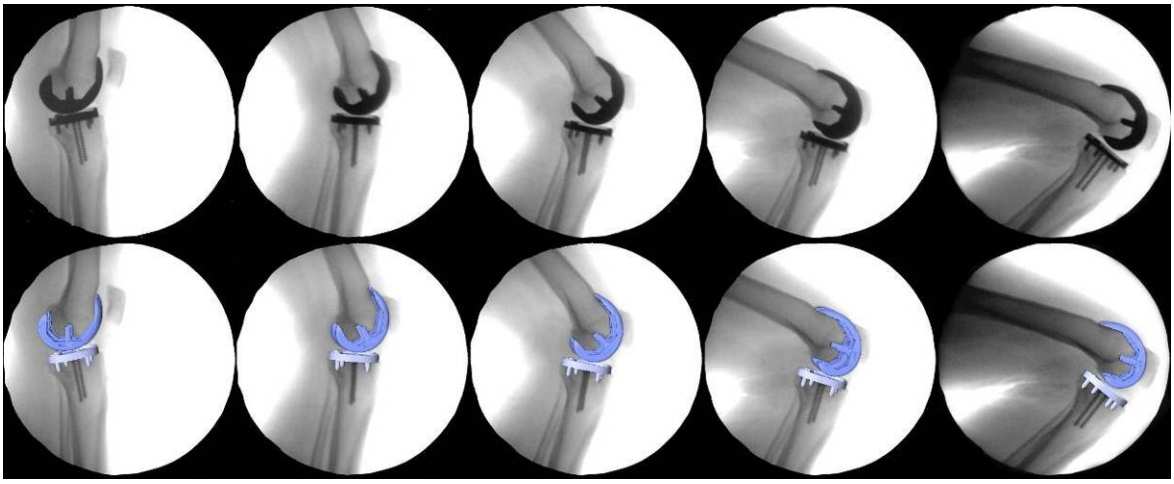

Figure 3-1: Series of fluoroscopy images and corresponding CAD model overlays.

The polyethylene inserts used in knee implants and neighboring soft tissues are invisible to X-rays. Therefore, this process entirely relies on image registration algorithms and does not take into account the interaction of neighboring objects. The error associated with the fluoroscopic process is a function of the resolution of the image used in the registration process. Higher the resolution of the image, lesser is the error. In an error analysis by Mahfouz et. al. (Mahfouz 2003) of the fluoroscopic process from video obtained using a commercially available C-arm system, the upper bound of the translational error in the antero-posterior, the superior-inferior and the medio-lateral directions were -0.023 ± 0.473 mm, 0.086 ± 0.449mm, and 1.054 ± 3.031mm respectively. The upper bound of the rotational error in the coronal plane, the axial plane and the sagittal plane were -0.068º ± 0.942º, 0.001º ± 0.771º, 0.253º ± 0.841º respectively. These errors are small when compared to the overall movements of the

knee joint, however, they are high for the measurement of deformation where sensitivity can be in the order of 0.1mm or less. Moreover, since the softer materials are invisible, their deformation, due to forces acting and as a result the possible changes in contact due to change in shape cannot be accounted for. This might not be a serious limitation for implanted joints as in normal joints due to the much stiffer components used. Nonetheless, direct calculation of polyethylene deformation from the assembly obtained using fluoroscopy is not suitable.

As a result, the calculations of in-vivo contact mechanics in knee implants from fluoroscopic measurements in this dissertation involves a two step approach – estimating the total contact forces acting on the system and then using those magnitudes to calculate deformations. The analysis is performed on kinematic data obtained for subjects performing a deep knee bend activity.

The total contact forces are calculated using a inverse dynamic rigid body model. Inverse dynamic modeling is proven to be a reliable and fast method of estimating forces from kinematics obtained from fluoroscopy (Komistek 2005). The greatest benefit of this method is that the second order differential equations of motion are a set of linear algebraic equations in terms of the forces. The femoral and tibial components in knee implants are made of steel which has a Young's modulus in the order of 10^2 GPa. On comparison, polyethylene has a Young's modulus in the order of 10^2 MPa. Also, the

deformation in polyethylene is negligible compared to the overall kinematics observed in the knee. Therefore, the contact forces can be calculated using a rigid body model without significant loss of accuracy. In this dissertation, the rigid body model used in this analysis has been modified from the one previously developed for the deep knee bend activity by Sharma et. al. (Sharma 2007, 2008).

Once the total contact force acting at the femorotibial interface is obtained, the force distributions on each condyle is calculated using a deformation contact model consisting of the rigid femoral component and a deformable polyethylene insert. Instead of using finite elements, which can be slow and requires considerable post processing, the polyethylene insert is modeled using discrete spring networks. Discrete spring networks have never been previously used with respect to implant mechanics. Also, most spring networks developed in the field of biomechanics have either been 2D or have used 3D tetrahedral structures using linear material models. Since hexahedral elements have been found to have higher accuracy than tetrahedral elements in FEA, therefore, this dissertation concentrates on creating 3D hexahedral spring networks. The physics associated with spring networks are different than the constitutive laws based on continuum. Therefore, this dissertation focuses on the determination of spring parameters for the incorporation of nonlinear materials. Hexahedral meshing of random geometry is a challenging task. It has not yet been possible to implement such an algorithm that works automatically for any geometry. This necessitates a significant amount of pre-

processing time that must be devoted in conducting FEA with hexahedral elements. In this regard spring networks, being a discrete element model not assuming continuum, offers a distinct advantage as once the nodes are generated, connection of two nodes creates an element. With very few nodes this can result in distortion of geometry, however, this problem can be resolved with sufficiently refined number of nodes. In this dissertation, a versatile approach for generating the nodes replicate the polyethylene geometry in TKAs is used. This approach is formulated assuming triangulated surface definitions of the CAD models.

Chapter 4

Materials and Methods

4.1 Generating Nodes in the Polyethylene:

After the orientation of the implant components are obtained from fluoroscopy the first step is to create the grid of nodes inside the polyethylene. This grid of nodes is used to check for the correctness of assembly, apply corrections when needed and compute surface distances and normals and is then further developed into the spring network with interconnections between them. Therefore, the objective is to find a way to automatically create this grid that is robust enough to be applicable for all knee implants. Different knee implants have differing geometries. However, the differences in the same genre of implants are mainly in the radii of the surfaces in contact without a huge difference in shape. The major differences in the designs occur when comparing fixed versus mobile (due to the attachment mechanisms of the polyethylene insert with the tibial component) or when comparing PCR versus PS implants (due to presence of the cam-post mechanism in the PS implants) (Figure 4-1).

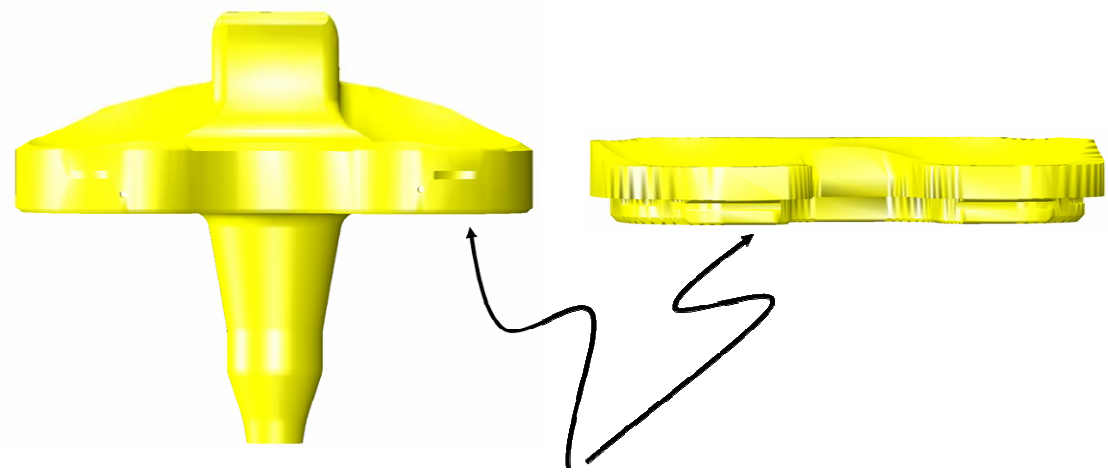

Figure 4-1: (Left) PS mobile bearing. (Right) PCR fixed bearing.

Nonetheless all knee implants are characterized by a mostly flat surface of the polyethylene component which rests on the tibial implanted base-plate. Being flat, this surface is easy to identify. The femoral condyle contact surfaces lie almost parallel to the flat surface. These surfaces are however curved. The grid of nodes is generated by using a ray-firing algorithm which generates rays normal to the flat surface and measures the intersection of the rays with the polyethylene surface. The nodes only need to be created once before the start of analysis. The sequence of the method is outlined below and assumes that the CAD model has triangulated surface definitions:

1. Let us assume that the insert is denoted as Body A and in this axis system ‘A1>’ represents the antero-posterior direction, ‘A2>’ represents the superior-inferior

direction and ‘A3>’ represents the medio-lateral direction. However, just as a cross-check the flat surface of the polyethylene is identified. It can generally be identified with the maximum number of nodes in the CAD model having one of their coordinates same and the maximum number of same normals defined. Incase the flat surface does not lie in the A1-A3 plane, the whole assembly is re-oriented so that the flat surface lies parallel to the A1-A3 plane (Figure 4-2).

2. Calculate the bounding box of the polyethylene component along the A1>, A2>, A3> axis. Depending on the dimensions of the bounding box calculate the number of nodes required along each dimension in order to ensure that a unit grid is approximately cubic (equal sides) in nature. For reasons that is explained later (refer to patch test), and to prevent distortion of geometry it is important to keep sufficient number of nodes per dimension.
3. Based on the number of nodes and the bounding box dimensions, a 2D grid of references points is created along the A1-A3 plane lying outside the polyethylene bounding box. Rays are initiated from these reference points in the A2> direction and the intersections of these rays with the CAD model surfaces are recorded.
4. With an automated process is mind, it is best and most generic to find the intersections of a ray with all the triangle definitions associated with the CAD model and then search for the correct intersections. Since, a triangulated surface represents a plane, there should be some intersection value of the ray with a triangle. The correct intersections are found based on the following logic:

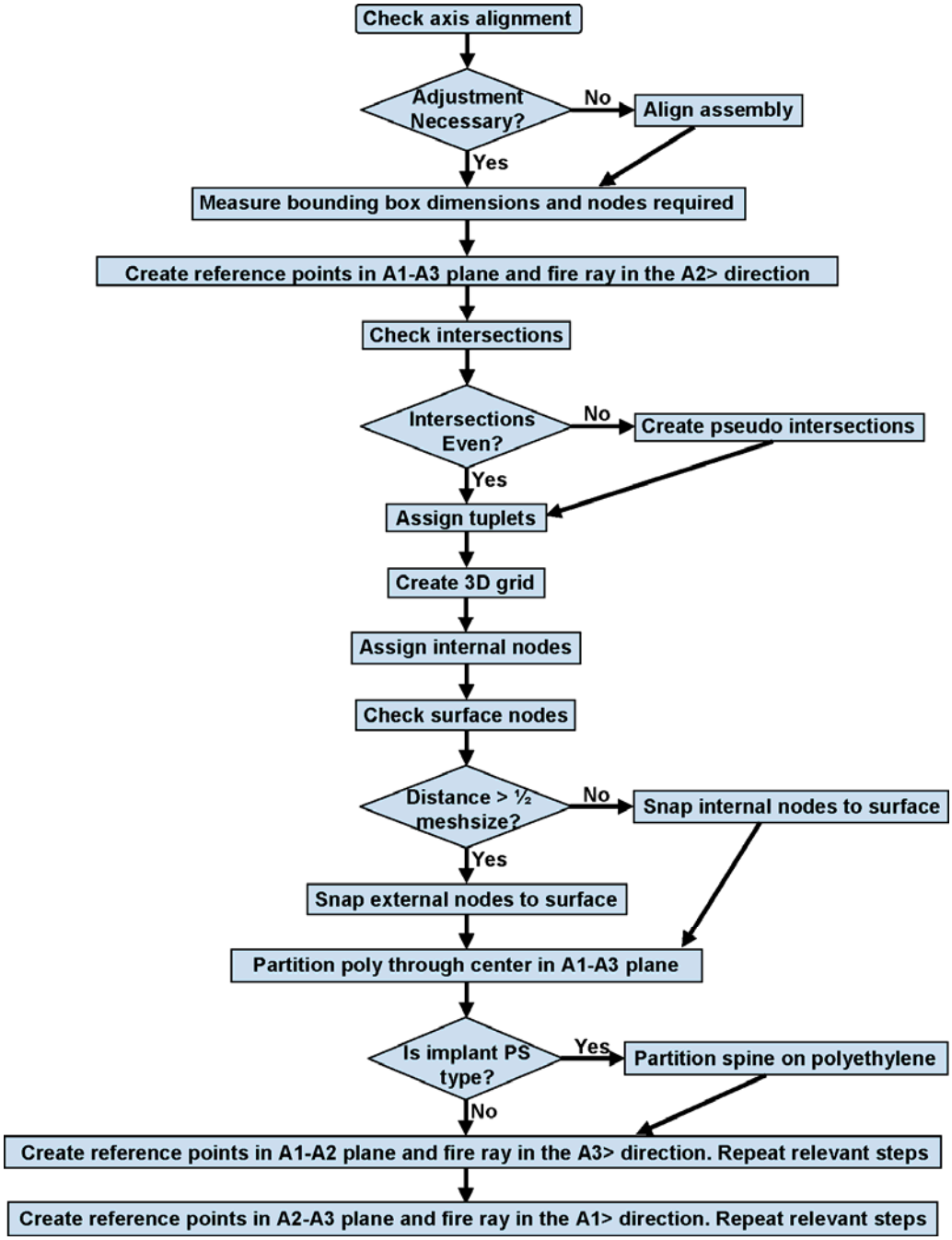

Figure 4-2: Flow chart used to create the nodes in the polyethylene.

I. Only the coordinates of the intersection of the ray that lies within the triangle are possible candidates (Figure 4-3).

II. All other intersections that do not lie within the triangle represents the possible intersection had the triangle been extended in space. An intersection at infinity represents the case when a triangle is parallel to the ray.

III. No possible intersections indicate that the point from which the ray is fired lies outside the polyethylene geometry.

IV. There can be cases when the same possible intersection point is associated with multiple triangles. This generally happens when the intersection falls on the common sides or vertices of the triangles. In this case, any triangle is chosen as it does not change the coordinates of the intersection

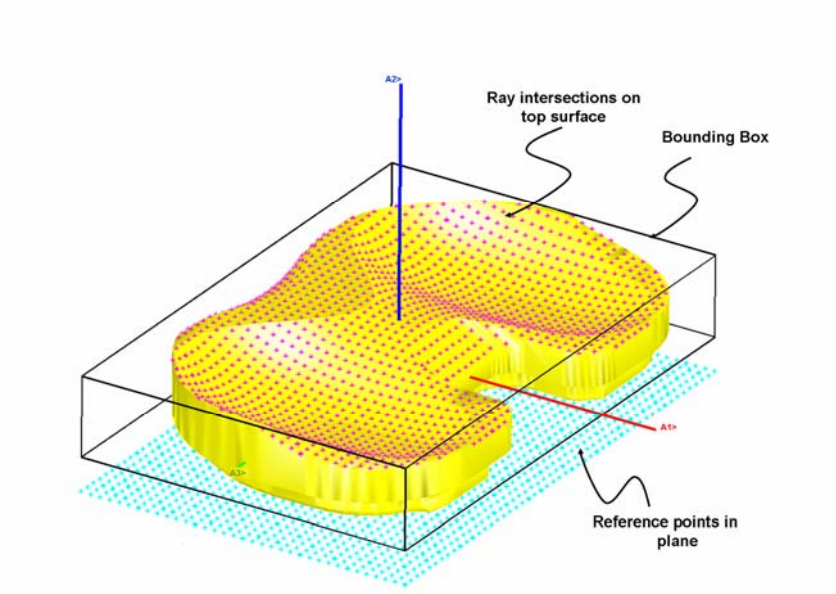

Figure 4-3: Reference nodes and corresponding intersections on the top surfaces.

5. Since, the reference points from which the rays are fired lie outside the polyethylene geometry, which is a closed geometry, ideally the number of intersections of each ray should always be even. However, sometimes due to slight gaps in the CAD models there can be cases when the number of intersections is odd. In those cases, the intersections of the neighboring rays are checked and pseudo-intersections are generated based on a simple average of the neighboring intersections (Figure 4-4).
6. In most cases the number of intersections should be two. This represents the scenario that between the two intersecting coordinates, the ray lies entirely inside the polyethylene geometry. However, due to some special features in the geometry (holes for attachment of polyethylene on the tibia, presence of the spine in polyethylene of PS implants, etc.) the number of intersections can be more than two but is always even. These represent cases where between the maximum and minimum intersecting coordinates, a ray lies partly inside the polyethylene geometry and partly outside. To correctly identify the lattice nodes in the A2> direction that lie inside the polyethylene geometry the ray intersections are assigned identification numbers (ID) in an ascending order based on their A2> coordinates. The number of interactions is broken into pairs based on an odd and the corresponding higher even number ID. Such pairs represent parts of the ray that lie inside the polyethylene (Figure 4-4).

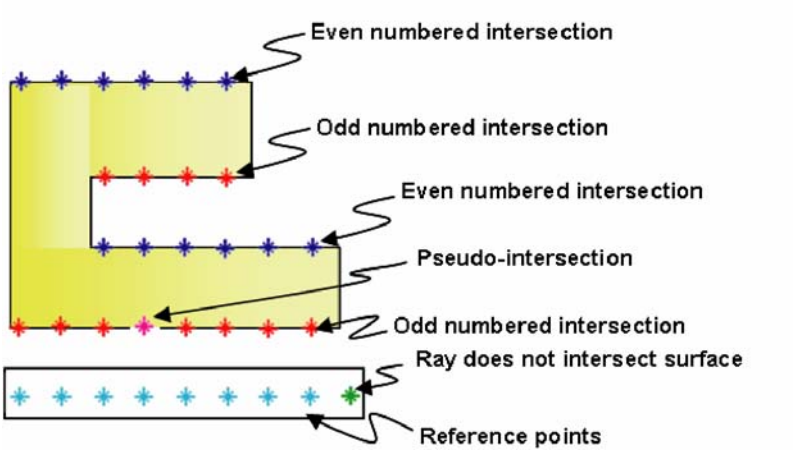

Figure 4-4: Generation of pseudo nodes in case of gaps and assigning pairs if intersections are more than two in order to identify parts of the ray inside the surface.

7. A 3D grid of possible nodes based on the bounding box dimensions is generated to calculate the possible y-coordinates that would be associated with each ray. Based on the maximum and minimum A2> coordinates of the pair created from the intersection of the rays, the nodes of the 3D grid created that lie inside (excluding the surface) the polyethylene are assigned.
8. To correctly form the surface geometry, the coordinates of the nodes must match the intersection coordinates. This is especially important at the surfaces in contact. This raises the concern of the grid quality near the surface. The internal nodes are all spaced equally. However, the surface nodes cannot be. Therefore, to keep mesh distortion low, the distance of the surface interaction from the nearest internal node (in the A2> direction) is calculated. If this distance is less than or equal to half the gridsize in the y-direction, the nearest internal node is moved to

the surface. If this distance is greater than half gridsize in the A2> direction, then the nearest external node is moved to the surface (Figure 4-5).

9. Due to intricacies in the geometry (small holes and edges) there is a possibility of no internal node or just one internal node between two intersecting pairs. This can happen when the geometry is small and the distance between the intersection coordinates is less than the gridsize. When there is no internal node and the length distance between the intersection coordinates is greater than half the gridsize, the two external nodes (top and bottom) closest to the surfaces are moved to the surface. If the distance between the intersection coordinates is less than half of gridsize, then only one node is added. This node is placed at the mean value of the intersection coordinates. A similar idea is used when there is just one internal node. If the distance between the intersection coordinates is less than half of gridsize then nothing is done. However, if the distance is greater than half gridsize, the internal node and one external node is matched to the surface. This is not an essential step to the performance of the network in general as long as the contact surfaces are not involved.
10. The above procedure should create a fairly structured grid of nodes. With sufficient number of nodes the whole structure of the polyethylene can be modeled pretty closely. However, it is to be noted, that since rays are fired in the A2> direction, there cannot be any intersections with the surfaces that are parallel

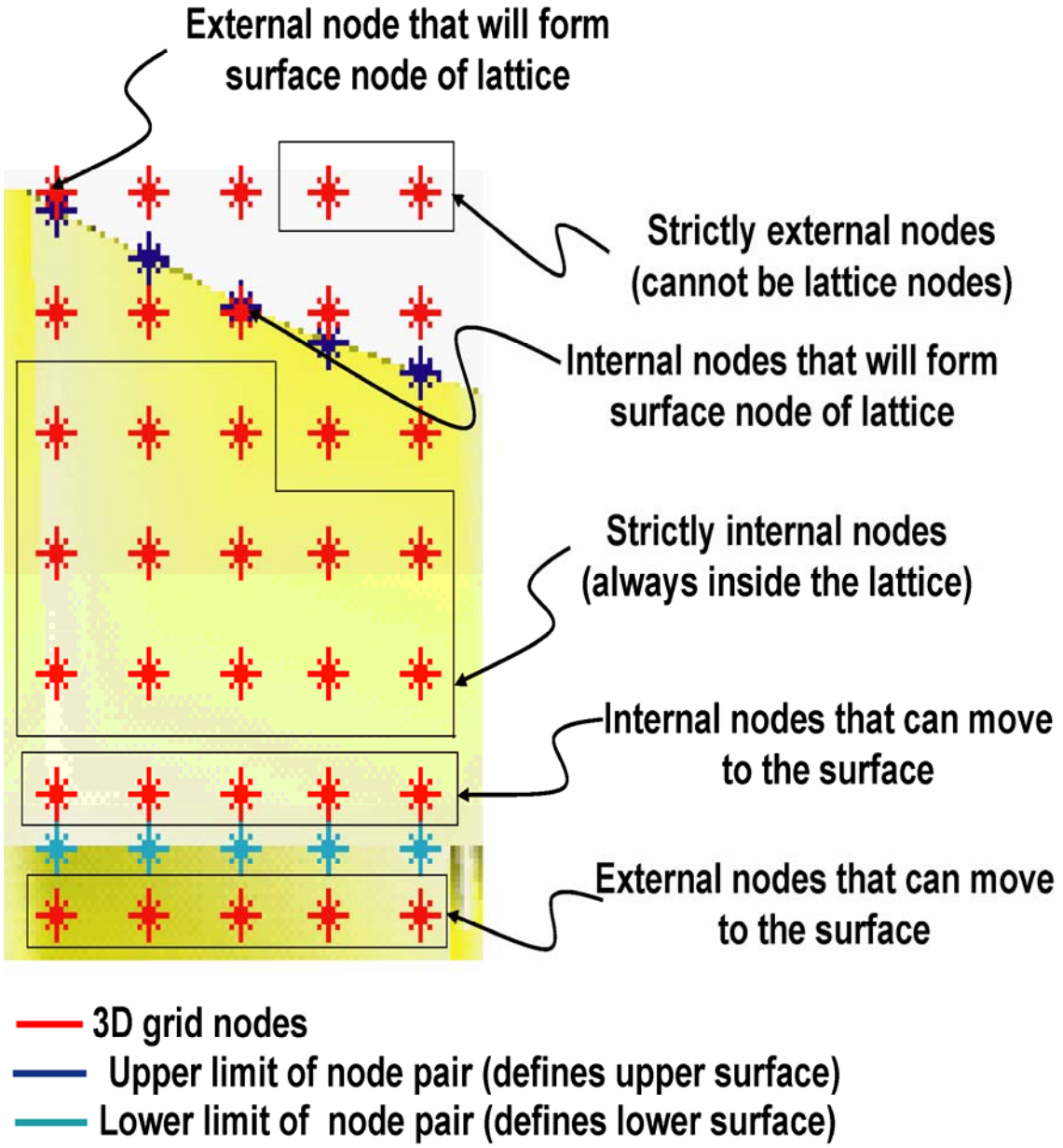

Figure 4-5: Identifying the nodes that would form the surface.

to the A2> axis. For more accurate geometrical representation, the above steps are repeated with reference points created in the A1-A2 plane and rays fired in the A3> direction and with reference points in the A2-A3 plane and rays fired in the A1> direction. This process can be carried out for as many planes desired.

11. Once, the grid nodes forming a part of the polyethylene insert are obtained, the nodes need to be assigned to either three types – contact nodes, internal nodes and boundary condition nodes. The contact nodes are all the nodes which lie on the top surface of the polyethylene. These are the nodes that would come in contact with the femur. The boundary condition nodes are the nodes on the bottom surface of the polyethylene. These are the nodes that would come in contact with the tibial component and would be used to assign boundary conditions. All other nodes lie inside the polyethylene geometry and are considered as internal nodes.
12. In order to facilitate measurement of distances on the surfaces, the contact nodes on the polyethylene surface are fitted with piecewise continuous cubic splines to create an UV grid. The U lines connect nodes having the same A3> coordinates and the V lines connect the nodes having the same A1> coordinates. These UV lines are also used to generate normal definitions at each node (Figure 4-6). The normal is defined as the average of the values obtained for the U and V lines associated with a particular node. The UV lines are also used to measure arc distances when required.

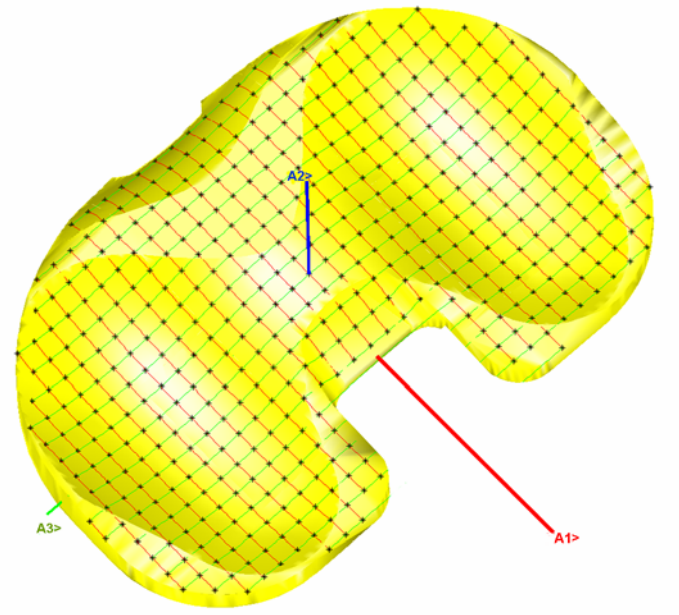

Figure 4-6: Creation of UV lines on the contact surfaces.

4.2 Femoral Nodes and Contact Detection:

At the beginning of the analysis, the algorithm outlined before is used to create nodes and UV line definitions for the femoral lower surface to measure arc lengths on the femoral surface that is used for slip calculations. For contact detection, rays are projected in the A2> direction from the contact nodes of the polyethylene lattice to generate interactions on the lower surface of the femur (Figure 4-7). The difference in the A2> coordinates between the intersections on the lower surface of the femur and the contact nodes of the polyethylene insert is used to check for contact. A negative value indicates contact while a positive value indicates separation. However, for numerical stability of the contact

algorithm any node having a distance value lesser than a desired tolerance is assumed to be in contact. For each time step, the orientation of the femur and polyethylene is fixed. However, during the deformation analysis, the nodes associated with the polyethylene can move in the A1> and A3> directions. Therefore, new rays are projected onto the femoral surface whenever contact needs to be calculated. Thus a small sliding formulation of the contact problem with node to node contact detection is executed at each time step. Also, this prevents intersection of the femoral and polyethylene nodes during the analysis since the contact nodes on the polyethylene and the femoral surfaces are always matched.

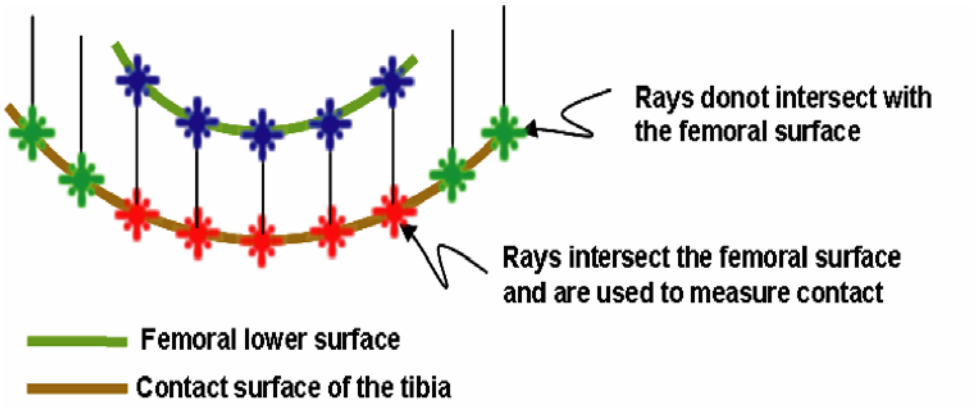

Figure 4-7: Rays are projected from the polyethylene surfaces nodes to create femoral nodes and check for contact.

4.3 Adjustment of Femoral Orientation:

Based on the transformations obtained from fluoroscopy, there can be three conditions for the articulation of the femoral condyles on the polyethylene:

1. Neither of the two femoral condyles are in contact with the polyethylene surface. This condition is not physically possible and is not considered.
2. Only one of the femoral condyles contacts the polyethylene while the other does not. This condition has been referred to as condylar lift-off and is quite often observed in knee implants and less frequently in normal knees.
3. Both the femoral condyles contact the polyethylene surface.

Telemetric studies have shown that the maximum force occurring between the femoral and the polyethylene components occur in the superior inferior direction with a very small amount of force in the medial-lateral and antero-posterior direction (D'Lima, 2007). Since deformation analysis is more sensitive than the error range of the fluoroscopic 3D to 2D registration process, a slight modification in the orientation of the femur with respect to the polyethylene is performed at the beginning of the analysis.

The purpose of the adjustment is to realign the coronal orientation of the femoral component so that both condyles of the femur come in contact with the polyethylene until there is a clear evidence of lift-off. A cut-off of 0.5mm in translation and 0.5º in rotation is used. These values are the general error estimates that are considered to be associated

with the fluoroscopic process. Though, lift-off is frequently observed in TKAs however, at the small values for which the correction is performed, there is no way of knowing whether the result is due to measurement error from fluoroscopy or otherwise. Therefore, by realigning the femur we take a much more conservative approach so that the possibility of lift-off is not over predicted. If the correction is performed, the femoral penetration and coronal angle is checked after the completion of the deformation analysis. If the final femoral penetration and coronal angle is more than the adjustments made, the original orientation of the femur is restored and the analysis is reconducted (Figure 4-8). The following logic is used:

1. The distance of the closest point of each femoral condyle to the corresponding polyethylene surface and the corresponding difference is measured.
2. Assuming small angles, the ratio of the difference of these distances with the intercondylar distance of the contact points projected onto the coronal plane generates the coronal inclination. If this angle ('A' in Figure 4-9) is found to be less than 0.5º, then the femoral component is rotated in the coronal plane till the difference becomes zero.
3. If the angle is greater than 0.5º, then no correction is performed.
4. The femoral condyles are always translated in the superior-inferior direction until it touches the polyethylene surface (the difference between the contact node in the polyethylene and the corresponding femoral node is zero). Whether there is contact on one condyle or both the condyles depends upon the coronal orientation

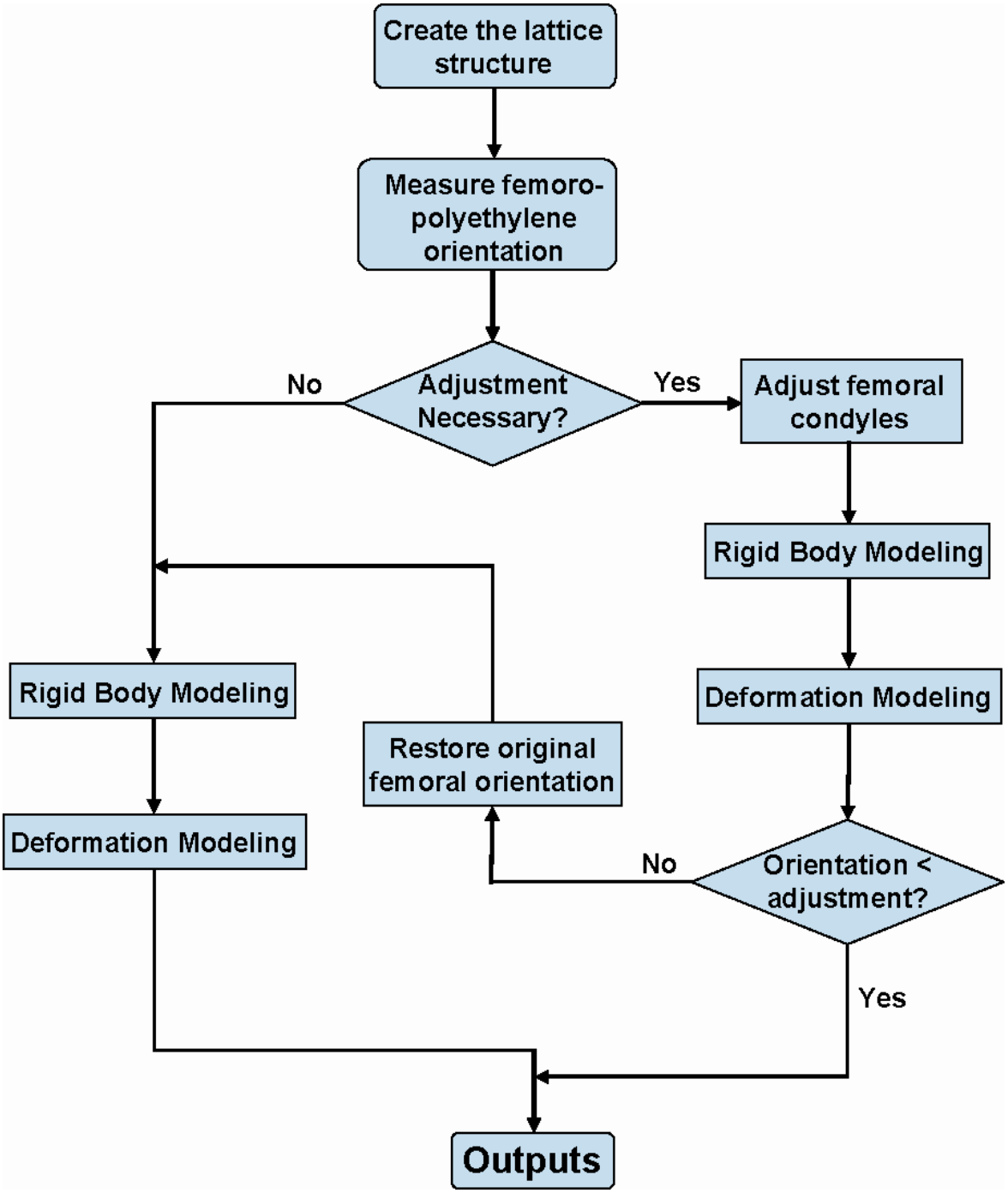

Figure 4-8: Flow chart of initial adjustment correction.

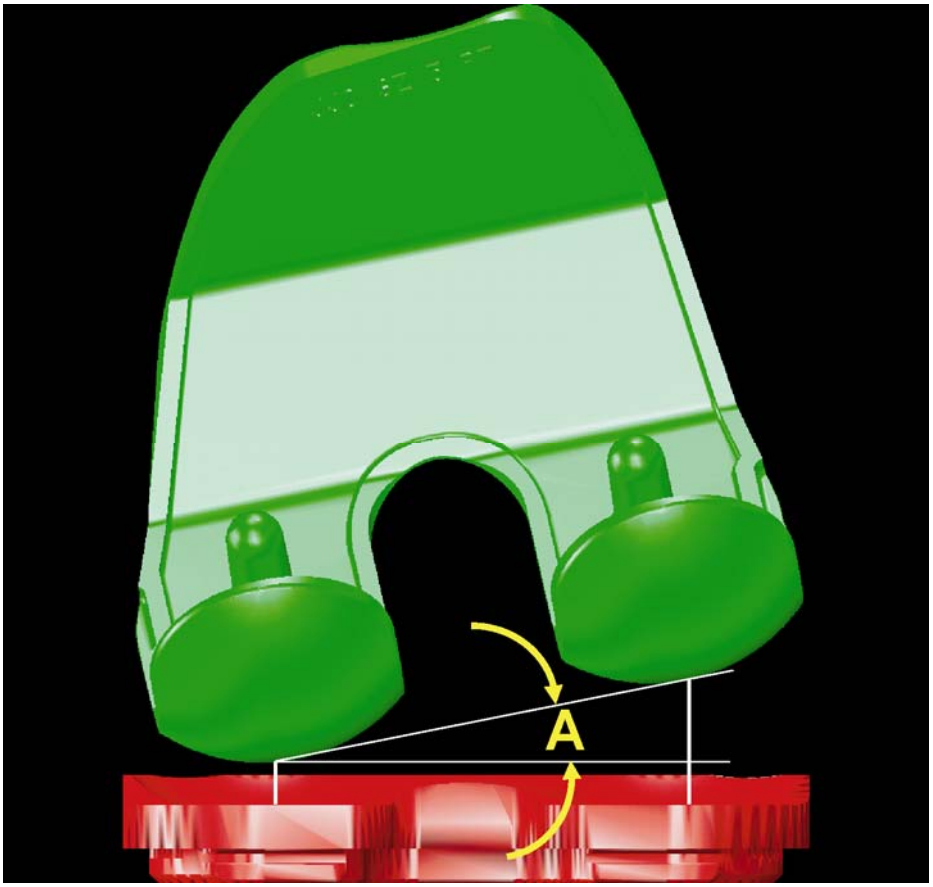

Figure 4-9: Coronal alignment of the femur with respect to the polyethylene.

4.4 Inverse Dynamic Rigid Body Modeling:

The purpose of the rigid body model was to estimate the total contact force acting interactively between the femoral component and the polyethylene and to generate the equations of motion related to the activity. This 3D model for the deep knee bend activity is based on the principles of inverse dynamics, utilizing the reduction technique (Komistek 2005) and was created in Autolev^{TM} (Online Dynamics Inc, Sunnyvale, CA) a symbolic manipulator based upon the concepts of Kane's dynamics.

The model consists of a kinematic chain from the ankle to the hip and consists of the femur, tibia and patella which were assumed to be rigid bodies (Figure 4-10). The hip joint was modeled as a resultant reaction force having three scalar components. The foot was not modeled as it remained fixed to the ground (heel not lifting up) during the activity. The ground reaction force, obtained from a force plate, was applied at the ankle. The tibia was assumed to rotate only in the sagittal plane about the ankle. The patellofemoral joint was modeled by a single contact point which started inferior but moved in the superior direction about its mass center with the increase in knee flexion. The closest point of the patella to the femoral implant was assumed to be the contact point. Incidence of patellar dislocation and separation was neglected and the patella was assumed to be always in contact with the femur. The patella was assumed to rotate only

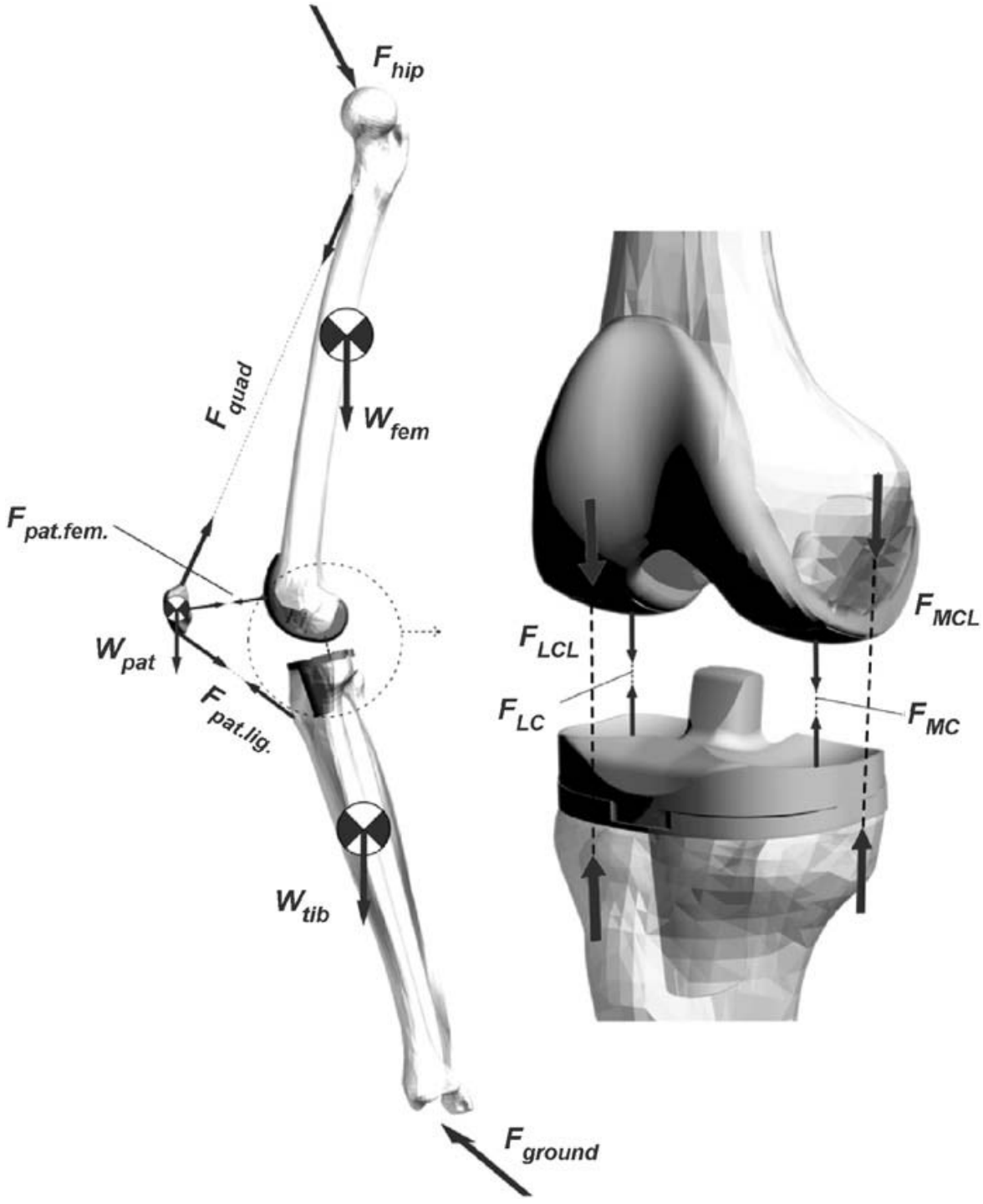

Figure 4-10: Schematic diagram of the rigid body model.

in the sagittal plane about its mass center which was assumed to be the centroid of the patellar bone.

At the first time increment the femur is assumed to be static with zero initial velocities. However, for all successive increments the femur is modeled to roll with slip on the polyethylene. The slip calculation is based on the lowest point of the femoral condyles. For pure rolling, the arc length of the femoral surface in between the two lowest points measured in between two time intervals must be equal to the arc length in the polyethylene surface corresponding to the projections of the lowest point. However, since the femur rolls with slip, the arc length in the femur is greater than the arc length in the polyethylene (Figure 4-11). The difference between the arc length traveled by the femoral contact points and the arc length of the polyethylene contact points are used to calculate the amount of slip. For equal slip on both the condyles, the difference in the arc length should be equal. However, due to the coupled axial rotation of the femur along with flexion, the arc length measured on the polyethylene surface is different on the two condyles. The difference in the arc length is assumed to be due to the axial rotation of the femur and the rotational axis is assumed to pass through the geometrical center of the femur. After correction in the arc lengths of the femur due to axial rotation, the amount of slip is calculated (Figure 4-12). Slip is entered into the system by the addition of a translation velocity (obtained after differentiating the slip length) in the femur in the direction of flexion.

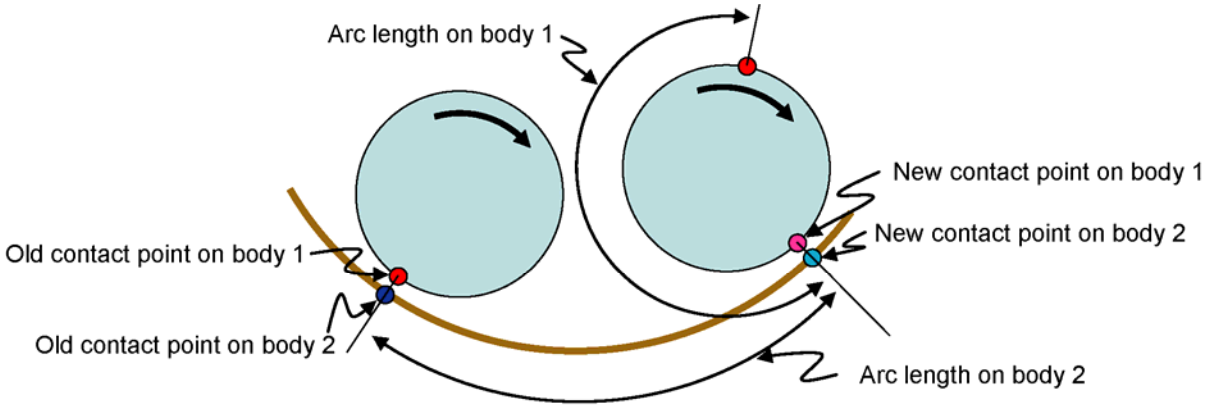

Figure 4-11: Contact behavior when two bodies roll against each other.

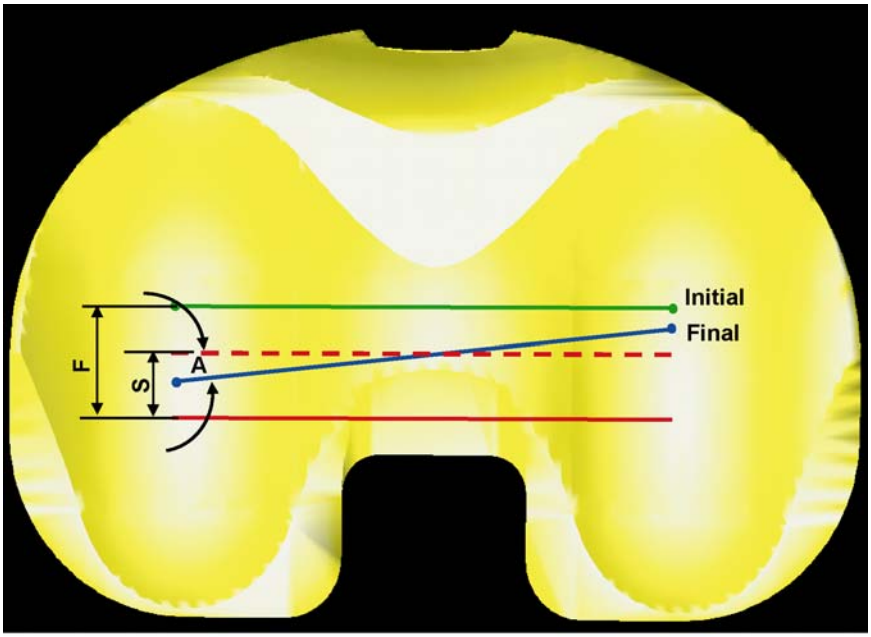

Figure 4-12: Amount of slip is based on the lowest points of the femur.

Since the femoral and polyethylene condyles are characterized by smooth quadratic surfaces their contact surfaces are elliptical and therefore the centroid of the ellipse that is formed due to the contact can be assumed to be the location for the resultant force and the contact point. Under this assumption, the point on the femur that was closest to the polyethylene surface was used as the contact point on each femoral condyle that is in contact with the polyethylene insert. It is to be noted that since the femoral and polyethylene surfaces are curved, the lowest point on the femoral condyle is not necessarily the contact point. The contact constraint was enforced by zero velocity in the normal direction of the points in contact. A frictional force in the direction opposite to the relative velocity of the points in contact was also incorporated (Figure 4-13). Coulomb frictional formulation was used where the magnitude of the frictional force was obtained as the product of a frictional coefficient and the normal force. A constant frictional coefficient of 0.05 was assumed. The contact forces were transferred to the global (polyethylene) coordinate system and summed up to obtain the total contact forces for use in the deformation modeling.

The collateral ligaments (medial and lateral) and the cruciate ligaments (when applicable) were incorporated in the model as non-linear elastic springs which carry a load only when extended. The posterior cruciate ligament (PCL) was divided into a posteromedial and anterolateral bundle (Hughston 1980; Burks 1990; Amis 2003;

Shin 2007). The anterior cruciate ligament (ACL) comprised of an anteromedial and a posterolateral bundle (Arnoczky 1983; Norwood 1979; Shin 2007). The lateral collateral ligament (LCL) was modeled as a single element (Abdel-Rahman 1998; Shin 2007). The medial collateral ligament (MCL) was divided into three bundles (Abdel-Rahman 1998; Caruntu 2004; Shin 2007). The force versus extension profile for the ligaments was formulated as combination of two linear springs to represent the toe region and the terminal stiffness region and is given by Shin et.al. (Shin 2007):

$$F = 0 \qquad \varepsilon \le 0$$

$$F = \frac{k}{2}(L - L_0) \qquad 0 \le \varepsilon \le 2\varepsilon_1$$

$$F = k\left[L - (1+\varepsilon_1)L_0\right] \qquad 2\varepsilon_1 \le \varepsilon$$

where

$L_0 = \text{Slack length}; L = \text{acutal length}; k = \text{stiffness coefficient}$

$\varepsilon_1 = 0.03(\text{a constant}); \varepsilon = \text{strain} = \dfrac{L - L_0}{L_0}$

The lengths of the ligaments are computed by tracking the distance between the proximal and distal ends. All other relevant ligament parameters are obtained from previously published literature Shin et. al. (Shin 2007).

The extensor mechanism (quadriceps muscle and patellar ligament) is the primary activator during a deep knee bend activity. In order to keep the system determinate, the quadriceps muscles were assumed to be a single muscle having its attachment points corresponding to the vastus intermedius. The quadriceps muscle and the patellar ligament

were modeled as massless and entered into the system as equal and opposite forces acting along their lengths. Wrapping of the quadriceps and the patellar ligament at higher flexion angles, when occurring, was taken into account. Since in this inverse dynamic model the muscles forces are computed therefore the model does not incorporate muscle activation dynamics.

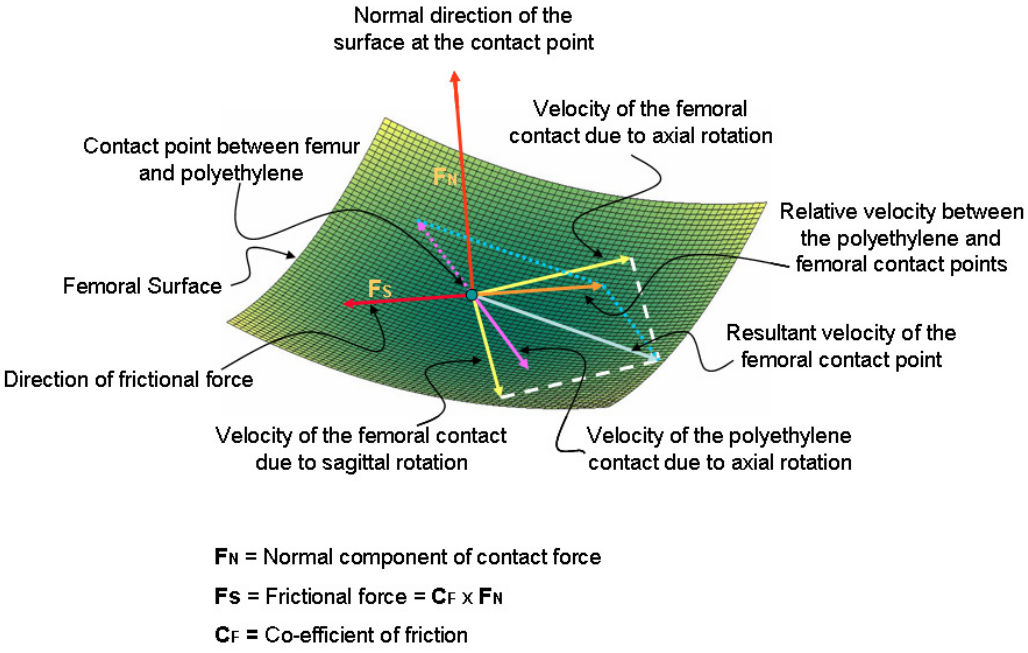

Figure 4-13: The direction of the femoro-polyethylene contact forces used in the model.

4.5 Deformation Modeling:

4.5.1 The Lattice Template:

For the deformation model to work, the grid of nodes, that were previously generated, need to be transformed into a discrete network by adding spring interactions between the neighboring nodes. In the discrete network, any two neighboring nodes are connected by a single spring. However, when considering more than two nodes in the structure a hexahedral (cubic) grid of connections is used. For eight nodes forming the corners of a cube several formulations of interconnections are possible. The behavior of the network depends on the interconnection chosen. For example a template might be used where connections are created among the nearest nodes. This generates a grid with connections along the edges of the cube. However, such a cube does not exhibit any Poisson ratio effect under uniaxial load conditions as the spring members perpendicular to the load do not deform and therefore do not carry any load in other directions. Therefore, in order to have an effect of unidirectional load on other directions diagonal members are needed. Use of a nearest and next to nearest neighbor algorithm creates additional diagonal members across the faces of the imaginary cube formed by 8 nodes at the corners. (Figure 4-14)

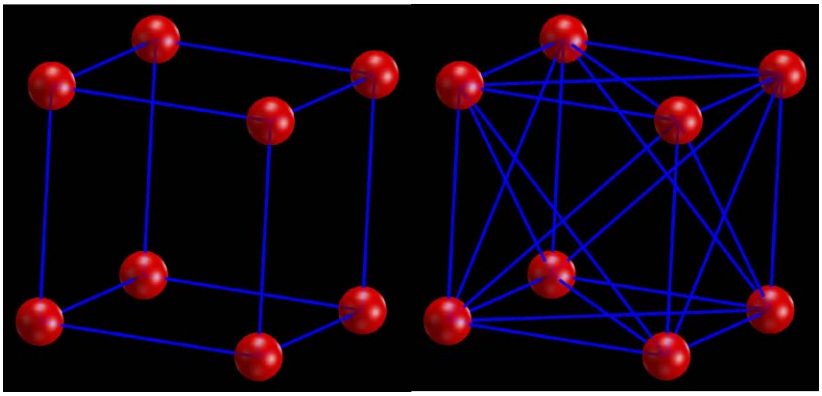

Figure 4-14: (Left) Connections formed by a nearest node template. (Right) Connections formed using a nearest plus next to nearest node template.

To model the polyethylene as generically as possible a combination of body centered cubic (BCC) and face centered cubic (FCC) template was used. This was analogous to using a nearest plus next-to-nearest plus next-to-next-to-nearest node algorithm. Thus in this case each internal node (not on the surface or edge) (green node in Figure 4-15) was connected to 26 of its neighbor nodes, 8 BCC nodes (red nodes in Figure 4-15) and 18 FCC nodes (blue nodes in Figure 4-15). It is to be noted that for a single cube of 8 nodes this template for connection generates ${}^{8}C_{2}$ = 28 connections. In other words for 8 nodes that form a cube, each node was connected to every other node in the grid. However, for more than 8 nodes in the network, when multiple cubes with 8 nodes can be formed, this template eliminates the double connections caused due to cubes in a grid sharing common faces. In other words for a 27 noded grid this template generates 158 connections as opposed to 224 that would have been obtained using 8 individual cubes having 28 connections each.

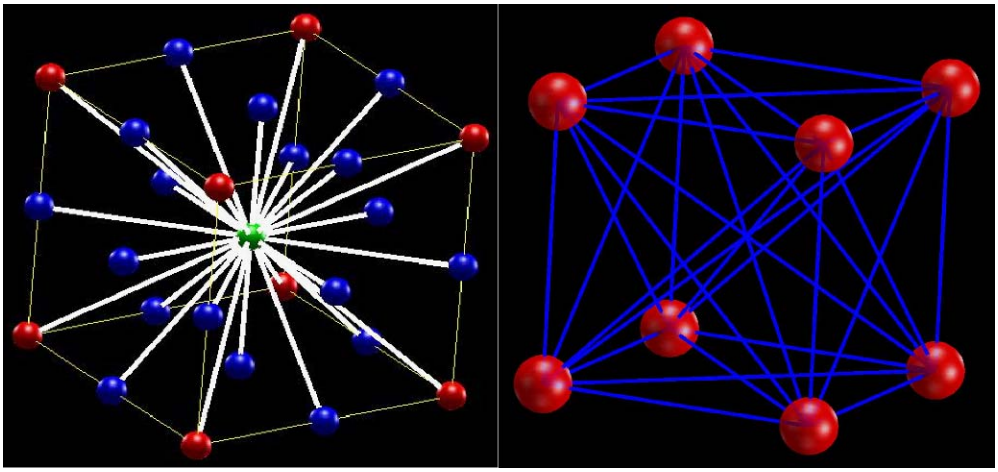

Figure 4-15: (Left) Unit cell of the template used. (Right) Connections for 8 nodes forming an imaginary cube

4.5.2 Calculating Spring Stiffness:

The idea behind material models is to find a constitutive relationship between stress and strain in the material and is independent of size or dimensions of the material. The principles of continuum mechanics aimed at the development of these constitutive relationships are based on the principles of strain energy. For any geometrical structure, its stiffness is a measure of its force versus deformation relationship and is associated with the potential energy stored in the system due to the deformation. Potential energy is the sum of the internal strain energy and the work done due to the forces acting on it. Thus stiffness of a structure depends both on the properties of the material as well as the geometry of the structure. Though, strains (ratio of deformation and original length) can be defined for a spring, there is no physical definition of stresses associated with a spring.

Springs are characterized by their force versus deformation relationship and store potential energy when they deform. Therefore, the stiffness associated with a spring is a function of both the material and the geometry it represents. For a spring of stiffness '*k*', the force in it and the energy stored can be computed as:

$$f = -\int k \partial r \quad \text{and} \quad E = -\int f \partial r$$

where f = Force in the spring

E = Potential energy in the spring

$|r|$ = Length of the spring

Assuming that stiffness of the spring is independent of the length of the spring and at zero deformation there in no energy stored in the spring, the force and energy associated with the springs have the following relationships:

$$f = -\int_{|R|}^{|r|} k \partial |r| . \left(\frac{\partial r}{\partial |r|} \right) = -(k \int_{|R|}^{|r|} \partial |r|) \vec{e} = -k(|r| - |R|) . \vec{e}$$

$$E_{ij} = -\int_{|R|}^{|r|} f \partial |r| . \left(\frac{\partial r}{\partial |r|} \right) = (k \int_{|R|}^{|r|} (|r| - |R|) \partial |r|) \vec{e} \vec{e} = \frac{1}{2} k (|r| - |R|)^2$$

where $|R|$ = Original spring length

$\frac{r}{|r|} = \vec{e}$ = unit vector along the spring length

The spring stiffness is calculated based on the equivalence of the total energy stored in a unit cell of the spring network of volume 'V' with that obtained using continuum.

$$U_{cell} = U_{continuum}$$

For this unit cell the total energy is:

$$U_{cell} = \sum_b E_b = \frac{1}{2}\sum_b^{N_b} (F \bullet u)^b$$

where b = subscript for bth spring

N_b = total number of springs = 26

E = Energy per spring

F = Force acting on each spring

u = Deformation of each spring

Assuming that the stiffness of the springs are independent of their initial lengths and spatially linear displacement fields *u*, i.e. we assume uniform strain fields, the total energy in an unit cell per unit volume reduces to:

$$U_{cell} = \frac{1}{2V}\sum_{b=1}^{26} (ku \bullet u)^b = \frac{1}{2V} k \sum_{b=1}^{26} l_i^b l_j^b \varepsilon_i \varepsilon_j$$

where k = Spring stiffness

V = Cell Volume

l = Spring length

Based on continuum mechanics the energy of the unit cell can be computed as:

$$U_{continnum} = \frac{1}{2}\int \sigma \bullet \varepsilon dV$$

where σ = stress

ε = strain

For linearly elastic materials and assuming small deformations the energy per unit volume is:

$$U_{continuum} = \frac{1}{2}\sigma_i \varepsilon_j = \frac{1}{2} C_{ij} \varepsilon_j \varepsilon_i$$

where C_{ij} = Stiffness tensor of the material

Equating the energy per unit volume for the unit cell with that obtained using continuum we have:

$$C_{ij} = \frac{k}{V} \sum_{b=1}^{26} l_i^b l_j^b$$

For the above spring network, the only material variable is the stiffness of the springs which was assumed to be the same for all the springs in the unit cell. Once the spring stiffness was defined, the Poisson's ratio was automatically defined by the structure of the network. For a linearly elastic material, there are two material variables defined as the Lame's constants. Therefore, the stiffness tensor of the spring network would not match the stiffness tensor of a material obtained using the principles of continuum mechanics. This problem can be solved by using different spring stiffness for the different spring elements defining the cube. However, this aspect has not been explored in this dissertation. Since the knee joint experiences maximum loads in the superior inferior direction, so the diagonal element in the compliance tensor matrix (obtained as the inverse of the stiffness tensor matrix) corresponding to superior inferior direction is compared to find the stiffness of each spring and we obtain:

$$k = EC$$

Where E = the Young's modulus of the material

C = a factor related to the geometry of the unit cube presented by the spring network and has a dimension of [L].

Since 'C' is a factor associated with the volume of the material represented by the unit cube, therefore it was assumed constant. Using this representation of the spring stiffness, both linear and nonlinear material behavior (assuming nonlinear elastic) was obtained. Since, $E = \frac{\partial \sigma}{\partial \varepsilon}$, therefore the expressions for stiffness, force and energy for the springs can be defined as:

$$k = \frac{\partial \sigma}{\partial \varepsilon} C$$

$$f = -\int_{|R|}^{|r|} k \partial r = -\int_{|R|}^{|r|} \left(\frac{\partial \sigma}{\partial \varepsilon}\right) C \partial r = -|R| C \vec{e} \int_{0}^{\sigma} \partial \sigma = -\sigma C |R| \vec{e}$$

$$\text{Since, } \frac{\partial \varepsilon}{\partial r} = \frac{\partial}{\partial r}\left(\frac{|r| - |R|}{|R|}\right) = \frac{1}{|R|}\frac{\partial |r|}{\partial r} = \frac{1}{|R|\vec{e}}$$

$$E = -\int_{|R|}^{|r|} f \partial r = \int_{0}^{\varepsilon} (\sigma C |R| \vec{e}) \partial \varepsilon \left(\frac{\partial r}{\partial \varepsilon}\right) = \int_{0}^{\varepsilon} (\sigma C |R| \vec{e}) \partial \varepsilon \left(|R| \vec{e}\right) = |R|^2 C \int_{0}^{\varepsilon} \sigma \partial \varepsilon$$

Using this formulation and a piecewise continuous relationship that is at least first order differentiable (to be able to calculate E), any stress strain relationships with linear or nonlinear elastic material models can be incorporated. In this dissertation, the stress strain relationship for the polyethylene used is based on the true stress strain data for polyethylene as reported by Halloran et. al. (Halloran 2005).

4.5.3 Creating the Global Stiffness Matrix:

A standard algorithm is used to assemble stiffness matrices:

1. Based on the lattice nodes already created and the BCC+FCC connection structure defined before, the number of element connections was calculated.
2. For each element, the element stiffness matrix was computed. For a spring element as used in our case the element stiffness matrix was of the following form

$K^s = \begin{bmatrix} \kappa^s & -\kappa^s \\ -\kappa^{sT} & \kappa^{sT} \end{bmatrix}_{6x6}$ where $\kappa^s = knn^T$ is a 3x3 subunit of the element stiffness matrix

and k = Spring stiffness

n = Unit vector associated with each spring

T = A subscript to indicate transpose

3. A simple spring can carry a load only when extended or deformed. So all the nodes in this deformation model were assigned 3 degrees of freedom. Therefore, the global stiffness matrix was 3Nx3N (N=number of nodes) which was assembled from the individual element stiffness matrix by matching the global degrees of freedom with the degrees of freedom associated for each element.
4. Depending on the number of nodes, the global stiffness matrices can be huge and can serve as a possible bottleneck in the speed of the total algorithm. Thus a vectorized approach was used in the global stiffness assembly routine. In this approach all loops are converted to matrix multiplications. Elimination of the loops increases speed of the computation but it is accomplished at the cost of a high amount of memory usage needed to store large matrices.

4.5.4 Assigning Boundary Conditions:

Since, the tibial component of knee implants is made of alloy steel, so it was considered to be rigid. Therefore, boundary conditions were applied at the nodes of the polyethylene that were in contact with the surface of the tibial component. Based on the attachment of the polyethylene to the tibial component, knee implants can be classified as fixed or mobile. Therefore depending on the type of implant modeled the following boundary conditions were applied:

1. If the implant modeled is of a fixed type, all the nodes at the bottom of the lattice are assumed to be fixed in all three directions and therefore their deformations were zeros. This is analogous to assuming that the polyethylene is rigidly connected to the tibia at these nodes.
2. For a mobile bearing implant, the nodes at the bottom of the flat surface resting on the tibia, were assumed to be fixed to the tibial component only in the A2> direction, but can freely deform in the A1> and A3> directions. This however leads to rigid body modes for the solution algorithm which causes singularity in the stiffness matrix. Therefore, to remove any rigid body motion, the two end nodes on the bottom surface measured in the A3> direction was fixed in the A1> and A3> directions.

The imposition of the boundary conditions essentially means that the deformation of the nodes on which the conditions have been imposed are known (zero in this case).

4.5.5 The Solution Algorithm:

The equation for solving deformation models under static conditions is:

$$KX = F$$

where K = The global stiffness matrix

X = A vector of displacements at each degree of freedom

F = A vector of the forces acting at each degree of freedom

Therefore, if the force was known at each node, the solution could be achieved in a single step. However, from the multidynamic rigid body model only the total contact force for the femoral and the polyethylene component can be calculated. As a result, the force distribution acting on the node must first be calculated before the final solution is possible. Thus the solution is essentially deformation driven rather than being force driven, where the aim is to find the correct deformation for the known total external force F_{ext}. The algorithm is outlined below:

1. Move the femur by a distance D.
2. Check elements in contact N_0 and the corresponding assumed nodal displacements $\{d_0\}$.
3. Calculate nodal forces $\{f_0\}=[K_0]\{d_0\}$. ($[K_0]$ is the global stiffness matrix associated with the undeformed structure).
4. Calculate actual nodal displacements $\{x_0\}=[K_0]^{-1}\{f_0\}$. ($\{x_0\}$ is in the global coordinates)**.**
5. Calculate the internal force $\{F_{int}\}$ based on $\{x_0\}$. This calculation includes the following substeps:

(A) Based on $\{x_0\}$ calculate the length $|r|$ and strain ε in each spring.

(B) Based on strain and material properties calculate force f_{el} and stiffness k_{el} of each spring. Note that f_{el} is a vector with components $(f_{el})_x$, $(f_{el})_y$, $(f_{el})_z$ in the A1>,A2>,A3>, directions.

(C) Sum spring contributions for each node to obtain the total force at a node f_{int}.

(D) Assemble f_{int} into the global internal force $\{F_{int}\}$.

(E) Compute $\{F_{int}\}_{NC}$ for the nodes not in contact and $\{F_{int}\}_C$ for the nodes in contact.

(F) Assemble the new global stiffness matrix K_1 based on the new spring stiffness k_{el}.

6. Check $\|\{F_{int}\}_{NC}\| < tolerance.$ If yes move to step 11 else move to step 7.
7. Define $\{f_1\} = -\{F_{int}\}$. Assign zeros at the degrees of freedom for the nodes in contact N_0.
8. Compute $\{\Delta x_1\} = [K_1]^{-1} \{f_1\}$.
9. $\{x_1\} = \{x_0\} + \{\Delta x_1\}$.
10. Repeat Steps 5 to 9 until; $\|\{F_{int}\}_{NC}\| < tolerance$.
11. Compute the total reaction force $F_{react} = \|\{F_{int}\}_C\|$ for the nodes in contact.
12. Check $(F_{react} - F_{applied}) < tolerance.$ If yes terminate. Else move to step 13.
13. Compute $D_{new} = \frac{F_{applied}}{F_{react}} xD$.

14. Repeat steps 2 to 12 until $(F_{react} - F_{applied}) < tolerance.$

The basic idea behind the algorithm is to start with an assumed displacement to calculate the nodal displacement and the force distribution for the whole network. Since only the nodes that are in contact are constrained and the remaining nodes are free to displace in any direction, they always remain in equilibrium. Therefore, the total internal reaction force in the non contact nodes should always be equal to zero and only the contact nodes would carry a distributed load based on the amount of penetration of the femoral surface on the polyethylene and that would be the reaction force for the assumed deformation.

For a nonlinear material formulation, the stiffness properties of the springs in the network change with respect to the current nodal deformation. Therefore, the current properties need to be computed on an element basis before they can be assigned globally. This is achieved in steps 5A to 5F. Also due to the change in the stiffness, the total amount of internal force in the structure also changes and therefore steps 7-10 is an iterative loop aimed to ensure that the nodes not in contact are in equilibrium and carry a zero force. Once the force associated with a particular deformation is obtained, a new deformation is calculated in order to match the total force driving the femoral component into the polyethylene (step 13). Since the external force versus deformation behavior of the structure is nonlinear so the current formulation is based on the secant slope of the material (Figure 4-17).

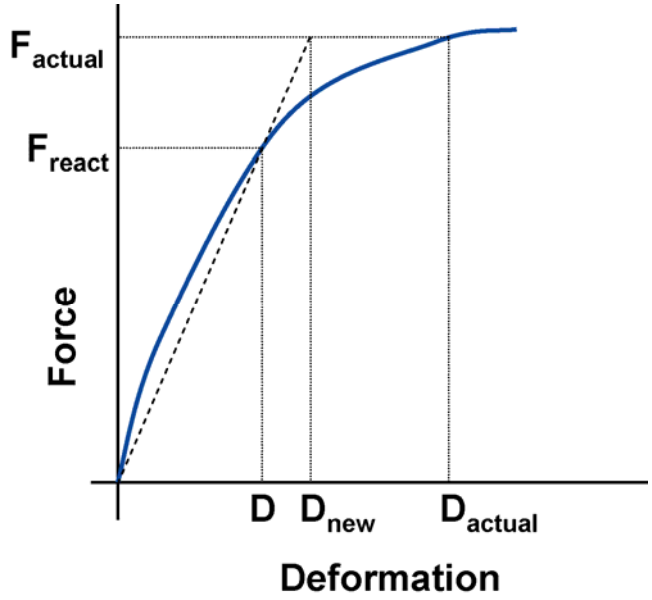

Figure 4-17: The secant slope is used for convergence in the nonlinear algorithm

For a linear elastic material formulation, since the stiffness of the structure does not depend on the current deformation, it has to be computed only once. This also eliminates the requirement for steps 5A to 5F as well as steps 6 to 10. As a result the solution can be obtained much faster using the following refined algorithm:

1. Move femur by a distance D.
2. Check elements in contact N_0 and the corresponding assumed nodal displacements $\{d_0\}$.
3. Calculate nodal forces $\{f_0\}=[K]\{d_0\}$. ($[K]$ is the stiffness matrix).
4. Calculate actual nodal displacements $\{x\}=[K]^{-1}\{f_0\}$
5. Calculate total reaction force F_{react}.
6. Check $(F_{react} - F_{ext}) < tolerance$. If yes move to step 15 else move to step 7.

7. Calculate residual force $F^* = F_{react} - F_{ext}$.
8. Create dummy nodal displacements $\{\Delta d\}$. It is a vector contains ones for nodes that are in contact and zeros elsewhere.
9. Calculate dummy nodal forces $\{\Delta f\} = [K]\{\Delta d\}$.
10. Calculate dummy nodal displacements $\{\Delta x\} = [K]^{-1} \{\Delta f\}$.
11. Calculate dummy reactions Δf_{react}.
12. Calculate scalar $\lambda = F^* / \Delta f_{react}$.
13. Move femur by distance $(D + \lambda)$.
14. Check new elements in contact N_1.
15. If $N_1 = N_0$, repeat steps 2 to 4, else repeat steps 2-15 until termination.

The basic idea behind the algorithm is that, since the material is assumed to be linearly elastic, its force versus deformation profile is also linear if the number of nodes in contact remains the same. Therefore, once the slope is correctly identified (using the dummy displacements), the correct solution can be obtained in a single step if the nodes that are in contact remain the same. If the number of nodes that are in contact changes due to the actual calculated deformation, the process has to be repeated. Since, steps 3-5 and 8-10 are similar, the only difference is that while $\{d_0\}$ represent actual values, $\{\Delta d\}$ contains unit deformation (for slope calculation), they are combined in the code so that the computations are conducted simultaneously.

4.5.6 Contact Areas and Contact Pressures:

Unlike finite element analysis which involve pressure over closure relationships for contact and, therefore, can output contact pressures associated with each node, the discrete element model can only predict the force distribution associated with the nodes in contact. For a lattice network in which the springs are interconnected, there are no concrete ways to identify the area of influence (Gonzalez 2008) that can be used to correctly predict the contact pressures. Therefore, we used an indirect approach for measuring contact pressures. First the total area in contact is calculated. The total area in contact is assumed to be the area of the femoral surface that interferes with the undeformed polyethylene surface. The associated area of influence is the ratio of the total contact area divided by the number of nodes found to be in contact. This is an approximate measure of the contact pressures as it assumes that the area of influence is equal for all the nodes in contact. Also the force associated with each node is obtained in the global reference frame. Therefore, the force obtained at each node is oriented along the normal direction associated with each node. Therefore contact pressure at each node is defined as:

$$P_i = \frac{F_i \bullet \vec{n}_i}{A_i} = \frac{F_i \bullet \vec{n}_i}{A/N} = \frac{(F_i \bullet \vec{n}_i)N}{\mathrm{A}}$$

where P_i = Contact pressure at each node

F_i = global force, at each node

$\vec{n}_i$ = unit normal vector at each node

A_i = area of influence at each node

A = Total area in contact

N = Number of nodes in contact

We also define average contact pressure as: $P_{avg} = \frac{\sum F_i}{A}$

Chapter 5

Error Analysis

5.1 Patch Test:

In simple terms, the patch test is any test conducted in a scenario where the analytical solution is known. This is a very important step to assure convergence of the deformation solution with sufficient mesh refinement. For our patch test we chose a box representing the polyethylene, which was assumed to be a linear, isotropic material. This box is rigidly fixed to a base-plate representing the tibial component and is deformed on the other side by the application of force on another rigid plate that can move. This represents the femur for our scenario. Contact can cause non-linearity in the system because the number of elements in contact can change. Therefore, the dimensions of the plate representing the femoral component are chosen to be slightly bigger than the polyethylene component, in order to ensure that all surface nodes of the polyethylene remain in contact (Figure 5-1). Thus this set up represents a truly linear problem – linear in geometry, linear in contact and linear in material.

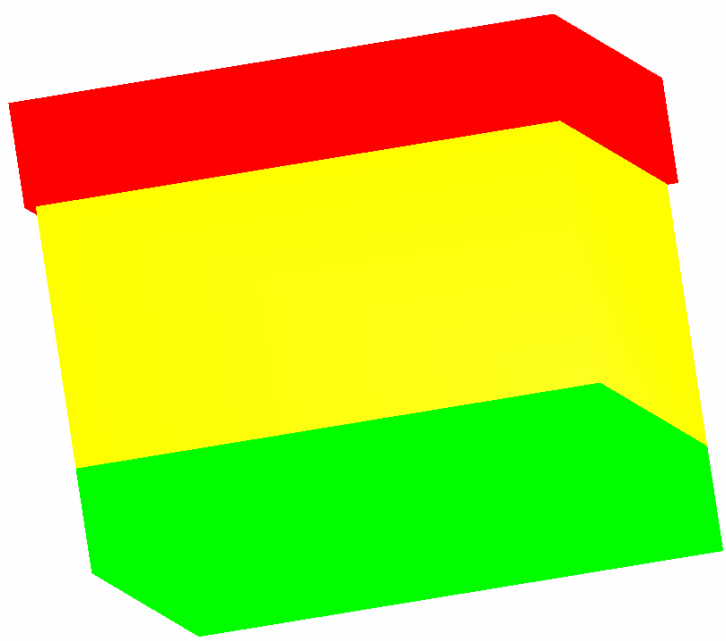

Figure 5-1: Set up used for the patch test.

The femur was assumed to be pressed down with a vertical load of 1000N. A linear elastic isotropic material model has two independent material constants which are also known as the Lame's constant. As stated before, for this current formulation of the discrete spring model only one material variable (which is assumed to be independent of the length of each spring) has been used. Under these conditions, the Poisson's ratio is a function of the structure of the network. Since, the maximum forces in knee occur in the superior-inferior direction with small forces in other directions (D'Lima 2007), we concentrated on how this spring network behaves under mesh refinement in the vertical direction (along the direction of the applied load) when compared against the actual analytical solution for polyethylene assuming it to be linear elastic with a Young's modulus of 561.5 MPa and a Young's modulus of 0.45 (Halloran 2005).

It has been previously documented that the presence of the diagonal springs produce an extra force that causes the elongation of the object to be shorter than expected and the spring model can behave stiffer (Maciel 2003). This effect is pronounced when the mesh size is course and thus represents a larger volume of the continuum and decreases with mesh refinement. Therefore, the result from the patch test is utilized to estimate the minimum mesh size that must be used so as to keep the error less than 2%. Therefore, for creating the nodes of the grid as described earlier, the number of nodes per dimension is selected so as to keep the sides of each mesh less than 1.5mm. Finer meshes can easily be selected at the expense of higher memory requirements due to the vectorization of the global stiffness assembly routine.

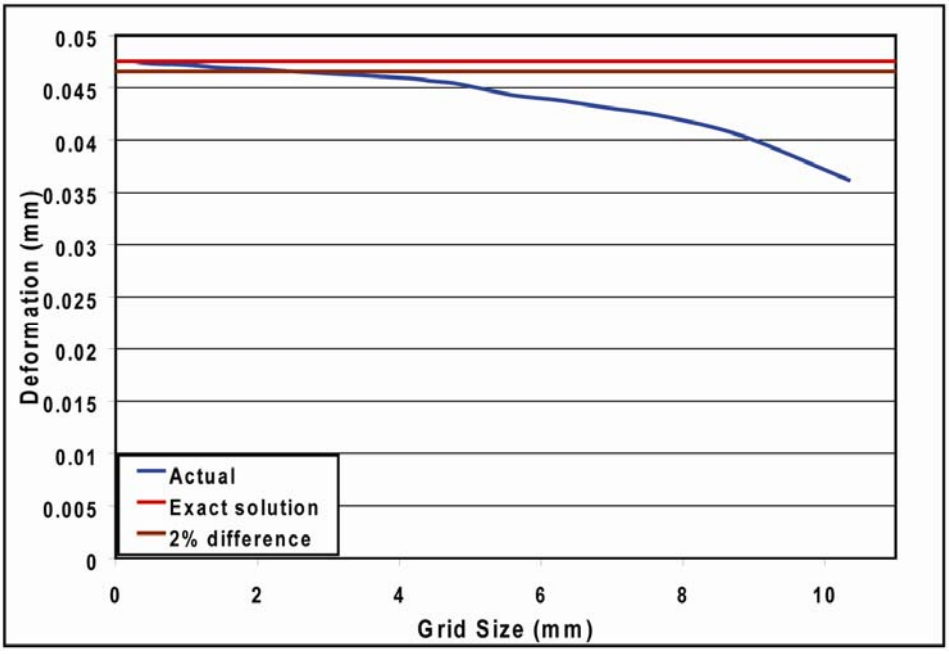

Figure 5-2: Effect of mesh refinement on deformation.

The variation of deformation with mesh size for a linear case exhibited by discrete spring models is a significant difference in its behavior when compared to finite elements. For this linear case tested above, the deformation predicted by finite elements, would be independent of mesh size. However, the actual stress and strain values in the solution accuracy of finite elements still increases with mesh refinement. Therefore to check the variation of contact pressure over the contact surface of the polyethylene the values obtained using the spring network model were compared with that obtained using finite elements implemented in Abaqus/Standard^{TM} (Dassault Systemes S.A.) where the polyethylene was modeled using C3D8 (8 noded brick) elements. For both the methods the number of nodes was matched and sufficient mesh refinement (1mm grid) was incorporated so that both the methods predict results with high accuracy.

Due to the effect of Poisson ratio in the material, the force distribution is not uniform at all the nodes. The contact pressure at the center nodes is higher than the contact pressure at the edge nodes. Both the methods exhibited similar results. While the maximum and minimum contact pressures predicted by finite elements were 9.11 MPa and 3.40 MPa respectively for the spring network model, the values were 8.64 MPa and 3.33 MPa respectively. Also, the variations of contact pressure along the contact area were similar in profile and symmetrical in distribution due to the regular geometries used.

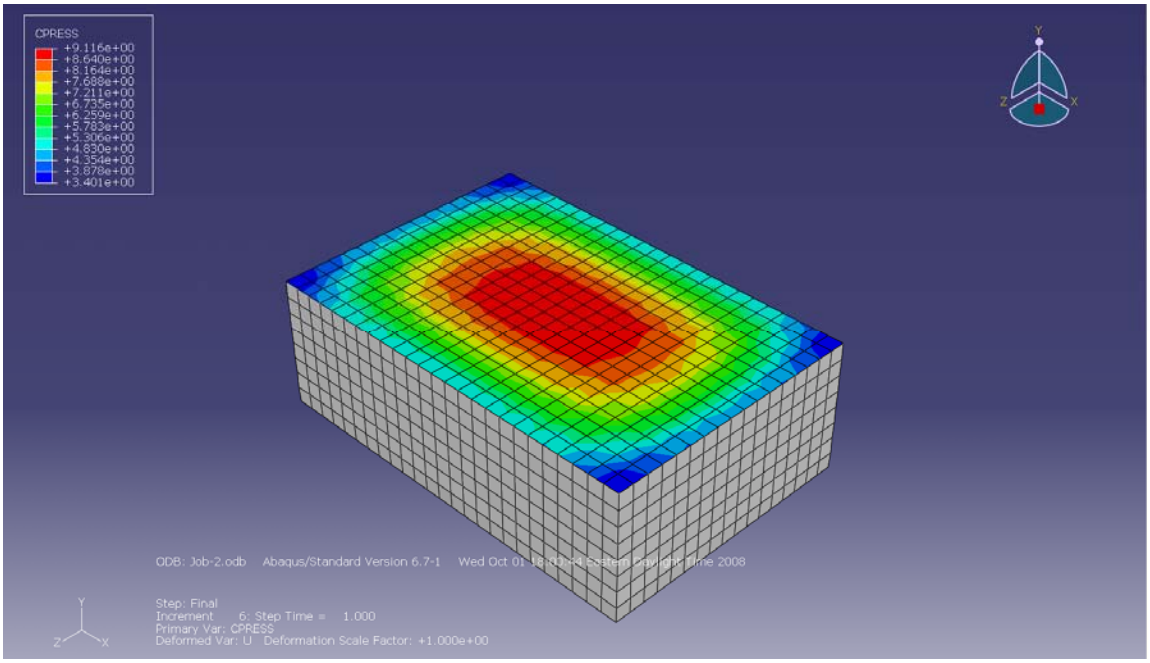

Figure 5-3: Pressure distributions obtained from finite elements.

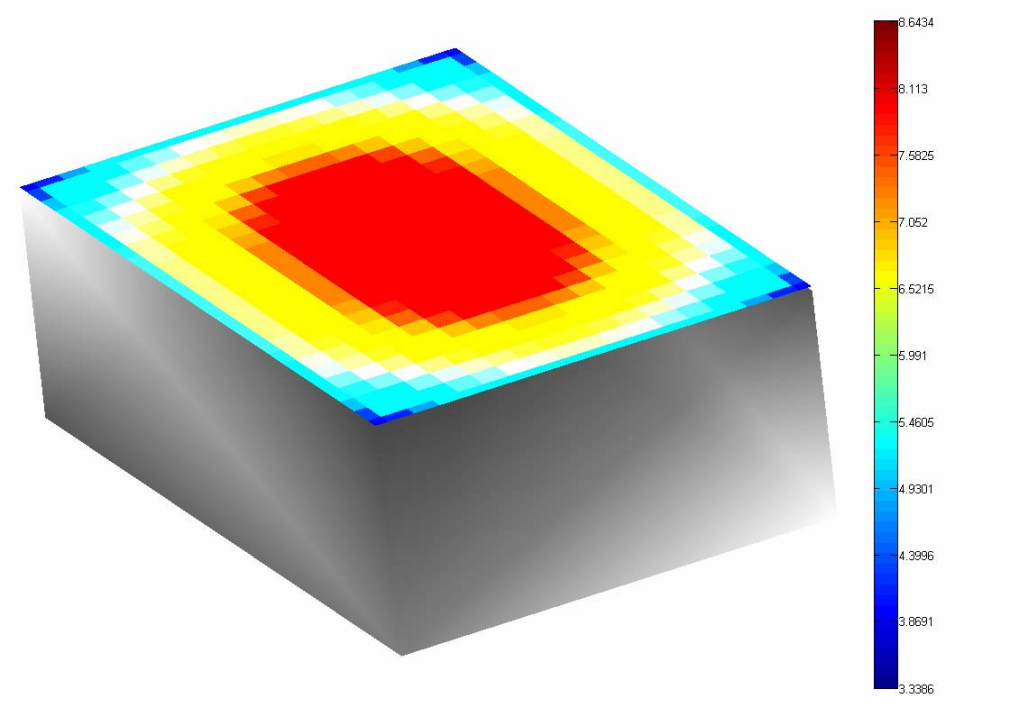

Figure 5-4: Pressure distribution obtained from the discrete spring network.

5.2 Performance of the Whole Method:

The method to calculate in vivo contact mechanics of total knee implant from kinematics obtained using fluoroscopy has two distinct components – estimation of the contact forces from rigid body modeling and then based on the contact forces, calculating the contact behavior at the femorotibial interface using the discrete element deformation model. For checking the performance of the method, an error analysis was conducted from data obtained with a telemetric implant. The comparisons of force were performed using the data from the telemetric implant (D'Lima 2005). However, the telemetric implant does not generate contact pressures and contact areas. Therefore, these values were compared with a static finite element analysis in Abaqus/Standard™ (Dassault Systemes S.A.).

Telemetric data was collected while the patient performed a deep knee bend activity from full extension to 120º of weight bearing flexion under fluoroscopic surveillance in the sagittal plane. Ground reaction force data obtained from a force plate was also simultaneously recorded. The telemetric knee is a fixed polyethylene type and a PCR type implant which measures the tibiofemoral contact forces with the help of 4 force transducers incorporated in the tibial component of the implant (D'Lima 2005). Sum of forces from all the sensors gives the total femorotibial force. For measurement of the

lateral and medial forces separately, the sensors are symmetrically placed with 2 each on the medial and the lateral side respectively (Figure 5-5).

For finite element modeling IGES CAD models of the components were used. The polyethylene was meshed at an approximate seed size (element size) of 1mm. The mesh contained a mixed linear hexahedral (C3D8) and linear tetrahedral (C3D4) element formulation and was obtained using Abaqus CAE^{TM} (Dassault Systemes S.A). The possible contact regions were meshed with hexahedral elements and the regions not in contact were meshed with tetrahedral elements to reduce time with the meshing process. The femoral component was assumed to be rigid and was modeled as a shell structure of quadratic elements (R3D4). Polyethylene was modeled using the Ramberg-Osgood equation which was found to closely match the stress strain data of polyethylene (Figure 5-6) as reported by Halloran et. al. (Halloran 2005).

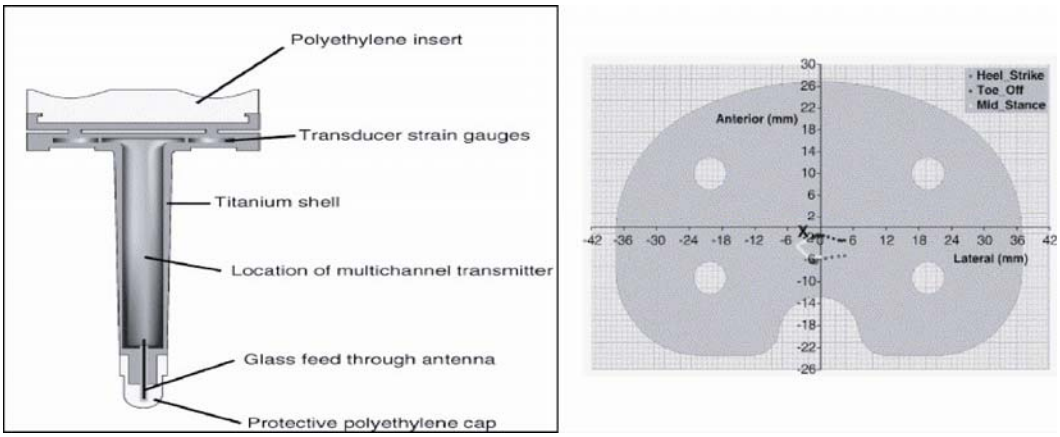

Figure 5-5: (Left) Polyethylene and tibial component of the telemetric implant. (Right) Location of the force transducers in the implant. (from D'Lima 2005).

In one dimension, the model is:

$$\varepsilon = \frac{\sigma}{E} + \alpha\left(\frac{|\sigma|}{\sigma^0}\right)^{n-1}\frac{\sigma}{E}$$

where ε = strain

σ = stress

σ^0 = yield stress

E = Young's modulus (initial slope of the stress strain curve)

α = yield offset

n = hardening exponent

Using a nonlinear curve fitting algorithm, the material parameters for the stress strain data of polyethylene using the above model was found to be

$E = 561.5, \alpha = 0.0389, \sigma^0 = 8.4194, n = 4.5485$.

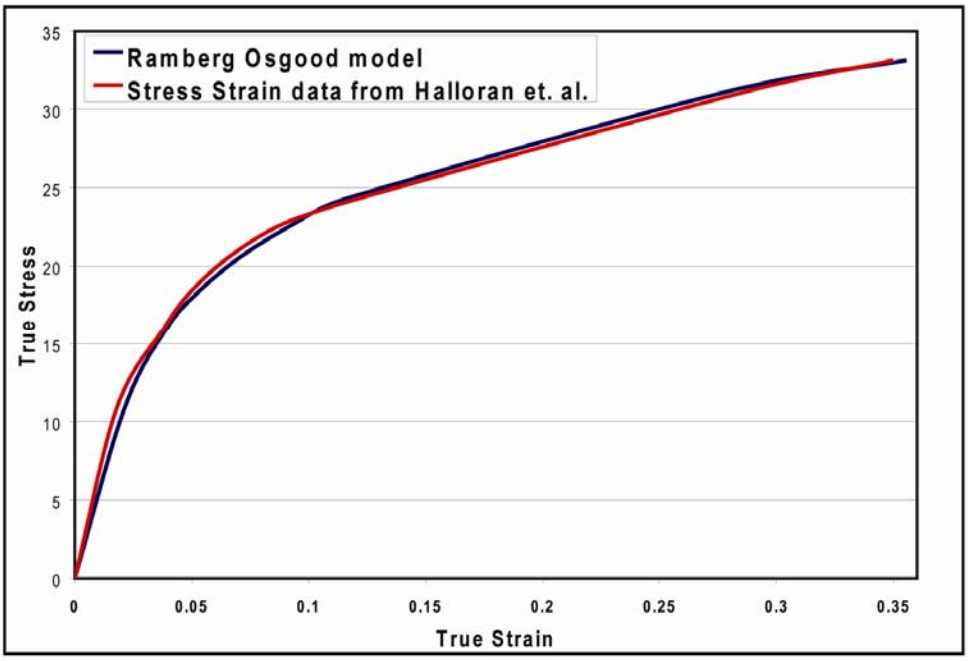

Figure 5-6: Comparison of the true stress strain data and the material model used for finite elements.

The lower surfaces of the polyethylene were considered to be completely fixed without any translation or rotation. The femoral component was fixed to prevent any rotation but was free to translate. The force was applied at a reference point on the femur. Separate surface to surface contacts were defined on the medial and the lateral condyles and a small sliding algorithm was selected for the analysis. The analysis was conducted at 15º flexion increments.

5.2.1 Comparison of Total Forces:

An overall comparison of the total force variations obtained from telemetry with respect to the total force predicted by the rigid model revealed three distinct regions (Figure 5-7). During high flexion and the maximum force region (Region A), the model was the most accurate and had a maximum difference of 0.15 BW compared with that obtained using telemetry. At this region, the telemetric implant measured a total femorotibial peak load of 3.84BW occurring at 103° of flexion, whereas the model predicted a peak load of 3.81BW at 100° of flexion. Between 10º and 60° of knee flexion (Region B), the model had a maximum difference of 0.3BW compared with the results obtained using telemetry. For the low-flexion, low-force region (Region C), the model had the highest amount of difference. In this region, the telemetric patient exhibited a surprisingly high force of approximately 1.5BW. We believe that this occurred because of the isometric contraction of the quadriceps at full extension. At full extension, the telemetric patient attempted to hyperextend his knee, leading to firing of the quadriceps muscle, which the model did not

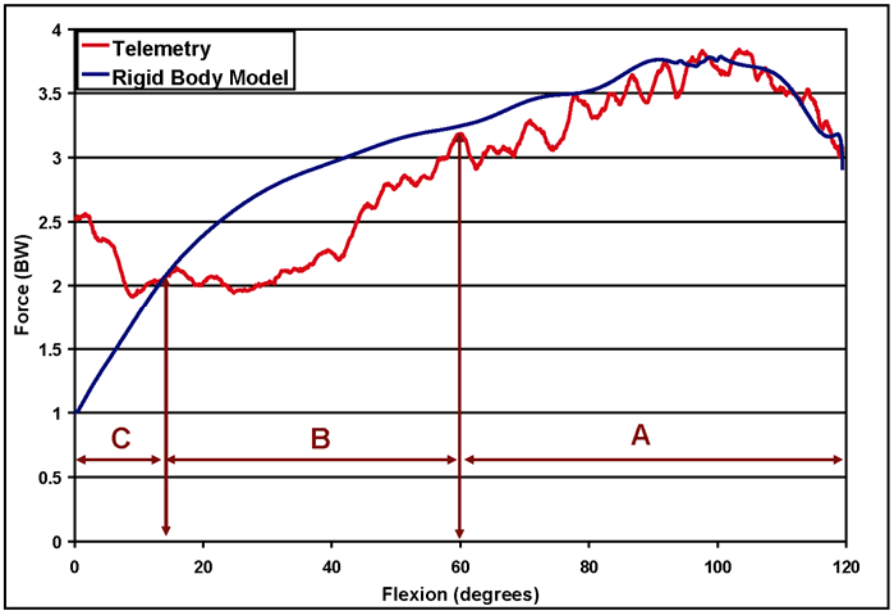

Figure 5-7: Comparison of the total forces.

take into account as it does not incorporate muscle activation dynamics. Also, the model started from a static initial condition and therefore, the initial force prediction is low.

5.2.2 Effect of Femoral Alignment Correction:

The model was found to be extremely insensitive (difference less than 0.001BW) in the prediction of the total forces acting on the femur when comparisons were made between the corrected femoral alignment as previously described to reduce over prediction of lift-off and the uncorrected femoral alignment directly obtained from fluoroscopy This is probably because the proposed correction is small with respect to the overall movement of the femoral component on the polyethylene through the flexion cycle. The deformation and the contact on the condyles were found to be significantly affected when the femoral

correction is applied before the start of the analysis when compared to the scenario when it was not performed. Even though there was no clear evidence of lift-off, if the uncorrected femoral orientation was used in the deformation analysis, both the deformation model predicted that the lateral condyle was not in contact at 15º and 30º of flexion. The problem was found to be that the maximum deformation in the medial aspect of the polyethylene was lesser than the difference between the probable contact point on the femur and the polyethylene on the lateral condyle. After using the proposed correction, this problem was not observed at any flexion increment.

5.2.3 Comparison of Medial-Lateral Condyle Force Distribution:

The medial and lateral contact force also exhibited similar variation through the flexion cycle as the total contact force. Thus they were the most accurate at the higher flexion ranges. However, at the beginning of the flexion cycle, the predicted forces were lesser than the magnitudes obtained from telemetry (Figures 5-8, 5-9). While the lateral-medial force distribution obtained using telemetry ranged between 0.78-1.23, the deformation model predicted a lateral medial force distribution from 0.87-1.15 (Figure 5-10).

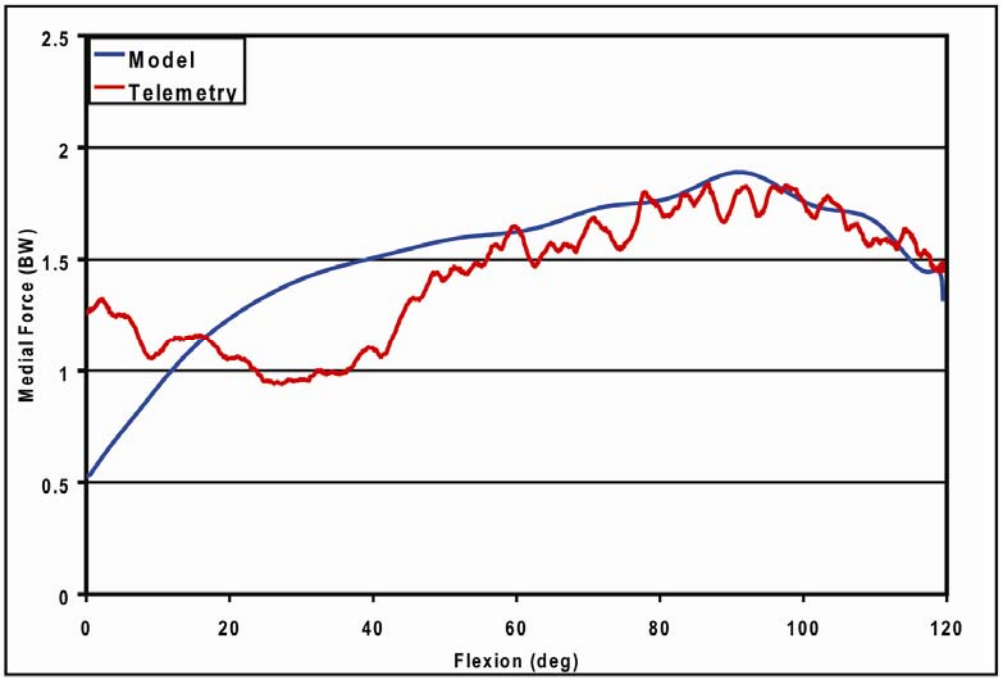

Figure 5-8: Comparison of the medial forces.

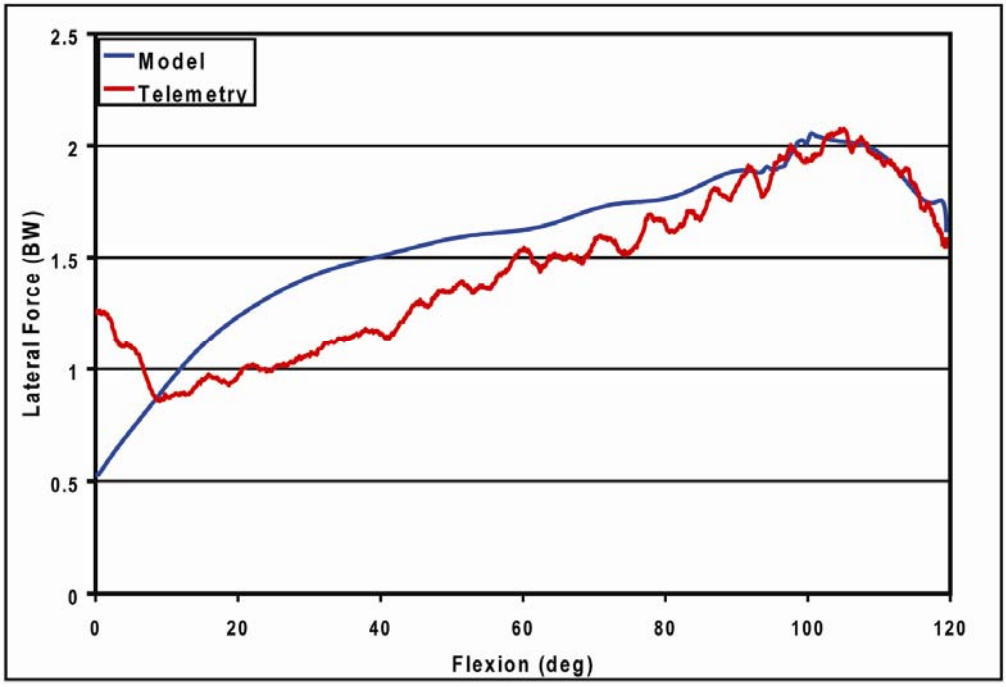

Figure 5-9: Comparison of the lateral forces.

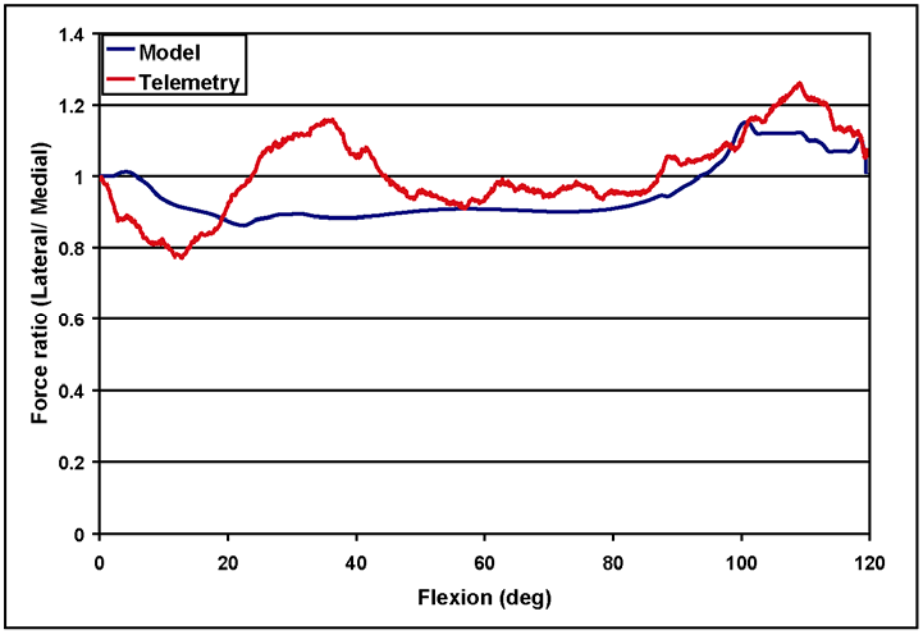

Figure 5-10: Comparison of lateral to medial force distribution ratio.

5.2.4 Comparison of Deformation:

Since the femoral component is assumed to be rigid, and moves into the polyethylene surface due to the force acting on it, so the maximum deformation in the polyethylene is analogous to the movement of the femur. The variation of the maximum deformation, with the increase in flexion angle in the polyethylene predicted by the spring lattice model, was very similar to that obtained using the finite element analysis. The maximum deformation in the lattice model for any flexion angle was slightly lesser than that of finite elements indicating that this model behaves a little stiffer when compared to finite elements. The maximum difference between the values predicted by finite element analysis and that obtained from the lattice model was less than 0.02mm (Figure 5-11).

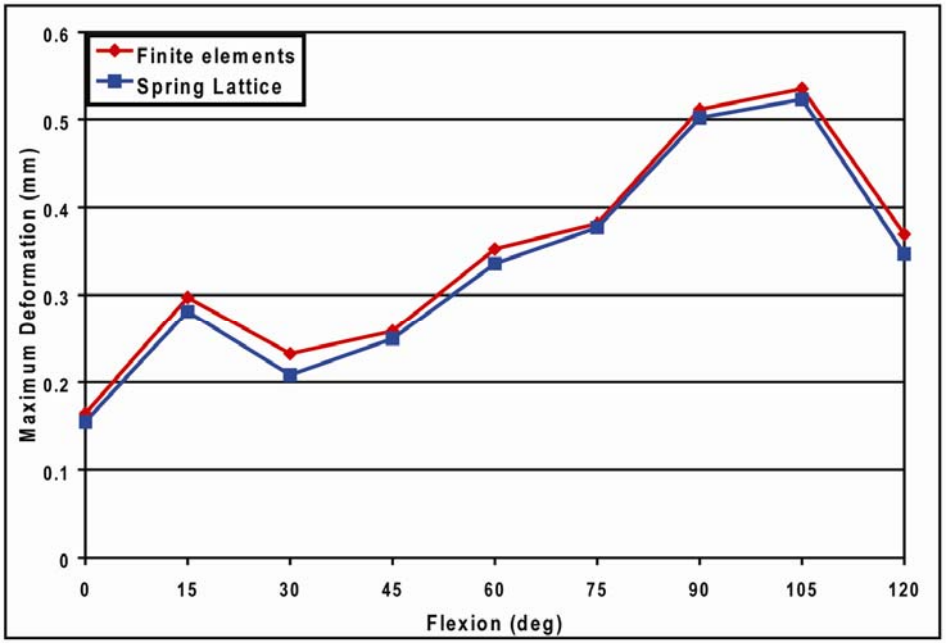

Figure 5-11: Comparison of maximum deformation.

5.2.5 Comparison of Contact Areas:

The variation of the medial and lateral contact areas with flexion as predicted by the spring lattice model with that of finite elements were similar (Figures 5-12, 5-13). However, in all cases the area calculated using the spring model were always lesser than that obtained using finite elements. This might be due to the small differences in the deformation between the two methods as observed previously and also different CAD models used in the process. The maximum difference in the contact areas for any condyle was less than $7mm^2$.

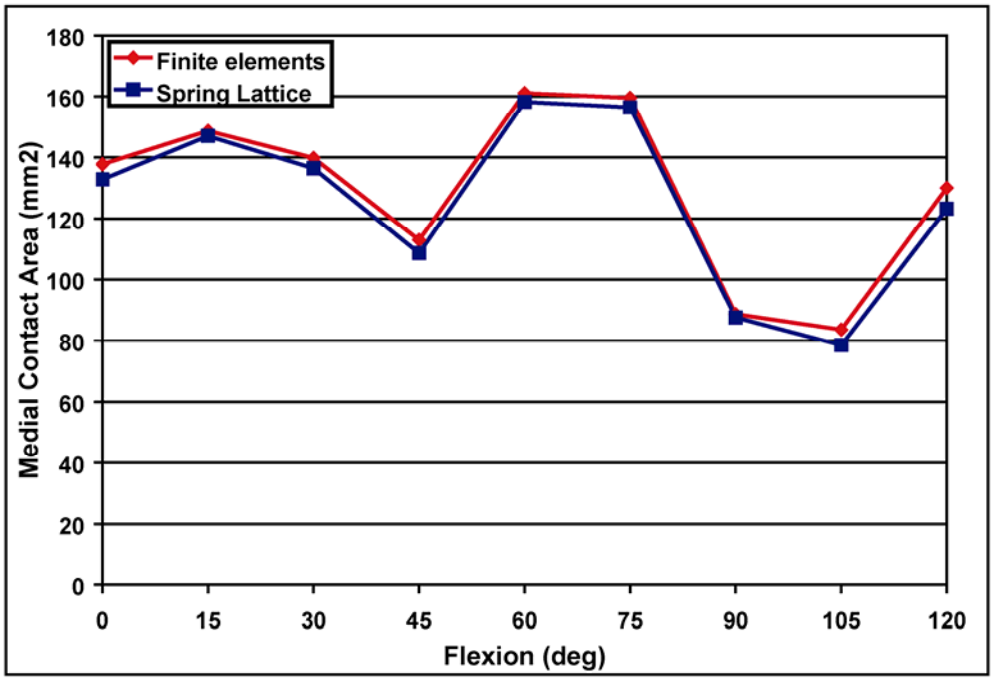

Figure 5-12: Comparison of medial contact area.

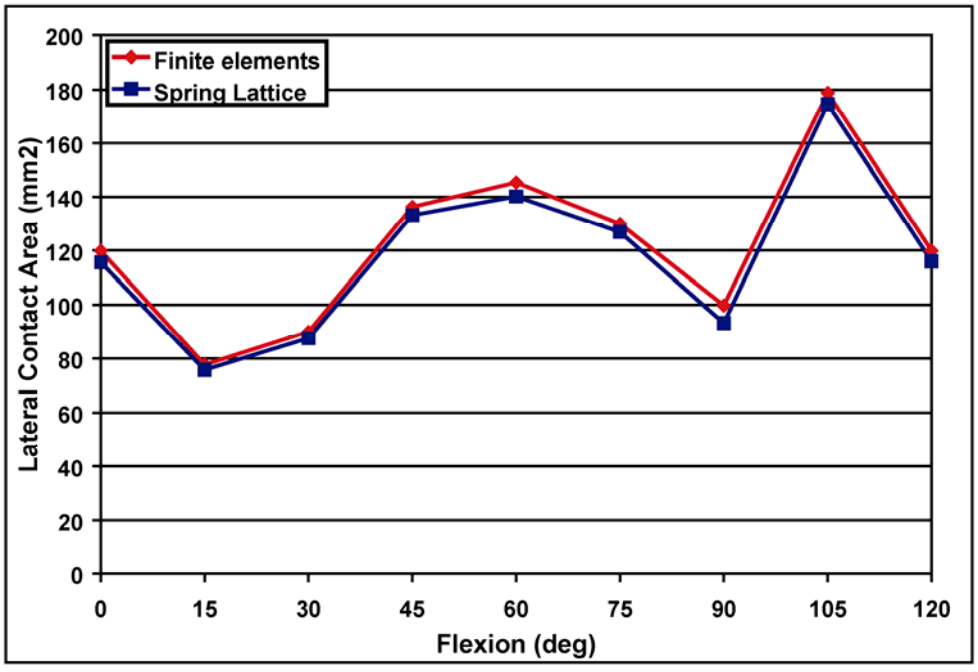

Figure 5-13: Comparison of lateral contact area.

5.2.6 Comparison of Force Distribution:

The femoral and the polyethylene components are characterized by quadratic surfaces at the condyles which come in contact. Under such circumstances, the contact is elliptical in nature where the maximum forces and pressures occur at the center of the contact followed by a decreasing value away from the center of the contact. Also, the variation of forces and pressures away from the center of the contact show an elliptical trend. The spring lattice model when compared to finite elements show a similar variation of the forces distribution indicating that the contact is elliptical in nature with maximum force occurring at the center of the contact (Figures 5-14, 5-15).

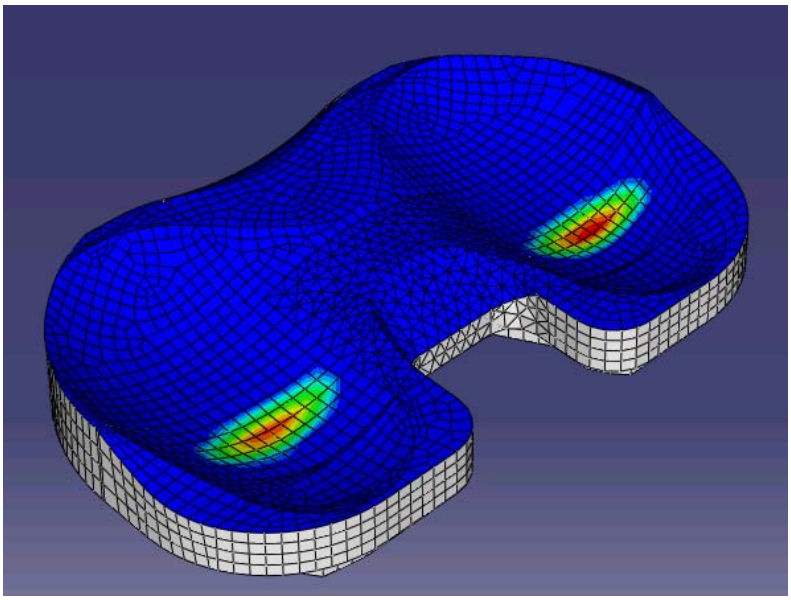

Figure 5-14: Pressure variation with finite elements across the contact region.

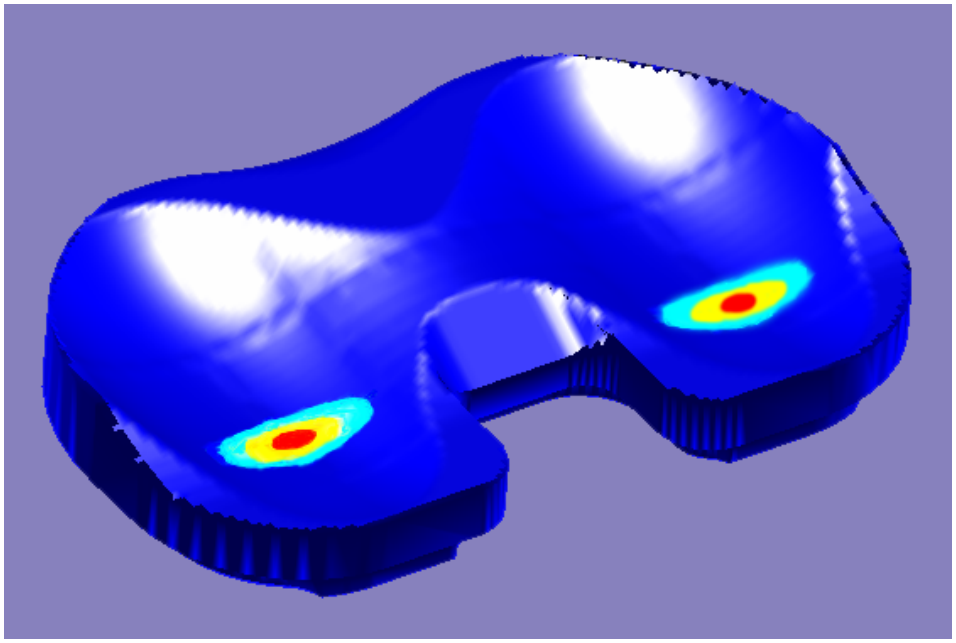

Figure 5-15: Pressure variation with spring lattice elements across the contact region.

Abaqus/ Standard does not output the force associated with each node. As stated before the spring lattice model, being discrete in nature, can only predict the force distributions. Therefore, the prediction of contact pressure from the lattice model is based on an assumed area of influence. When comparing the maximum contact pressures, the maximum difference between the lattice model and the results obtained using finite elements were found to be less than 15%. However, when comparing the average contact pressures defined as the ratio of the total forces divided by the area in contact, the difference was found to be less than 5%. This is because the average contact pressures are independent of the assumed area of influence.

5.2.7 Speed of computation:

Use of nonlinear material models require repeated calculations of the stiffness matrix and its inverse. The algorithms for the discrete spring element model are coded in Matlab (Matworks Inc.). Also, the time associated for the final solution is sensitive to the initial deformation used. As a result the solution time using the lattice model under the current formulation when using a 1.8 GHz Core 2Duo Processor was found to vary between 32 sec to 3.6 minutes. Nonetheless, this was found to be much faster than finite elements using Abaqus which took from 56 minutes to 1.8 hours.

Chapter 6

In Vivo Mechanics of Knee Implants

Knee implant designs undergo extensive clinical tests before being released in the market. However, in vivo performances of implants vary considerably than found in the normal knee. Nonetheless, there are various types of knee implants in the market with excellent long term results. Therefore the above method was used to study the in vivo performance in 6 popular designs so as to get a general idea about the magnitudes of the contact forces and the forces in the quadriceps mechanism during a deep knee activity.

The study was conducted on 6 different types of implants implanted on 29 subjects - 5 PFC Sigma fixed bearing traditional TKA (Sigma FB), 5 PFC Sigma mobile bearing traditional TKA (Sigma MB), 5 LPS Flex fixed bearing high flexion TKA (LPS-Flex), 5 Nexgen PCR fixed bearing high flexion TKA (CR-Flex), 5 Natural Knee II fixed bearing traditional TKA with congruent insert fixed (NKII CP), 4 Natural Knee II fixed bearing traditional TKA with ultra congruent insert (NKII UCP). While the first two implants are

manufactured by Depuy Orthopaedics Inc. (Warsaw, IN), the other implants are manufactured by Zimmer Inc. (Warsaw, IN). The subjects were matched so that the groups were similar to age, weight, body mass index, pre-operative range of motion and postoperative alignment. All implantations were judged clinically successful (Hospital for Special Surgery knee scores >90) with no ligamentous laxity or pain. None of the patients had any incidence of lift off. However, the patients were not matched based on their in vivo kinematics. Also, since the sample size is small therefore, the derived mechanics may be affected by individual patient outliers.

The Sigma FB and Sigma MB are PS type designs with symmetrical condyles and incorporate a femoral component with multiple radii (radius decreasing with increasing flexion) in the sagittal plane. Due to the ability of the polyethylene insert to rotate axially, the mobile bearing design incorporates a polyethylene design that is much more conforming and constrained in the coronal plane. The high flexion designs LPS-Flex and the CR-Flex incorporate modifications in the component geometry to account for high flexion. The sagittal radii of the femoral J curve for the CR-Flex when compared with its traditional counterpart are smaller starting at 90º flexion through deep flexion. The sagittal radii of the LPS-Flex are smaller than its traditional counterpart in flexion transitioning to the same contour at approximately 30º of flexion. In both designs, approximately 2 mm of additional bone is resected posteriorly to allow the condyle to sweep further in deep flexion to increase contact area. The CR-Flex has asymmetrical

condyles whereas the LPS-Flex has symmetric condyles. Also, in general the LPS-Flex has smaller sagittal radii from mid flexion through deep flexion compared with the CR-Flex. The Natural Knee II is a fixed bearing traditional design with asymmetrical condyles and offers variations in the polyethylene bearing design – the standard congruent (CP) and the ultra-congruent (UCP). Whether to use the congruent or ultra-congruent polyethylene design is an intra-operative decision taken by the surgeon as both designs use the same femoral and tibial components. The CP insert is the more conventional design and is used when the PCL is retained by the surgeon. However, if the surgeon for some reason decides to resect the PCL then he uses the ultra-congruent design. Since for the CP insert the PCL is present to provide rollback to the knee joint while for the UCP insert it is absent, so the designs of these polyethylene inserts are slightly different. The ultra-congruent design has a much steeper anterior slope and a much posterior inflexion point so as to constrain the anterior movement of the femoral component, thus ensuring a favorable condition for posterior movement.

6.1 Femorotibial Contact Mechanics:

Both the medial and lateral contact forces increased with the increase in knee flexion and the total contact force varies from, on average, about 0.8BW at the start of flexion to about 3.7BW at the end of flexion. In some patients, the total contact forces reached values as high has 4.2 BW. However, the total contact force was not equally distributed between the medial and lateral condyles. On average, the medio-lateral force distribution ranged from 60%-40% to 75%-25% throughout the flexion cycle across all the implants. Also for the symmetrical condylar designs, the medio-lateral forced distribution generally increased with flexion. However, for the asymmetrical condyle designs the variation of medio-lateral force distribution was much lesser and no distinct trend was observed. Also no significant difference was observed in the medial forces observed in the implants (Figure 6-1). However, the lateral forces were found to be more variable depending on the type of implant. In this regard, the implants with asymmetrical condyles experienced the highest amount of lateral forces (Figure 6-2). The lateral forces were found to have a high correlation with the amount of axial rotation. The asymmetrical condyle designed implants experienced consistent higher axial rotation of the femur with respect to the femur and that might be the cause for the higher lateral forces.

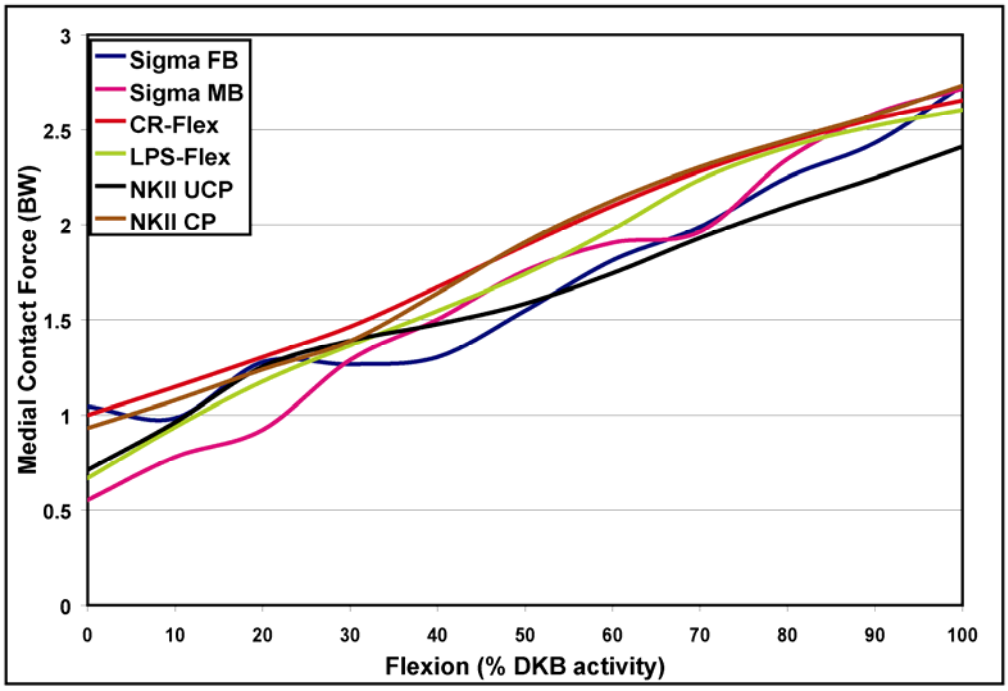

Figure 6-1: Total contact forces in the medial condyles.

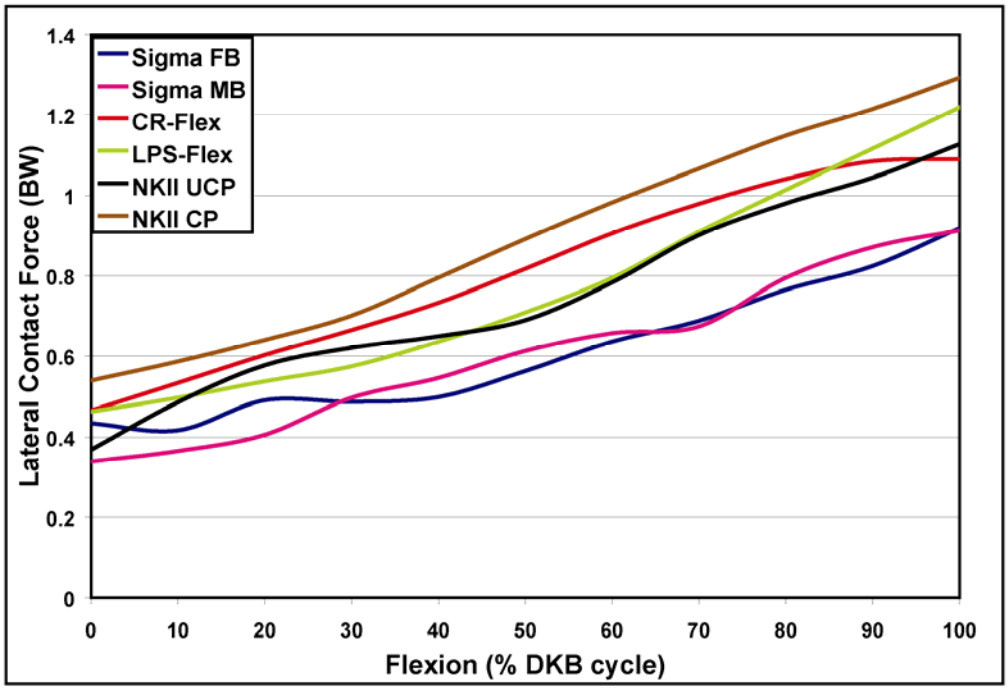

Figure 6-2: Total contact forces in the lateral condyles.

When the total force is resolved into the axial (superior-inferior), and shear (medio-lateral and antero-posterior) directions, the maximum force occurs in the superior-inferior direction and accounts for 98-99% of the total load. The maximum magnitude of the shear forces was found to be 0.51BW. In some of the patients the contact forces also decreased at high flexion angles.

There was no consistent variation between the medial and lateral condyle contact areas with flexion and high standard deviations were observed for each patient with the same implant and across the implants (Figures 6-3, 6-4). The contact areas are a function of deformation as well as the geometry and the orientation of the components. In this regard asymmetrical designs generally experienced higher contact areas on the lateral side than on the medial side as the radii in the medial condyle in these designs are generally smaller. Also interestingly, the contact areas in the PFC Sigma MB and FB decreased with increase in flexion. The PFC Sigmas have much larger femoral radii in the deeper flexion ranges and a higher amount of conformity than the other designs. This effect was much more noticeable on the lateral side due to the smaller magnitudes of contact forces, than on the medial side where the effect was somewhat negated by the increase of contact area due to increased deformation and higher medial contact forces. The LPS-Flex and CR-Flex designs as well as the NKII designs have smaller femoral radii at the higher flexion ranges and, the contact areas was found to increase in higher flexion regions.

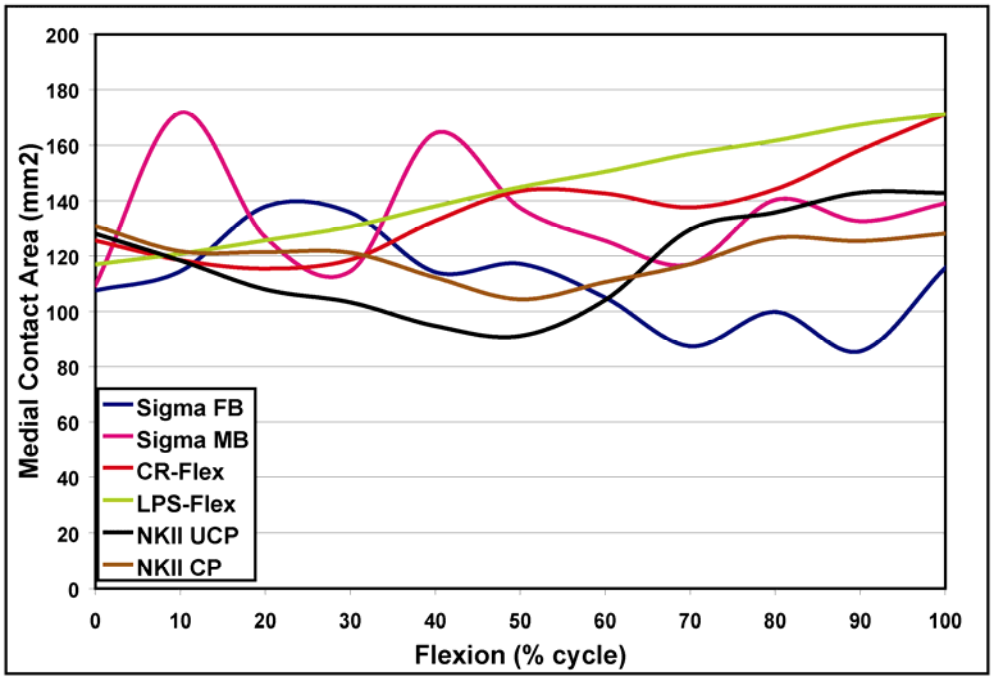

Figure 6-3: Contact areas in the medial condyles.

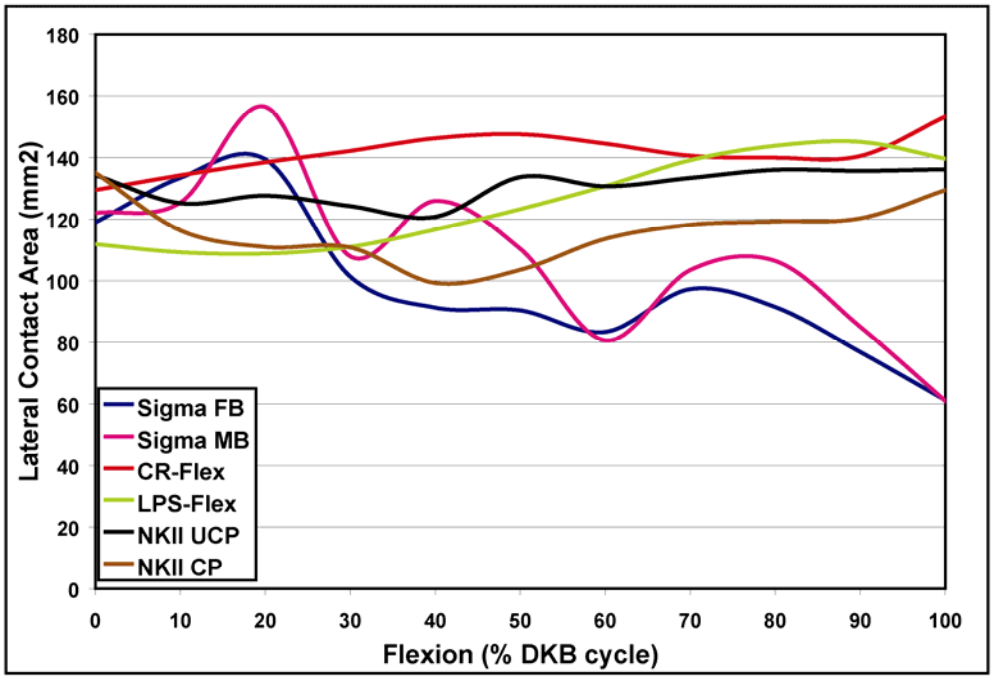

Figure 6-4: Contact areas in the lateral condyles.

Both the medial and the lateral contact pressures increased with increasing flexion and were higher on the medial condyle than on the lateral condyles due to the higher amount of forces on those condyles (Figures 6-5, 6-6). This correlates well with the retrieval studies which show that the wear on the medial side is more than the wear on the lateral side (Wasielewski 1994; Currier 2005). Due to the decrease in contact area observed in the Sigma implants at higher flexion, the average contact pressures increased the most in these implants with increasing flexion. Two patients implanted with Sigma fixed bearing implants, were found to have higher average contact pressure on the medial side than the yield strength of polyethylene (~ 21 MPa).

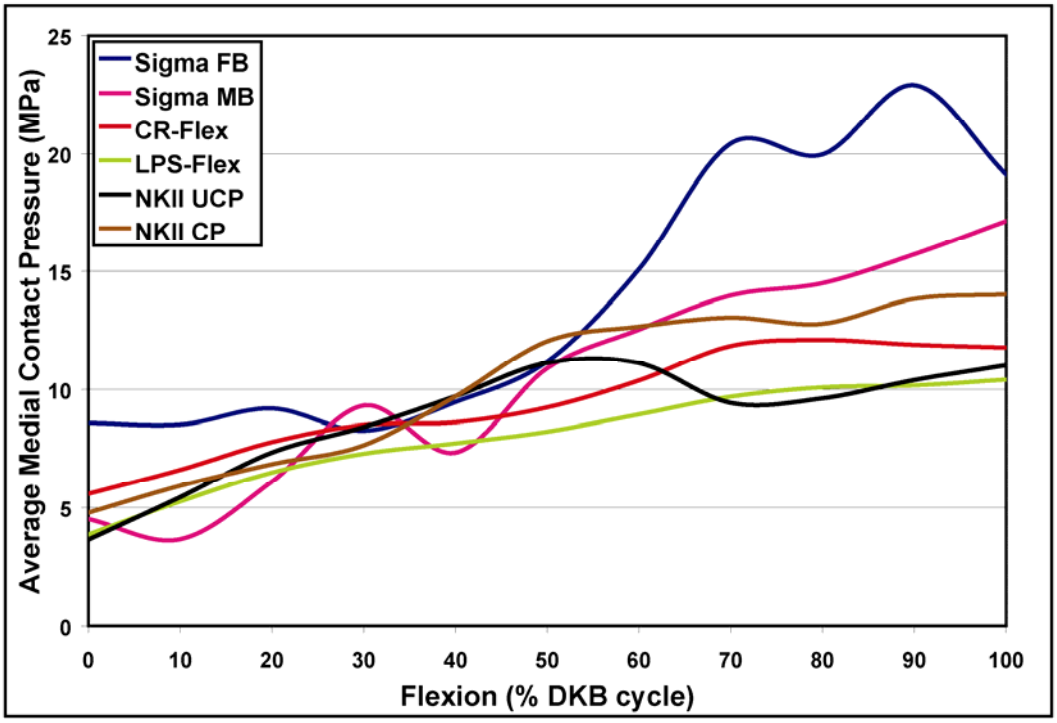

Figure 6-5: Average contact pressure in the medial condyle.

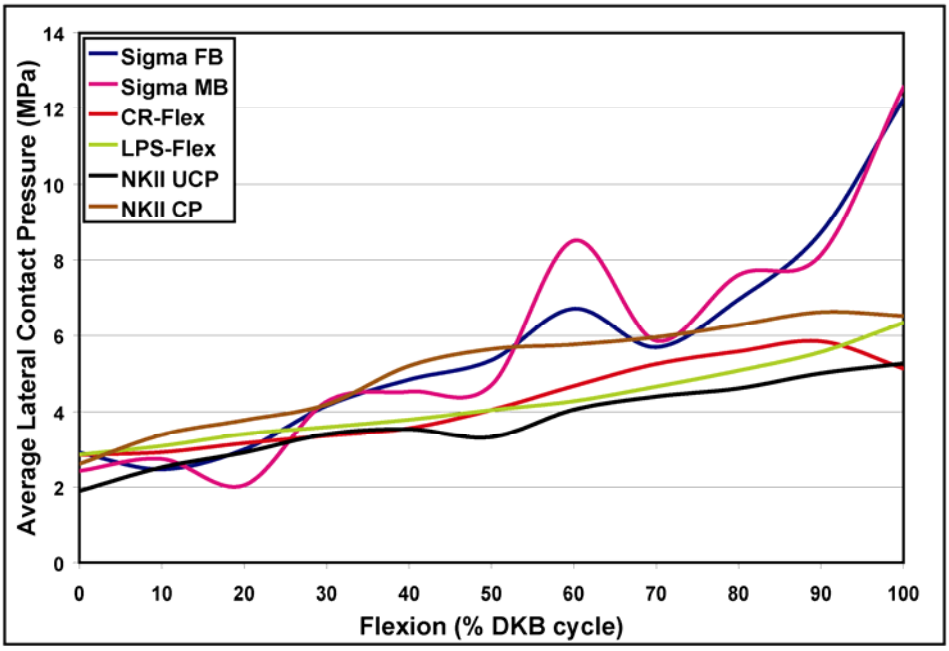

Figure 6-6: Average contact pressure in the lateral condyle.

6.2 Quadriceps Mechanism Forces:

The quadriceps muscle is the main force producer during a deep knee activity. For the asymmetrical condylar design, the quadriceps forces were similar throughout the flexion cycle. However, for the symmetrical condylar designs the quadriceps forces were generally low during low to mid flexion. However, at higher flexion the values were similar and ranging about 2.8BW to 3.3BW (Figure 6-7). The variation of the ratio between the patellofemoral force and the quadriceps force increased and varied from about 0.2 at full extension to about 1.0 at full flexion with increasing flexion (Figure 6-8). The force ratio between the patellar ligament and the quadriceps decreased from 1.0 at full extension to about 0.45 at full flexion (Figure 6-9).

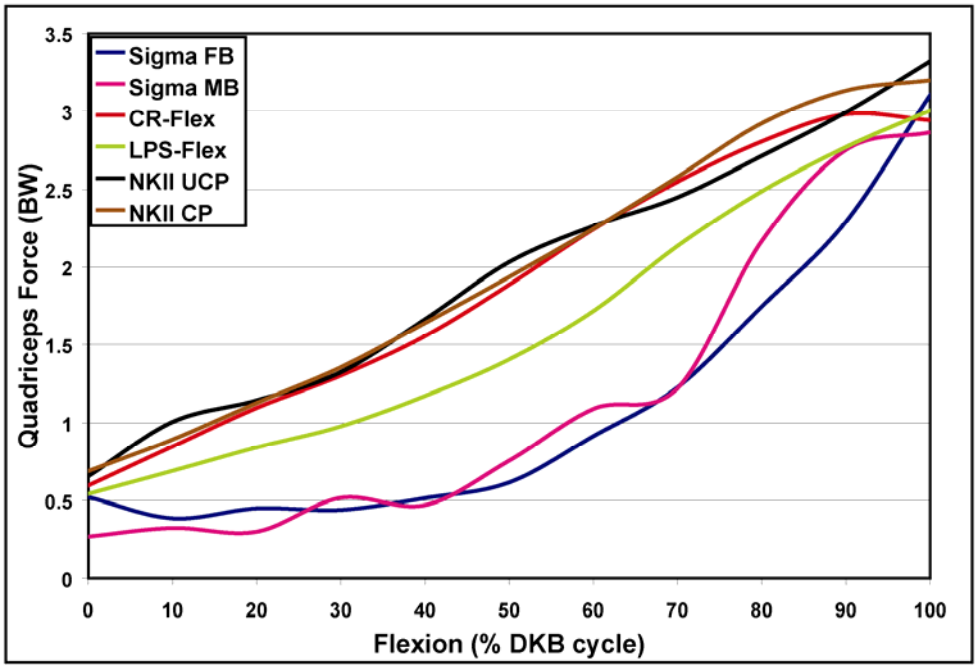

Figure 6-7: Magnitude of quadriceps forces.

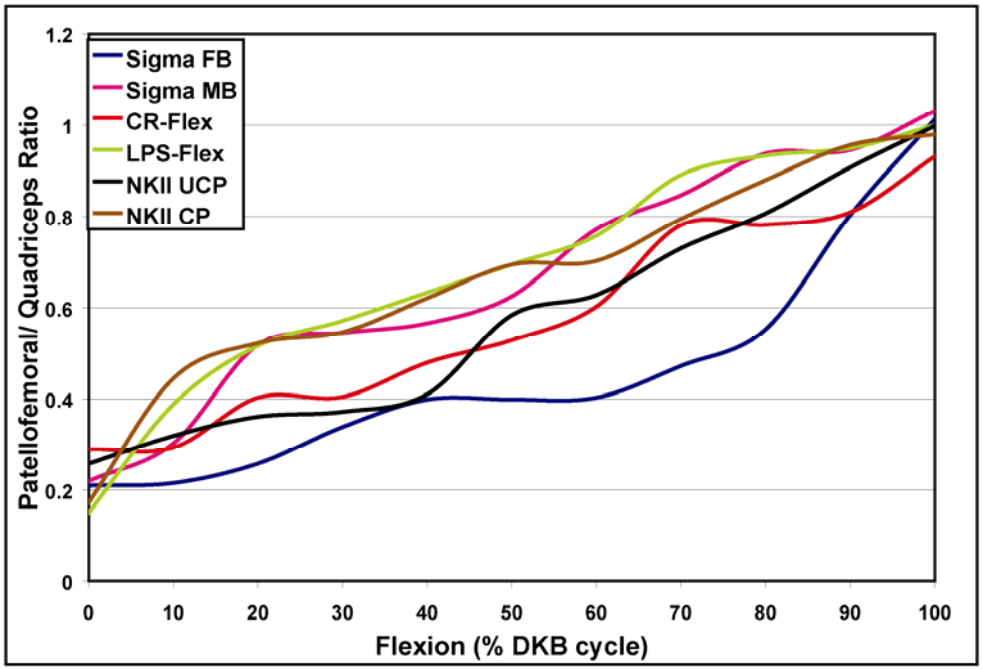

Figure 6-8: Variation of the patellofemoral to quadriceps force ratio.

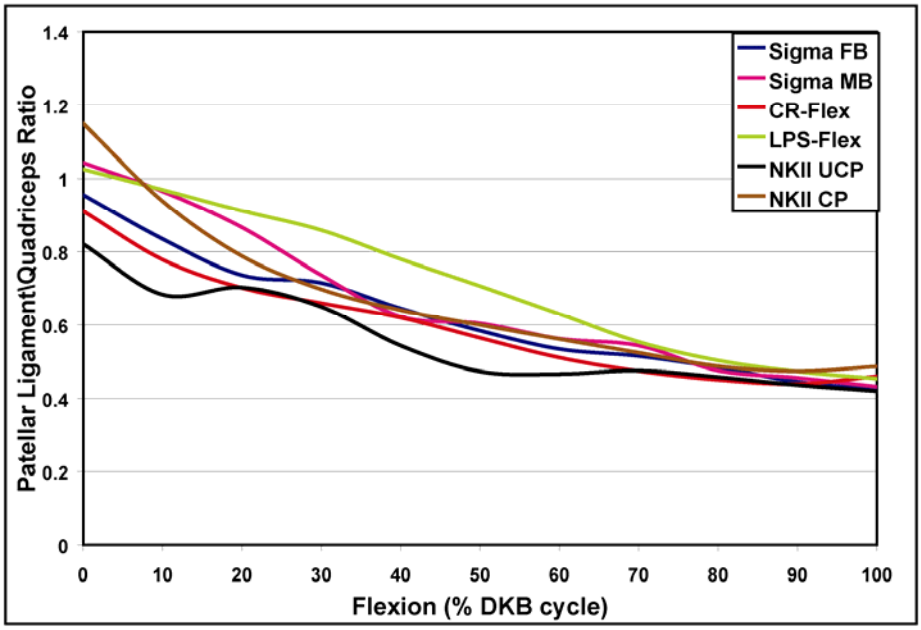

Figure 6-9: Variation of the patellar ligament to quadriceps force ratio.

No noticeable differences were observed across the various implants with respect to the variation of the patellofemoral and patellar ligament force ratios with the forces in the quadriceps.

Since, the mass of the patella is small, inertia effects due to the patella is also small as the accelerations in the patella are not very high. As a result the patella acts similar to a three force system, where the values of the patellofemoral force and the forces in the extensor mechanism is mainly governed by the angle between the patellar ligament and the quadriceps with respect to the patella longitudinal axis and was found to influence the force ratios. At full extension, these angles are low and the quadriceps muscle and the patellar ligament are almost along the same axis. Thus the forces in them are almost

equal, resulting in low patellofemoral force. In deeper flexion, the quadriceps muscle vector becomes more aligned to the patellofemoral force vector causing the patellofemoral force to increase. However, at increasing flexion angle, the angle between the quadriceps force and the patellar ligament force increases causing the force in the patellar ligament to decrease.

In some patients, the quadriceps force decreased with high flexion (Figure 6-10). As a result the patellar ligament forces, the patellofemoral forces and the contact forces in the knee also decreased. The decrease in the quadriceps force is observed due to the increase in the moment arm (Churchill 2001; Browne 2005).

The moment arm of the quadriceps depends upon the angle of the quadriceps with respect to the femur and location of the femorotibial contact point. Generally, with increase in flexion, the femorotibial contact point moves posterior, increasing the moment arm. However, this is associated with the decrease in angle of the quadriceps with respect to the femur tending to increase the moment arm. Due to wrapping of the quadriceps on the femur at higher flexion, the angle of the quadriceps with respect to the femur does not change. In this case, whether the contact force increases or decreases depends on whether the femoral condyles move anterior or posterior.

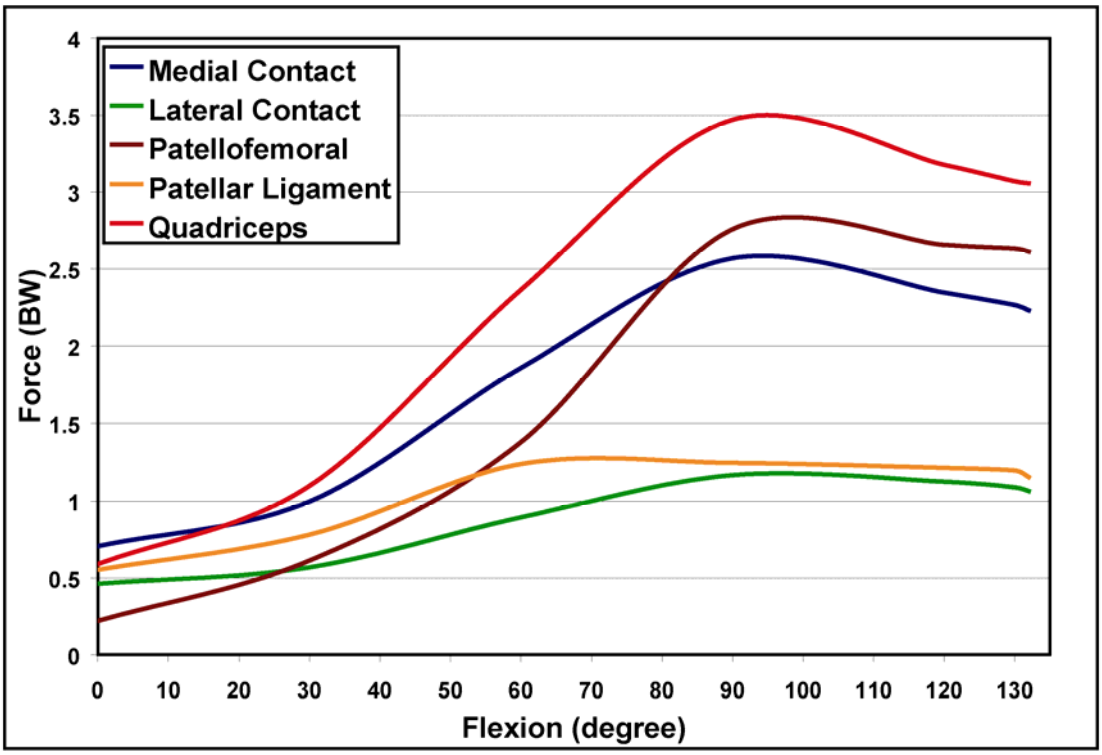

Figure 6-10: Sample patient where the force decreased at high flexion.

Chapter 7

Contributions and Future Work

In summary this dissertation is focused and streamlined towards the development of a methodology to predict the contact mechanics in knee implants from the kinematic data obtained using fluoroscopy during a deep knee activity. It not only works accurately but also presents far reaching implications from the perspective of a process that is fast and can be easily automated to work without any external preprocessing requirements. In this regard the uniqueness and contributions to the field of biomechanics are:

1. Development of a detailed methodology pertaining to the measurement of contact forces and contact stresses, using kinematics derived from fluoroscopy, taking into account errors involved in the process and possible means of correction.
2. Implementation of a multidynamic mathematical model for the deep knee activity that utilizes a new, more accurate and automated method for characterizing the slip and/or roll movement of the femoral component on the polyethylene insert and calculates the in vivo forces at the femoropolyethylene articulation.

3. Introduction and development of a detailed methodology pertaining to the use of hexahedral discrete lattice model for deformation modeling of polyethylene in knee implants as a tool that is not only accurate but fast and automatic without any separate preprocessing requirements. Therefore, it can be used as an efficient contact algorithm in multidynamic simulations.
4. Introduction and development of an algorithm to create a 3D cubic grid from triangulated surface defined models that is customized for knee implants but can easily be extended to other joints.
5. Verification of the computational model using a telemetric knee data and finite elements in order to determine the accuracy of this in vivo process to determine the in vivo mechanics.
6. Studying the contact behavior in some popular knee designs and determination of the in vivo mechanics of the quadriceps mechanism and understanding the influence of the quadriceps muscle in the in vivo mechanics of the knee joint during a deep knee bend activity.

Though the process has been validated, however, some limitations still remain which we intend to improve with future work:

1. The multidynamic rigid body used to estimate the total contact forces starts from a static condition and does not assume muscle activation dynamics. Muscle activations can substantially change the force carried experienced in it. We would

like to incorporate EMG data so as to be able to characterize muscle activations. Also, the model does neglects lift-off. Lift-off causes the contact forces to pass through only one condyle and would thus increase the contact pressures experienced at the condyles.

2. In the current formulation, polyethylene is modeled as non linear elastic and the springs are assumed to be independent of original length and thus there is just one variable tuning the behavior of the network. In the future, we would like to incorporate additional springs and dampers in series and parallel so as to be able to characterize more advanced properties like viscoelasticity and viscoplasticity. Also, we would like to work on using different spring stiffness along different directions so that 3D deformation in polyethylene as well as other materials can be more accurately predicted.
3. Currently, using this method only deep knee bend activity in TKAs has been studied. We would like to extend the algorithms so that diverse activities involving more joints can be studied.

REFERENCES

References – Websites

1. Ahlfeld Sports Medicine Orthopaedic Centre website." *Patient Education – Knee Joint Anatomy*". Visited on 10-09-2008.
   Link :- http://yoursportsdoc.com/pages-subsections/ht_k_anat.html

2. Queen's University Faculty of Applied Science website. "Dr. Kevin Deluzio's homepage". Visited on 10-09-2008.
   Link to QUEENS :- http://me.queensu.ca/people/deluzio/KneeOsteoarthritis.php

3. American Academy of Family Physicians website. "*Acute Knee Injuries: Use of decision rules for selective radiograph ordering*". Visited on 10-09-2008.
   Link :-http://www.aafp.org/afp/991201ap/2599.html

4. SEER's Training website. "*Planes of the Body*". Visited on 10-09-2008.
   Link :- http://training.seer.cancer.gov/module_anatomy/unit1_3_terminology2_planes.html

References – Publications

1. Abdel-Rahman EM, Hefzy MS, 1998: "*Three-Dimensional Dynamic Behaviour of the Human Knee Joint under Impact Loading*." Medical Engineering Physics 20, 276-290.
2. Ahmed AM, Burke DL, 1983: "*In Vitro Measurement of Static Pressure Distribution in Synovial Joints – Part I: Tibial Surface of the Knee*." Journal of Biomechanical Engineering 105: 216-225.
3. Alexander S, 1998: "*Amorphous solids: their structure, lattice dynamics and elasticity*." Physics Reports, 296, 65-236.
4. Alexander EJ, Andriacchi TP, 2001: "*Correcting for deformation in skin-based marker systems*." Journal of Biomechanics, 34(3), 355-361.
5. Amis AA, Bull AMJ, Gupte CM, Hijazi I, Race A, Robinson JR, 2003: "*Biomechanics of the PCL and related structures: posterolateral, posteromedial and meniscofemoral ligaments.*" Knee Surgery, Sports Traumatology, Arthroscopy 11, 271-281.
6. Anderson FC, Pandy M.G, 1999: "*A dynamic optimization solution for vertical jumping in three dimensions*." Computer Methods in Biomechanics and Biomedical Engineering 2, 201-231.

7. Anderson FC, Pandy MG, 2001: "*Dynamic Optimization of Human Walking*." Journal of Biomechanical Engineering 123, 381-190.

8. Andriacchi TP, Alexander EJ, 2000: "*Studies of Human Locomotion: Past Present and Future*." Journal of Biomechanics 33, 1217-1224.

9. Arnockzky SP, 1983: "*Anatomy of the anterior cruciate ligaments*." Clinical Orthopedics 172: 19-25.

10. Ateshian GA, Kwak SD, Soslowsky LJ, Mow VC, 1994: "*A Stereophotogrammetric Method for Determining In Situ Contact Areas in Diarthrodial Joints, a Comparison with Other Methods*." Journal of Biomechanics 27, 111-124.

11. Aubel A, Thalmann D, 2001: "*Interactive Modeling of Human Musculature.*" Computer Animation 2001, Seoul.

12. Banks SA, Hodge WA, 1996: "*Accurate Measurement of Three-Dimensional Knee Replacement Kinematics using Single Plane Fluoroscopy*." IEEE Transactions on Biomedical Engineering 43(6), 638-649.

13. Baraff D, Witkin A, 1998: "*Large Steps in Cloth Simulation*." Proceedings of ACM SIGGRAPH, ACM Press, pp. 43-54.

14. Bartel DL, Burstein AH, Toda MD, Edwards Dl, 1985: "*The Effect of Conformity and Plastic Thickness on Contact Stresses in Metal Backed Plastic Implants*." Journal of Biomechanical Engineering 107, 193-199.

15. Bartel DL, Bicknell VL, Ithaca, Wright TM, 1986: "*The Effect of Conformity, Thickness and Material on Stresses in Ultra-High Molecular Weight Components for Total Joint Replacement*." Journal of Bone and Joint Surgery (Am) 68-A (7), 1041-1051.

16. Bartel DL, Rawlinson JJ, Burstein AH, Ranawat CS, Flynn WF, 1995: "*Stresses in Polyethylene Components of Contemporary Total Knee Replacements*." Clinical Orthopaedics and Related Research 317, 76-82.

17. Bei Y, 2003: "*Dynamic simulation of knee joint contact during human movement*." PhD Dissertation, University of Florida.

18. Bendjaballah MZ, Shirazi-Adl A, Zukor DJ, 1997: "*Finite element analysis of human knee joint in varus-valgus*." Clinical Biomechanics 12, 139-148.

19. Benedetti MG, Cappozzo A, 1994: "*Anatomical landmark definition and identification in computer aided movement analysis in a rehabilitation context II.*" (Internal Report). Universita Degli Studi La Sapienza, pp 1-31.

20. Benoit DL, Ramsey DK, Lamontagne M, Xu L, Wretenberg P, Renstrom P, 2006: "*Effect of skin movement artifact on knee kinematics during gait and cutting motions measured in vivo*." Gait and Posture 24(2), 152-164.

21. Black JD, Matejczyk MB, Greenwald AS, 1981: "*Reversible Cartilage Staining Technique for Defining Articular Weight Bearing Surfaces*." Clin Orthop 159, 265-267.

22. Blankevoort L, Kuiper JH, Huiskes R, Grotenbeor, HJ, 1991: "*Articular contact in a three-dimensional model of the knee*." Journal of Biomechanics 24, 1019-1031.

23. Bolander JE, Sukumar N, 2005: "*Irregular lattice model for quasistatic crack propagation*." Physical Review B 71(094106), 1-12.

24. Bourguignon D, Cani MP, 2000: "*Controlling Anisotropy in Mass-Spring Systems*." Computer Animation and Simulation Interlaken ., 113-123,

25. Brand RA, Crowninshield RD, Wittock CE, Pedersen DR, Clark CR, Vankrieken FM, 1982: "*A Model of Lower Extremity Muscular Anatomy*." Journal of Biomechanics 104(4), 304-310.

26. Brown J, Montgomery K, 2001: "*A microsurgery simulation system*." In Proceedings of Medical Image Computing and Computer Assisted Intervention - MICCAI .

27. Brown J. et al., 2001: "*Real-Time Simulation of Deformable Objects: Tools and Applications.*" In Computer Animation, Seoul .

28. Browne C, Hermida JC, Bergula A, Colewell CW Jr., D'Lima DD, 2005: "*Patellofemoral forces after total knee arthroplasty: effect of extensor moment arm*." The Knee 12, 81-88.

29. Buechel FF, Pappas MJ, Makris G, 1991: "*Evaluation of Contact Stress in Metal Backed Patellar Replacements*." Clinical Orthopaedics and Related Research 273: 190-197.

30. Burda Z, 1998: "*Lattice models of random geometries*." Acta Physica Polonica B 29 (3), 573-617.

31. Burks RT, 1990; "*Gross anatomy*". In: Daniel DM, Akeson WH, O'Connor JJ (Eds.), "*Knee Ligaments: Structure, Function, Injury and Repair*." Raven Press, New York. pp 59-76.

32. Burny F, Donkerwolcke M, Moulart F, Bourgois R, Puers R, Van Schuylenberg K, Barbosa M, Paiva O, Rodes F, Beguert JB, Lawes P, 2000: "*Concept Design and Fabrication of Smart Orthopedic Implants*." Medical Engineering Physics 22, 469-479.

33. Cappozzo A, Catani F, Della CU, Leardini A, 1993: "*Calibrated Anatomical Systems Technique in 3-D Motion Analysis Assessment of Artifacts.*" Proceedings of the International Symposium on 3D Analysis of Human Movement. Poiters, France, Jul 1, 45-52.

34. Caruntu DI, Hefzy MS, 2004: "*3-D anatomically based dynamic modeling of the human knee to include tibio-femoral and patello-femoral joints*." ASME Journal of Biomechanical Engineering 126(1), 44-53.

35. Chao EYS, 1980: "*Justification of Triaxial Goniometry for the Measurement of Joint Rotation*." Journal of Biomechanics 13, 989-1006.

36. Churchill DL, Incavo SJ, Johnson CC, Beynnon RD, 2001: "*The influence of femoral rollback on patellofemoral contact loads in total knee arthroplasty*." Journal of Arthroplasty 16, 909-918.

37. Cohen ZA, Roglic H, Grelsamer RP, Henry JH, Levine WN, Mow VC, Ateshian GA, 2001: "*Patellofemoral stresses during open and closed kinetic chain exercises. An analysis using computer simulation*." American Journal of Sports Medicine 29, 480-487.

38. Cohen ZA, Henry J H, McCarthy D.M, Mow VC, Ateshian GA, 2003: "*Computer simulations of patellofemoral joint surgery. Patient-specific models for tuberosity transfer*." American Journal of Sports Medicine, 31, 87-98

39. Costa IF, Balaniuk R, 2001: "*LEM -An approach for real time physically based soft tissue simulation*." In Proceedings of IEEE International Conference on Robotics and Automation.

40. Cotin S, 1997: "*Mod`eles anatomiques d´eformables en temps r´eel (in French)*." PhD Dissertation, Universit´e de Nice, France.

41. Cotin S, Delingette H, Ayache N, 1999: "*Real-time elastic deformations of soft tissues for surgery simulation*." In IEEE Transactions on Visualizations and Computer Graphics.

42. Currier JH, Bill MA, Mayor MB, 2005: "*Analysis of Wear Asymmetry in a Series of 94 Retrieved Polyethylene Tibial Bearing*." Journal of Biomechanics 38, 367-375.

43. D'Lima DD, Chen PC, Colwell CW, 2001: "*Polyethylene Contact Stresses, Articular Congruity and Knee Alignment*." Clinical Orthopaedics and Related Research 393, 232-238.

44. D'Lima DD, Townsend CP, Arms SW, Morris BA, Colwell CW Jr., 2005: "*An Implantable Telemetry Device to Measure Intra-Articular Tibial Forces*." Journal of Biomechanics 38, 299-304.

45. D'Lima DD, Patil S, Steklov N, Chien S, Colewell CW Jr., 2007: "*In Vivo Knee Moments and Shear after Total Knee Arthroplasty*." Journal of Biomechanics 40, S11-S17.

46. Davoodi R, Loeb GE, 2001: "*Conversion of SIMM to SIMULINK for faster development of musculoskeletal models*." Proceedings of IFESS, Cleveland, Ohio, 282-284.

47. Davoodi R, Brown IE, Loeb GE, 2003: "*Advanced modeling environment for developing and testing FES control systems*." Medical Engineering and Physics 25, 3-9.

48. De S, Bathe KJ, 2001: "*The method of finite spheres: A summary of recent developments*." Proceedings of MIT Conference on Computational Fluid and Solid Mechanics.

49. Debunne G, Desbrun M, Barr A, Cani MP, 1999: "*Interactive multi resolution animation of deformable models*." Proceedings of EACG Conference on Eurographics.

50. Delp SL, Kocmond JH, Stern SH, 1995: "*Tradeoffs between motion and stability in posterior substituting knee arthroplasty design*." Journal of Biomechanics 28, 1155-1166.

51. Delp SL, Arnold AS, Piazza SJ, 1998: "*Graphics-based modeling and analysis of gait abnormalities*." Biomedical Materials and Engineering 8, 227-240.

52. DesJardins JD, Walker PS, Haider H, Perry J, 2000: "*The use of a Force-Controlled Dynamic Knee Simulator to Quantify the Mechanical Performance of Total Knee Replacement Designs during Functional Activity*." Journal of Biomechanics 33, 1231-1242.

53. Dimaio SP, Salcudean SE, 2002: "*Simulated interactive needle insertion*." Proceedings of International Symposium on Haptic Interfaces for Virtual Environment and Teleoperator System.

54. Elias JJ, Wilson DR, Adamson R, Cosgarea AJ, 2004: "*Evaluation of a computational model used to predict the patellofemoral contact pressure distribution*." Journal of Biomechanics 37(3), 295-302.

55. Fregly BJ, Bei Y, Sylvester ME, 2003: "*Experimental evaluation of a multibody dynamic model to predict contact pressures in knee replacements*." Journal of Biomechanics 36, 1659-1668.

56. Fregly BJ, Sawyer WG, Harman MK, Banks SA, 2005: "*Computational Wear Prediction of a Total Knee Replacement from In Vivo Kinematics*." Journal of Biomechanics 38, 305-314.

57. Giddings VL, Kurtz S.M, Eddin AA, 2001: "*Total knee replacement polyethylene stresses during loading in a knee simulator*." Journal of Tribology 123, 842-847.

58. Godest AC, deCloke S, et.al., 2000: "*A Computational Model for the Prediction of Total Knee Replacement Kinematics in the Sagittal Plane*." Journal of Biomechanics 33, 435-442.

59. Godest AC, Beaugonin M, Haug E, Taylor M, Gregson PJ, 2002: "*Simulation of a Knee Joint Replacement during Gait Cycle using Explicit Finite Element Analysis*." Journal of Biomechanics 35, 267-275.

60. Gonzalez AP, Esteve CF, Bru JLS, Marin FTS, Vergara M, Cervantes PJR, 2008: "*A modified elastic foundation contact mo0del for application in 3D models of the prosthetic knee*." Medical Engineering and Physics 30, 387-398.

61. Grachien F, Arnold R, Rohlmann A, Bergmann G, 2007: "I*mplantable 9-channel telemetry system for in vivo load measurements with orthopedic implants*." IEEE Trans Biomed Engg 54(2), 253-261.

62. Greenwald AS, O'Connor JJ, 1971: "*The Transmission of Load through the Hip Joint*." Journal of Biomechanics 4, 507-528.

63. Halloran JP, Petrella AJ, Rullkoetter PJ, 2005: "*Explicit Finite Element Modeling of Total Knee Replacement Mechanics*." Journal of Biomechanics 38, 323-331.

64. Harman M, DesJardins J, Banks S, Benson L, LaBerge M, Hodge W, 2001: "*Damage Patterns on Polyethylene Inserts After Retrieval and After Wear Simulation*." Proceedings 47th Orthopaedic Research Society, 1003.

65. Heimke G, Leyen S, Willmann G, 2002: "*Knee Arthroplasty: Recently Developed Ceramics Offer New Solution*." Biomaterials 23, 1539-1551.

66. Hertz H, 1881: "*Uebes die Beruehrung fester elastische Koerper (On the Contact of Elastic Solids)*." J. fues. Reine und angewandte Mathematik 92, 156-171.

67. Hoff WA, Komistek RD, Dennis DA, Gabriel SM, Walker SA, 1998: "*Three-Dimensional Determination of Femoral-Tibial Contact Positions under In Vivo Conditions using Fluoroscopy*." Clinical Biomechanics 13, 455-472.

68. Holden JP, Orsini JA, Siegel KL, Kepple TM, Gerber LH, Stanhope SJ, 1997: "*Surface Movement Errors in Shank Kinematics and Knee Kinetics during Gait*." Gait and Posture 3, 217-227.

69. Hood RW, Wright TM, Burstein AH, 1983: "*Retrieval Analysis of Total Knee Prostheses: A Method and its Application to 48 Total Condylar Prostheses*." Journal of Biomedical Materials Research 17, 829-842.

70. Howling GI, Barnett PI, Tipper JL, Stone MH, Fisher J, Ingham E, 2001: "*Quantitative Characterization of Polyethylene Debris Isolated from Periprosthetic Tissue in Early Failure Knee Implants and Early and Late Failure of Charnley Hip Implants*." Journal of Biomedical Materials Research 58, 415-420.

71. Hughston JC, Bowden JA, Andrews JR, Norwood LA, 1980: "*Acute tears of the posterior cruciate ligament.*" Journal of Bone and Joint Surgery 62A: 438-450.

72. James D, Pai D, 2001: "*A unified treatment of elastostatic contact simulation for real-time haptics*." Journal of Haptics-e.

73. Jin ZM, Dowson D, Fisher J, 1995: "*Contact pressure prediction in total knee joint replacements. Part I: general elasticity solution for elliptical layered contacts*." Journal of Engineering in Medicine, 1995, 209(H1), 1-8.

74. Karrholm J, 1989: "*Roentgen Stereophotogrammetry, Review of Orthopaedic applications*." Acta Orthopaedics Scandinavica 60(4), 491-503.

75. Kauffman KR, Kovacevic N, Irby SE, Colwell CW, 1996: "*Instrumented Implant for Measuring Tibiofemoral Forces*." Journal of Biomechanics 29, 667-671.

76. Kim J, De S, Srinivasan MA, 2002: "*Computationally efficient techniques for real time surgical simulation with force feedback*." Proceedings of International Symposium on Haptic Interfaces for Virtual Environment and Teleoperator System.

77. Komistek RD, Stiehl JB, Dennis DA, 1998: "*Mathematical Model of the Lower Extremity Joint Reaction Forces using Kane's Method of Dynamics*." Journal of Biomechanics 31, 185-189.

78. Komistek RD, Dennis DA, Mahfouz M., 2003: "*In vivo fluoroscopic analysis of the normal human knee*." Clinical Orthopaedics and Related Research 410, 69-81.

79. Komistek RD, Kane TR, Mahfouz MR, Ochoa JA, Dennis DA, 2005: "*Knee Mechanics: A Review of Past and Present Techniques to Determine In Vivo Loads*." Journal of Biomechanics 38, 215-228.

80. Kurosawa H, Fukubayashi T, Nakajima H, 1980: "*Load Bearing Mode of the Knee Joint: Physical Behavior of the Knee Joint with or without the Menisci*." Clinical Orthopaedics 149, 283-290.

81. Kwak SD, Blankevoort L, Ateshian GA, 2000: "*A mathematical formulation for 3D quasi-static multibody models of diarthrodial joints*." Computational Methods in Biomechanical and Biomedical Engineering 3, 41-64.

82. LaFortune MA, Cavanagh PR, Sommer HJ, Kalenak A, 1992: "*Three-Dimensional Kinematics of the Human Leg During Walking*." Journal of Biomechanics 25, 347-357.

83. Lee Y, Terzopoulos D, 1995: "*Realistic Modeling for Facial Animation*." Proceedings of SIGGRAPH 95, Computer Graphics Proceedings, Annual Conference Series, pp. 55-62, Los Angeles.

84. Lewis G, 1998: "*Contact Stress at Articular Surfaces in Total Joint Replacements. Part II: Analytical and Numerical Methods*." Journal of Biomedical Materials 8(2), 91-110.

85. Li S, Burnstein AH, 1994: "*Ultra-High Molecular Weight Polyethylene: The Material and its use in Total Joint Implants*." Journal of Bone and Joint Surgery 76-A, 1080-1090.

86. Li G, Sakamoto M, Chao EYS, 1997: "*A comparison of different methods in predicting static pressure distribution in articulating joints*." Journal of Biomechanics 30, 635-638.

87. Li G, Rudy TW, Sakane M, Kanamori A, Ma CB, Woo SLY, 1999:" *Importance of quadriceps and hamstring muscle loading on knee kinematics and in-situ forces in the ACL*." Journal of Biomechanics 32(4), 395-400.

88. Lu TW, Taylor SJG, O'Connor JJ, Walker PS, 1997: "*Influence of Muscle Activity on the Forces in the Femur: An In Vivo Study*." Journal of Biomechanics 30, 1101-1106.

89. Lucchetti L, Cappozzo A, Capello A, Della Croce U, 1998: "*Skin movement artifact assessment and compensation in the estimation of knee-joint kinematics*." Journal of Biomechanics 31, 977-984.

90. Machan S, 2004: "*Finite Element Analysis of Polyethylene Stresses in Total Knee Replacements*." PhD Dissertation, University of Sydney, Australia.

91. Maciel A, Boulic R, Thalmann D, 2003: "*Deformable tissue parameterized by properties of real biological tissue*." IS4TM, Juan-Ies-Pins, France. Lecture notes in computer science: surgery simulation and soft tissue modeling, Springer-Verlag.

92. Mahfouz MR, Hoff WA, Komistek, RD, Dennis DA: "*A robust method for registration of three-dimensional knee implant models to two-dimensional fluoroscopy images*." IEEE Transactions on Medical Imaging; 22(12), 2003.

93. Mendoza C, Laugier C, 2003: "*Simulating soft tissue cutting using finite element models*." In Proceedings of IEEE International Conference on Robotics and Automation.

94. Mikosz RP, Andriacchi TP, Andersson GB, 1988: "*Model Analysis of Factors Influencing the Prediction of Muscle Forces at the Knee*." Journal of Orthopaedic Research 6, 205-214.

95. Morris BA, D'Lima DD, Slamin J, Kovacevic N, Arms SW, Townshed CP, Colwell CW, 2001: "*e-knee: Evolution of the Electronic Knee Prosthesis*." Journal of Bone and Joint Surgery 83A (suppl 2 part 2), 62-66.

96. Murphy M, 1990: "*Geometry and the kinematics of the normal human knee*." PhD Dissertation. Department of Mechanical Engineering, MIT, Cambridge, MA, USA.

97. Nedel LP, Thalmann D, 1998: "*Real Time Muscle Deformations Using Mass-Spring Systems*." Computer Graphics International 1998, pp. 156-165, Hannover 1998.

98. Neptune RR, Wright IC, Bogert, AJ van den, 2000: "*A method for numerical simulation of single limb ground contact events: application to heel-toe running*." Computer Methods in Biomechanics and Biomedical Engineering 3, 321-334.

99. Nilsson KG, Karrholm J, Linder L, 1995: "*Femoral Component Migration in Total Knee Arthroplasty: Randomized Study Comparing Cemented and Uncemented Fixation of the Miller-Galante Design*." Journal of Orthopaedic Research 13(3), 347-356.

100. Norwood LA, Cross MJ, 1979: "Anterior cruciate ligament: functional anatomy of its bundles in rotary instabilities." American Journal of Sports Medicine 7(1): 23-26.

101. Nuño N, Ahmed AM, 2001: "*Sagittal profile of the femoral condyles and its application to femorotibial contact analysis*." Journal of Biomechanical Engineering 123, 18-26.

102. Ochoa JA, Sommerich RE, Zalenski EB, 1993: "*Application of an Innovative Experimental Method to Characterize Contact Mechanics of Total Joint Replacements*." Proceedings 39th Annual Orthopaedic Research Society, San Francisco, California.

103. Otto JK, Callaghan JJ, Brown TD, 2001: "*Mobility and contact mechanics of a rotating platform total knee replacement*." Clinical Orthopaedics and Related Research 392, 24-37.

104. Pandy MG, Sasaki K, Kim S, 1997: "*A Three-dimensional musculoskeletal model of the human knee joint. Part 1: Theoretical Construction*." Computer Methods in Biomechanics and Biomedical Engineering 1, 87-108.

105. Paul JP, 1965: "*Bio-engineering Studies of the Forces Transmitted by Joints. Engineering Analysis*." In: Kenedi, R.M. (ed.), Biomechanics and Related Bio-Engineering Topics. Pergamon Press, Oxford, 369-380.

106. Paul JP, 1976: "*Approaches to Design: Force Actions Transmitted by Joints in the Human Body*." Proceedings of the Royal Society of London 192, 163-172.

107. Périé D, Hobatho MC, 1998: "*In vivo determination of contact areas and pressure of the femorotibial joint using non-linear finite element analysis*." Clinical Biomechanics 13, 394-402.

108. Piazza SJ, Delp SL, 2001: "*Three-Dimensional Dynamic Simulation of Total Knee Replacement Motion during a Step-Up Task*." Journal of Biomechanical Engineering 123, 599-606.

109. Picinbono G, Delingette H, Ayache N, 2002: "*Nonlinear and anisotropic elastic soft tissue models for medical simulation*." Proceedings of IEEE International Conference on Robotics and Automation.

110. Rand JA, Trousdale RT, Ilstrup DM, Harmsen WS, 2003: "*Factors Affecting the Durability of Primary Total Knee Prosthesis*." Journal of Bone and Joint Surgery (Am) 85-A (2), 259-265.

111. Rawlinson JJ, Bartel DL, 2002: "*Flat medial-lateral conformity in total knee replacements does not minimize contact stress*." Journal of Biomechanics 35, 27-34.

112. Roberts AP, Garboczi EJ, 2002: "*Elastic properties of model random three-dimensional open cell solids*." Journal of the Mechanics and Physics of Solids 50, 33-55.

113. Sathasivam S, Walker PS, 1998: "*A Computer Model to Predict Subsurface Damage in Tibial inserts on Total knees*." Journal of Orthopaedic Research 16, 564-571.

114. Sathasivam S, Walker PS, 1999: "*The conflicting requirements of laxity and conformity in total knee replacements*." Journal of Biomechanics 32, 239-247.

115. Seireg A, Arvikar RJ, 1973: "*The Prediction of Muscular Load Sharing and Joint Forces in the Lower Extremities during Walking*." Journal of Biomechanics 6, 89-102.

116. Sharma A, Komistek RD, Ranawat CS, Dennis DA, Mahfouz MR, 2007: "*In-vivo contact pressures in total knee arthroplasty*." Journal of Arthroplasty 22(3), 404-416.

117. Sharma A, Komistek RD, Scuderi GR, Cates HE: "*High Flexion TKA Designs: What are their In Vivo Contact Mechanics? "* Clin Orthop Relat Res, 464: 117-126, 2007.

118. Sharma A, Leszko F, Komistek RD, Scuderi GR, Castes HE, Liu F: "*In Vivo Patellofemoral Forces in High Flexion Total Knee Arthroplasty*." Journal of Biomechanics 41(3): 642-648, 2008.

119. Shin CS, Chaudhari AM, Andriacchi TP, 2007: "*The influence of deceleration forces on ACL strain during single leg landing: A simulation study*." Journal of Biomechanics 40, 1145-1152.

120. Starzewski MO, 2002: " *Lattice models in micromechanics*." Appl. Mech. Rev. 55 (1), 35-59.

121. Stewart T, Jin ZM, Shaw D, Auger DD, Stone M, Fisher J, 1995: "*Experimental and Theoretical Study of the Contact Mechanics of Five Total Knee Joint Replacements*." Proceedings of the Institution of Mech Eng [H] 209, 255-231.

122. Sundaraj K, 2004: "*Real-time dynamic simulation and 3D interaction of biological tissue: Application to medical simulators*." PhD Dissertation. Institut National Polytechnique De Grenoble, France.

123. Tashman S, Anderst W, 2003: "*In-vivo measurement of dynamic joint motion using high speed biplane radiography and CTL: application to canine ACL deficiency*." Journal of Biomechanical Engineering 125, 238-245.

124. Taylor SJG, Walker PS, Perry JS, Cannon SR, Woledge R, 1998: "*The Forces in the Distal Femur and the Knee during Walking and other Activities Measured by Telemetry*." Journal of Arthroplasty 13, 428-437.

125. Taylor SJG, Walker PS, 2001: "*Forces and Moments Telemetered from Two Distal Femoral Replacements during Various Activities*." Journal of Biomechanics 34, 839-848.

126. Terzopoulos D, Waters K, 1990: "*Physically-Based Facial Modeling, Analysis, and Animation*." The Journal of Visualization and Computer Animation, 1, 73-80.

127. Tseng DC, Lin JY, 2000: "*A hybrid physical deformation modeling for laparoscopic surgery simulation*." In proceedings of IEEE International Conference of Engineering on Medicine and Biology Society.

128. Valstar ER, deJong FW, Vrooman HA, Rozing PM, Reiber JHC, 2001: "*Model Based Roentgen Stereophotogrammetry of Orthopaedic Implants*." Journal of Biomechanics 34, 715-722.

129. Walker PS, 1988: "*Bearing Surface Design in Total Knee Arthroplasty*." Engineering Medicine 17(4), 149-154.

130. Walker PS, Blunn GW, Broome DR, Perry J, Watkins A, Sathasivam S, Dewar M, Paul JP, 1997: "*A knee simulating machine for performance evaluation of total knee replacements*." Journal of Biomechanics 30, 83-89.

131. Walker PS, Sathasivam S, 1999: "*The Design of Guide Surfaces for Fixed Bearing and Mobile Bearing Knee Replacements*." Journal of Biomechanics 32(1), 27-34.

132. Wasielewski RC, Galante JO, et.al., 1994: "*Wear Patterns on Retrieved Polyethylene Tibial Inserts and Their Relationship to Technical Considerations during Total Knee Arthroplasty*." Clinical Orthopaedics and Related Research 299, 31-43.

133. Wasielewski RC, Parks N, Williams I, et.al, 1997: "*Tibial Insert Undersurface as a Contributing Source of Polyethylene Wear Debris*." Clinical Orthopaedics 345, 53-59.

134. Waters K, 1987: "*A muscle model for animating three dimensional facial expression*." Proceedings of ACM SIGGRAPH.

135. Williams IR, Mayor MB, Collier JP, 1998: "*The Impact of Sterilization Method on Wear in Knee Arthroplasty*." Clinical Orthopaedics and Related Research 356, 170-180.

136. Wimmer MA, Andriacchi TP, 1997: "*Tractive Forces during Rolling Motion of the Knee Implications for Wear in Total Knee Replacement*." Journal of Biomechanics 30, 131-137.

137. Wismans J, Veldpaus F, Janssen J, Huson A, Struben P, 1980: "*A three-dimensional mathematical model of the knee joint*." Journal of Biomechanics 13, 677-685.

138. Wroblewski BM, Siney PD, Fleming PA, 1999: "*Low Friction Arthroplasty of the Hip using Alumina Ceramic and Crosslinked Polyethylene – a Ten Year Follow Up Report*." Journal of Bone and Joint Surgery 81-B, 54-55.

139. Yao JQ, Seedhom BB, 1991: "*A New Technique for Measuring Contact Areas in Human Joint – the '3S technique*." Proceedings of the Institution of Mech. Engg. [H] 205: 69-72.

140. Zdero R, Fenton PV, Rudan J, Bryant JT, 2001: "*Fuji film and Ultrasound Measurement of Total Knee Arthroplasties Contact Areas*." Journal of Arthroplasty 16(3), 369-375.

APPENDIXES

Appendix A - Referencing Terminology

The following directions and planes are used in the medical field and also in the field to biomechanics to describe the locations on the human body:

- Superior or Cranial – direction towards the head or the upper part of the body (above).
- Inferior or Caudal – direction away from the head and towards the lower part of the body (below).
- Medial – direction towards the midline of the body (inner side).
- Lateral – direction away from the midline of the body (outer side).
- Anterior or Ventral – direction towards the front of the body (front).
- Posterior or Dorsal – direction towards the back of the body (back).
- Proximal –direction towards or nearest the trunk or the point of origin of a body part (closer).
- Distal – direction away or farthest from the trunk or the point of origin of a body part (farther).
- Superficial – direction towards the surface of the body (external).

- Profundum – direction away from the surface of the body (internal).
- Sagittal or Lateral – plane perpendicular to the ground in the antero-posterior direction dividing the body into right and left. A sagittal plane which divides the body into two equal halves is also known as the Medial Plane.
- Coronal or Frontal – plane perpendicular to the ground in the medio-lateral direction dividing the body into front and back.
- Transverse or Horizontal– plane parallel to the ground dividing the body into upper and lower.

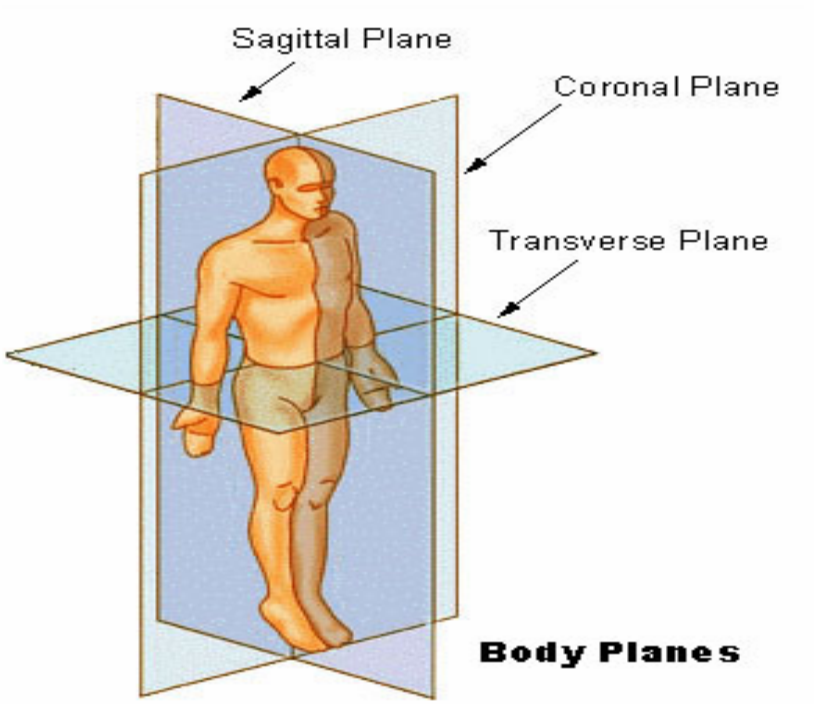

The Anatomical Planes defined in the Human Body (from SEER, 2008).

Appendix B – Anatomy of the Knee

Bone Structure

The knee joint is made up of three bones – the femur (thigh bone), the tibia (shin bone) and the patella (knee cap). There is one more bone in the lower leg, the fibula, but it does not form a part of the knee joint. However, it does serve as an attachment site for soft tissues associated with the knee.

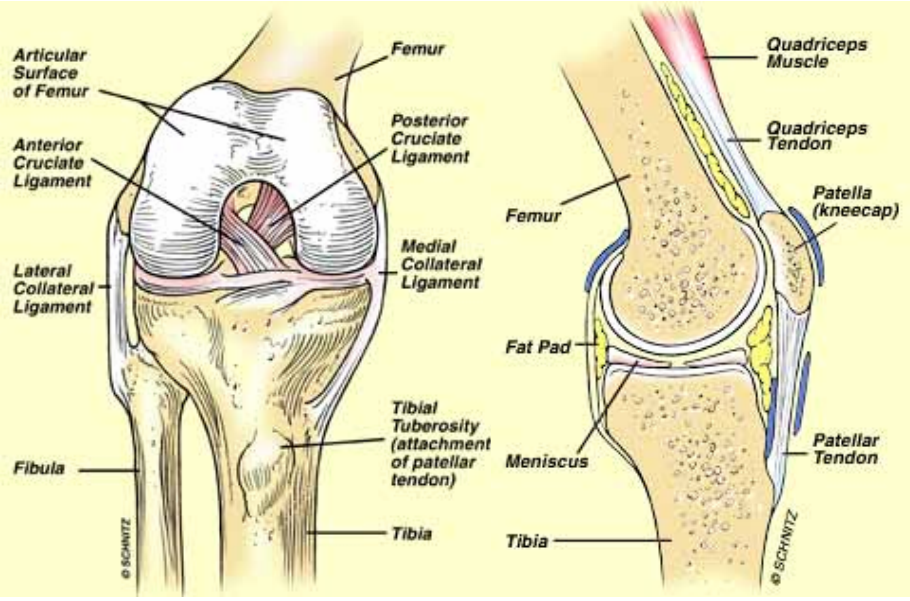

(Left) Anterior view (Right) Medial view of the Normal Knee (from Ahlfeld Sports Medicine Orthopaedic Centre, 2008).

The femur and the tibia are the two longest bones in the body and form the femoro-tibial articulation. The inferior end of the femur has two convex shaped condyles which are positioned medially and laterally and are separated by the intercondylar notch in the posterior direction and the trochlear groove in the anterior direction. The condyles have varying radii of curvatures when moving in the antero-posterior direction. Femoro-tibial articulation is achieved by the contact of the femoral condyles with shallow concave shaped condyles present in the tibia. The femoro-tibial articulation carries the maximum load passing through the knee joint. To accommodate this, the femur and tibia is made of hard cortical bone on the outside and soft and more compressible cancellous bone on the inside.

The patella is a sesamoid bone (formed completely within the structure of a tendon). The patello-femoral articulation is achieved by the contact of the patella on the medial and lateral condyles of the femur just adjacent to the trochlear groove, the place where the patella is located. The function of the patella is to increase the lever arm of the quadriceps extensor mechanism and to provide antero-posterior constraint for the femur.

Articular Cartilage and Meniscus

Cartilage is a collagen based soft viscoelastic material and is attached to the end of the knee joint bones where articulation occurs. This makes the mating surfaces almost frictionless and helps in smooth motion in the knee with less wear and tear. This is also

facilitated by the viscous, protein filled, synovial fluid which is filled up in the joint capsule and acts as the natural lubricant.

Between the articular cartilage coated ends of the femur and tibia are two crescent shaped pieces of fibrocartilage, called the meniscus. Due to their wedge-like shape, which deepens to cup-shape for the femur to articulate and move, they increase the contact area of the bones. Thus they serve to cushion the joint against impact type loads and distribute the compressive and shear loads across vulnerable articular cartilage surfaces. They also contribute in overall joint stability.

Ligamentous Structures

Ligaments are fibrous tissues, carrying only tensile loads, connected from bone to bone which help in stabilization of the joint. There are two main groups of ligaments that play a significant role in the control and stabilization of the knee joint – the collateral ligaments and the cruciate ligaments.

The collateral ligaments attach at the sides of the joint laterally and medially. The lateral collateral ligament is a round cord-like ligament that attaches on the outer side of the lateral femoral condyles and on the superior end of the fibula. The medial collateral ligament is a flat band like ligament attached to the outer side of the medial condyle of the femur and extends downwards to attach on the tibia on the antero-medial aspect. The

medial and lateral collateral ligaments assist in supporting the knee during abduction-adduction (valgus-varus) motion.

The cruciate ligaments are found at the centre of the knee within the joint space and are so named because the two ligaments in this group cross each other. The anterior cruciate ligament (ACL) inserts on the anterior end between the tibial condyles and on the medial side of the femoral lateral condyle. The posterior cruciate ligament (PCL) is attached more laterally on the tibia compared to the ACL and inserts on the medial side of the medial femoral condyle. The PCL is located posteriorly compared to the ACL. These ligaments are flat in cross-section and are twisted between their insertion points. These ligaments stabilize the knee against antero-posterior translations as well as the medial and lateral rotations of the tibia relative to the femur. The ACL restrains anterior subluxation while the PCL restrains posterior subluxation of the tibia.

Muscle Structures

Muscles are the motion generators in the human body and connect to the bone through the tendons. Force is generated in them during the extension of the fibers. The major muscle groups in the upper leg are the quadriceps and the hamstrings. In the lower leg the largest muscle group is the gastrocnemius. All these muscles are biarticulate, that is, they work on more than one joint. However, the level of activity for one joint is much more than the other joint.

The quadriceps, technically known as, the quadriceps femoris muscle group is made up of four muscles located anteriorly in the upper leg - rectus femoris, vastus laterlis, vastus medialis and vastus intermedius. Except for the rectus femoris, which inserts in the ilium (one of the bones making the pelvis), all the muscles insert on the femur. All the four muscles coalesce to form the quadriceps tendon. The quadriceps tendon, containing the patella bone, attaches the quadriceps muscle group to the anterior tibial bone and is known as the patellar tendon in the region between the patella and the tibia. The quadriceps muscles are the primary extensors of the knee.

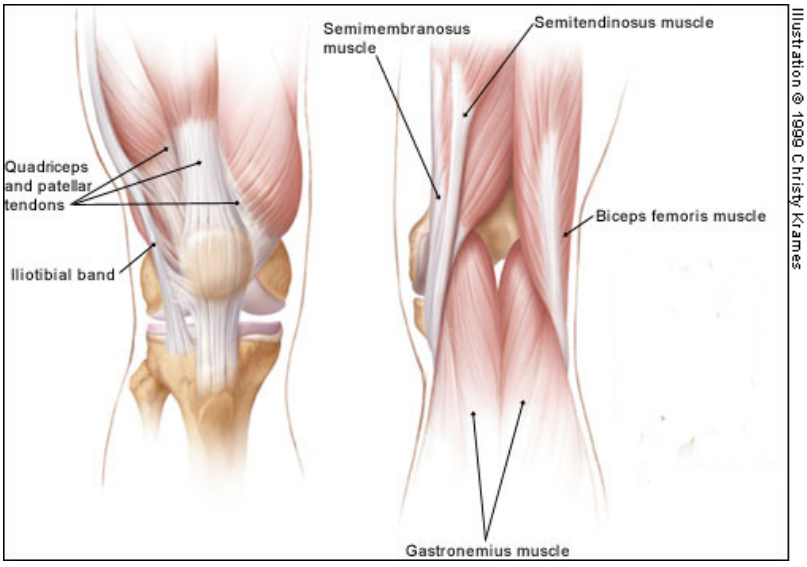

Major Muscles used in the Flexion and Extension of the Knee (Modified from American Academy of Family Physicians, 2008).

The hamstring muscle group is situated posteriorly on the upper leg and is made up of three separate muscles – biceps femoris (lateral side), semitendinosus and semimembranosus (medial side). Other medial thigh muscles, the gracilis, the pectinius and the adductor longus/ brevis/ magnus are not technically part of the hamstring group. All the hamstring muscles have one of their insertion points on the ischium (one of the bones making the pelvis) while the other insertion points lie on the fibula and femur (for biceps femoris) and on the tibia (for semitendinosus and semimembranosus). The hamstring muscles are the primary flexors of the leg.

The gastrocnemius muscle group, commonly known as the calf muscles, is located posteriorly in the lower leg and is made of three muscles - soleus, medial gastrocnemius and lateral gastrocnemius. While the soleus inserts in the fibula and the tibia, the medial and lateral gastrocnemius muscles insert on the posterior aspect of the femoral condyles. All the three muscles coalesce to from the Achilles tendon, which is attached to the back of the heel. Though these muscles primarily function in extending the heel, they also assist in the flexion of the leg.

Osteoarthritis in the Knee

Osteoarthritis is a degenerative joint disease caused due to the break down of the articular cartilage. Over a period of time, as the articular cartilage is worn away, bone to bone contact sets in. This leads to excessive joint pain and causes roughening and even wearing away of the bone articulation. Bony protrusions, known as osteophytes may also appear at the edge of the bone. This results in significant pain, inflammation and a loss of function and mobility. Though ideally osteoarthritis should develop during old age, however, early onset of the disease is accelerated by injuries, trauma and bone deformities. Treatments such as weight loss, braces, orthotics, steroid injections and physical therapy can alleviate the symptoms associated with mild to medium level of osteoarthritis. However, in severe cases the only choice remains is to undergo a knee replacement surgery. Knee replacement surgery consists of replacing the degenerated contact surfaces at the knee. If the arthritis affects only one side of the joint then it is replaced with a unicondylar knee replacement which resurfaces only the single damaged femoral and tibial condyle. If the arthritis affects the whole joint then a total knee arthroplasty (TKA) is used. Apart from restructuring both the femoral and tibial condyles, this type of replacement also has a component that fits with the patella.

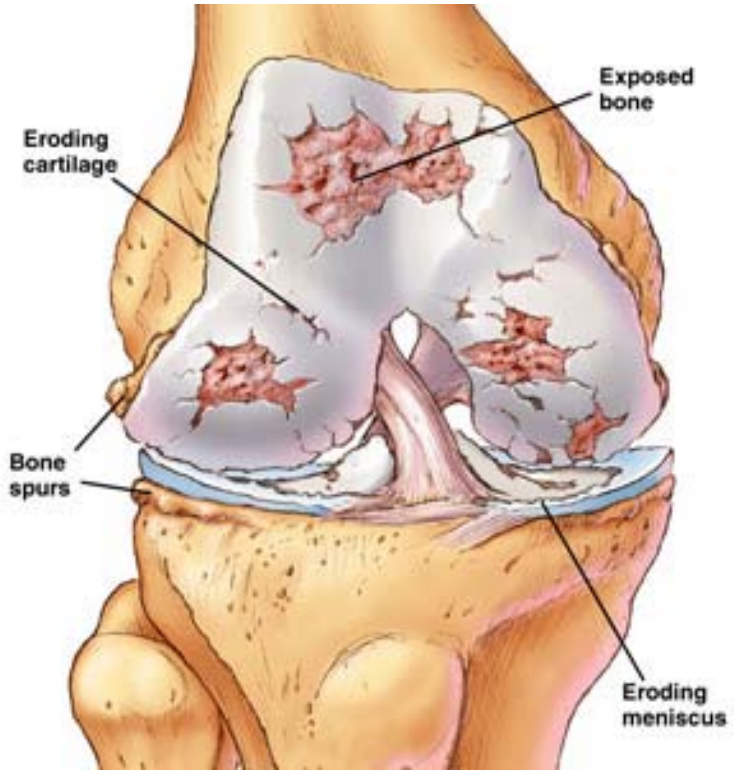

Deterioration in the Knee caused by Osteoarthritis (from Queen's University, 2008).

Appendix C – Kane's Dynamics

Kane's method combines the advantages of both Newton-Euler methods and the Lagrangian method (Huston, 1990). By using generalized forces, this method avoids the incorporation of non-contributing interactive and constraint forces between the bodies. Also this method avoids the use of energy functions. Finally, in this method differentiation needed to compute velocities and accelerations are obtained through the use of vector products.

The governing equation for Kane's method is that the sum of the generalized active forces and the generalized reactive forces should be zero. The key component while conducting an analysis with the Kane's method lies in development and the use of "partial velocities" and "partial angular velocities".

Calculating the partial velocities:

Generalized coordinates, q_r – These are defined as time varying translations and rotations selected to define the position of all points and the orientation of rigid bodies.

$$q_r \qquad (r = 1, ..., n)$$

Where 'n' is the number of degrees of freedom.

Generalized speeds, $\boldsymbol{u_r}$ – These are defined as time varying linear functions of $\dot{q}_r$'s (derivative with respect to time) selected so as to simplify expressions for velocities of points and angular velocities of rigid bodies.

$$u_r = \sum_{s=1}^{n} Y_{rs}\,\dot{q}_s + Z_r \qquad (r = 1, ..., n)$$

Where 'Y_{rs}' and 'Z_r' are functions of '$q_1, ..., q_n$' and time 't'.

Partial angular velocities, $\boldsymbol{\omega_r}$, **and partial velocities**, $\boldsymbol{v_r}$ – These are time varying linear functions of u_r's, determined by inspection, which greatly facilitate the formulation of the equations of motion.

$$\omega = \sum_{r=1}^{n} \omega_r u_r + \omega_t$$

$$v = \sum_{r=1}^{n} v_r u_r + v_t$$

Where 'ω' is the angular velocity of the rigid body, 'v' is the velocity of a point, and, 'ω_r','v_r','ω_t' and 'v_t' are the functions of '$q_1,.....,q_n$' and 't'. In principle, partial angular velocities need only be formed for those rigid bodies subjected to applied torques and possessing inertia, while partial velocities need only be forces for those points subjected to applied forces or possessing mass.

Using the partial velocities:

Generalized active forces, F_r – These are the quantities formed by taking the dot products of partial velocities and active (i.e. applied) forces and dot products of partial angular velocities and active torques. For each point 'P_i' subjected to an applied force,

$$(F_r)_{P_i} = v_r^{P_i} \cdot R_{P_i} \qquad (r = 1,.....,n)$$

Where '$v_r^{P_i}$' is the r^{th} partial velocity of 'P_i' and 'R_{P_i}' is the resultant of all contact and distance forces acting on 'P_i'. Similarly, for each rigid body 'B_j' subjected to an applied torque,

$$(F_r)_{B_j} = \omega_r^{B_j} \cdot T_{B_j} \qquad (r = 1, ..., n)$$

Where '$\omega_r^{B_j}$' is the r^{th} partial velocity of 'B_j' and 'T_{B_j}' is the resultant of all couples acting on 'B_j'. The r^{th} generalized active force 'F_r' can then be determined by summing the results over all points 'P_i' and all rigid bodies 'B_j':

$$F_r = \sum_{i=1}^{\kappa} (F_r)_{P_i} + \sum_{j=1}^{\lambda} (F_r)_{B_j} \qquad (r = 1, ..., n)$$

Where 'κ' is the number of points subjected to applied forces and 'λ' is the number of rigid bodies subjected to applied torques.

Generalized inertia forces, $\boldsymbol{F_r^*}$ - These are the quantities formed by taking the dot products of partial velocities and inertia forces and dot products of partial angular velocities and inertia torques. For each point 'P_i' possessing mass,

$$(F_r^*)_{P_i} = v_r^{P_i} \cdot R_{P_i}^* \qquad (r = 1, ..., n)$$

Where '$v_r^{P_i}$' is the r^{th} partial velocity of 'P_i' and '$R_{P_i}^*$' is the inertia force for 'P_i' and is defined as

$$R_{P_i}^* = -m_{P_i} a^{P_i}$$

Where 'm_{P_i}' is the mass of 'P_i' and 'a^{P_i}' is the acceleration of 'P_i'.Similarly, for each rigid body 'B_j' possessing inertia,

$$(F_r^*)_{B_j} = \omega_r^{B_j} \cdot T_{B_j}^* \qquad (r = 1, ..., n)$$

Where '$\omega_r^{B_j}$' is the r^{th} partial velocity of 'B_j' and '$T_{B_j}^*$' is the inertia torque for 'B_j' and is defined as

$$T_{B_j}^* = -\alpha^{B_j} \cdot I^{B_j/B_j*} - \omega^{B_j} \times I^{B_j/B_j*} \cdot \omega^{B_j}$$

Where 'I^{B_j/B_j*}' is the inertia dyadic of 'B_j' about its mass centre 'B_j^*', 'ω^{B_j}' is the angular velocity of 'B_j' and 'α^{B_j}' is the angular acceleration of 'B_j'.

The r^{th} generalized active force 'F_r^*' can then be determined by summing the results over all points 'P_i' and all rigid bodies'B_j':

$$F_r^* = \sum_{i=1}^{\mu} (F_r^*)_{P_i} + \sum_{j=1}^{\eta} (F_r^*)_{B_j} \qquad (r = 1, ..., n)$$

Where 'μ' is the number of points possessing mass and 'η' is the number of rigid bodies possessing inertia.

Equations of motion:

The equations of motion can be generated by adding all the generalized active forces and the generalized reactive forces and then equating the results to zero.

$$F_r + F_r^* = 0 \qquad (r = 1, ..., n)$$

In this method statics problems can be solved by considering $F_r = 0$.

Appendix D – In Vivo TKA Mechanics Data

Table D-1: Total contact forces in the medial condyle (BW)

	Sigma FB		Sigma MB		CR-Flex		LPS-Flex		NKII UCP		NKII CP	
% DKB	*Mean*	*Std Dev*	*Mean*	*Std Dev*	*Mean*	*Std Dev*	*Mean*	*Std Dev*	*Mean*	*Std Dev*	*Mean*	*Std Dev*
0	1.04	0.42	0.55	0.22	1.00	0.19	0.67	0.26	0.71	0.32	0.93	0.14
10	0.98	0.42	0.78	0.14	1.15	0.28	0.94	0.34	0.96	0.42	1.08	0.24
20	1.28	0.34	0.92	0.22	1.30	0.35	1.18	0.41	1.25	0.50	1.24	0.34
30	1.26	0.34	1.29	0.29	1.46	0.38	1.36	0.41	1.39	0.55	1.39	0.36
40	1.30	0.24	1.50	0.12	1.67	0.36	1.55	0.38	1.48	0.58	1.64	0.34
50	1.55	0.34	1.76	0.08	1.89	0.35	1.74	0.34	1.58	0.66	1.91	0.33
60	1.81	0.22	1.91	0.13	2.10	0.36	1.98	0.27	1.74	0.74	2.13	0.32
70	1.99	0.35	1.96	0.23	2.28	0.37	2.24	0.24	1.93	0.79	2.31	0.31
80	2.25	0.23	2.35	0.24	2.43	0.37	2.41	0.26	2.10	0.75	2.45	0.33
90	2.43	0.26	2.59	0.20	2.56	0.36	2.52	0.25	2.25	0.68	2.58	0.34
100	2.73	0.12	2.72	0.08	2.66	0.33	2.61	0.27	2.41	0.68	2.73	0.34

Table D-2: Total contact forces in the lateral condyle (BW)

	Sigma FB		Sigma MB		CR-Flex		LPS-Flex		NKII UCP		NKII CP	
% DKB	*Mean*	*Std Dev*	*Mean*	*Std Dev*	*Mean*	*Std Dev*	*Mean*	*Std Dev*	*Mean*	*Std Dev*	*Mean*	*Std Dev*
0	0.43	0.11	0.34	0.06	0.47	0.12	0.46	0.13	0.37	0.15	0.54	0.06
10	0.42	0.11	0.37	0.04	0.53	0.09	0.50	0.11	0.49	0.12	0.59	0.09
20	0.49	0.09	0.41	0.06	0.60	0.11	0.54	0.13	0.58	0.15	0.64	0.12
30	0.49	0.09	0.50	0.07	0.66	0.13	0.57	0.15	0.62	0.16	0.70	0.12
40	0.50	0.06	0.55	0.03	0.73	0.14	0.64	0.12	0.65	0.17	0.80	0.11
50	0.56	0.09	0.61	0.02	0.82	0.13	0.71	0.11	0.69	0.18	0.89	0.11
60	0.64	0.07	0.66	0.04	0.91	0.13	0.79	0.09	0.78	0.16	0.98	0.11
70	0.69	0.11	0.67	0.07	0.98	0.13	0.91	0.09	0.90	0.16	1.07	0.12
80	0.77	0.08	0.79	0.08	1.04	0.13	1.01	0.12	0.98	0.18	1.15	0.13
90	0.82	0.08	0.87	0.06	1.09	0.15	1.12	0.15	1.04	0.18	1.22	0.17
100	0.92	0.03	0.91	0.03	1.09	0.17	1.22	0.18	1.13	0.21	1.29	0.17

Table D-3: Contact area in the medial condyle (mm^2)

	Sigma FB		Sigma MB		CR-Flex		LPS-Flex		NKII UCP		NKII CP	
% DKB	*Mean*	*Std Dev*	*Mean*	*Std Dev*	*Mean*	*Std Dev*	*Mean*	*Std Dev*	*Mean*	*Std Dev*	*Mean*	*Std Dev*
0	107.6	33.8	109.5	37.6	125.6	32.8	117.0	24.6	128.1	17.5	130.9	23.8
10	114.5	66.9	171.6	21.1	118.5	25.8	120.9	21.7	118.4	24.0	121.8	21.5
20	137.9	51.8	126.8	32.6	115.5	30.8	125.7	33.0	107.9	16.6	121.5	26.4
30	135.8	39.3	114.5	19.7	118.7	31.3	130.7	35.6	103.3	20.3	121.2	24.0
40	114.2	30.3	164.3	43.6	132.8	31.9	138.0	32.6	94.7	12.6	112.2	22.7
50	117.2	34.1	137.4	19.2	143.5	37.5	144.9	30.3	91.1	5.9	104.4	15.8
60	105.0	21.0	125.5	16.2	142.6	33.6	150.5	27.3	104.2	14.8	110.6	17.3
70	87.3	34.3	117.1	9.1	137.6	34.7	156.8	25.6	129.6	19.2	117.1	20.4
80	99.8	36.2	140.3	40.2	144.1	35.3	161.6	24.6	135.8	36.3	126.6	20.2
90	85.5	33.9	132.7	12.8	158.2	44.6	167.4	18.4	142.9	52.5	125.5	22.2
100	115.8	16.9	139.1	46.0	171.2	61.9	171.1	22.1	142.8	34.6	128.2	20.5

Table D-4: Contact area in the lateral condyle (mm^2)

	Sigma FB		Sigma MB		CR-Flex		LPS-Flex		NKII UCP		NKII CP	
% DKB	*Mean*	*Std Dev*	*Mean*	*Std Dev*	*Mean*	*Std Dev*	*Mean*	*Std Dev*	*Mean*	*Std Dev*	*Mean*	*Std Dev*
0	119.0	11.7	122.0	25.4	129.5	51.6	111.9	21.0	134.3	50.9	135.0	21.1
10	133.4	11.5	125.4	41.7	134.2	50.1	109.3	22.3	125.2	20.4	116.4	23.9
20	139.3	29.5	156.3	35.0	138.4	52.1	108.8	31.5	127.6	29.6	111.0	18.7
30	101.3	27.1	108.0	60.3	142.1	50.4	111.1	32.9	124.2	43.8	110.8	21.2
40	91.2	26.0	125.9	80.6	146.2	48.9	116.7	28.5	120.8	33.3	99.2	10.6
50	90.3	28.2	110.4	29.4	147.5	54.3	123.3	29.3	133.6	21.5	103.6	15.3
60	83.3	34.8	80.5	34.5	144.4	53.3	130.7	29.8	130.7	28.9	113.7	21.1
70	97.3	21.3	103.5	29.3	140.5	54.6	139.1	33.1	133.4	22.9	118.2	19.3
80	91.4	27.4	106.4	44.6	139.9	52.7	143.8	35.9	136.0	23.4	119.2	14.8
90	76.8	8.6	84.9	18.5	140.5	46.9	145.0	34.9	135.7	32.3	120.3	14.5
100	61.2	10.4	61.0	11.4	153.2	46.1	139.6	33.1	136.2	11.1	129.4	16.4

Table D-5: Average contact pressures in the medial condyle (MPa)

	Sigma FB		Sigma MB		CR-Flex		LPS-Flex		NKII UCP		NKII CP	
% DKB	*Mean*	*Std Dev*	*Mean*	*Std Dev*	*Mean*	*Std Dev*	*Mean*	*Std Dev*	*Mean*	*Std Dev*	*Mean*	*Std Dev*
0	8.59	4.31	4.52	1.29	5.59	1.32	3.86	1.40	3.65	1.87	4.79	1.43
10	8.52	4.22	3.66	0.34	6.61	1.38	5.27	1.86	5.45	2.59	5.93	1.95
20	9.20	6.61	6.12	1.39	7.78	1.85	6.50	2.21	7.35	2.27	6.85	2.60
30	8.26	4.13	9.33	2.56	8.50	1.98	7.30	2.24	8.42	2.05	7.65	2.70
40	9.48	1.99	7.35	2.97	8.62	1.85	7.73	1.94	9.72	2.69	9.71	2.79
50	11.20	2.58	10.91	1.51	9.25	2.58	8.22	1.69	11.13	4.65	12.05	3.31
60	15.10	2.36	12.55	1.54	10.38	3.00	8.95	1.30	11.12	5.63	12.67	3.21
70	20.44	8.20	13.98	1.89	11.85	3.76	9.70	1.09	9.43	3.75	13.05	3.27
80	19.97	7.88	14.50	5.24	12.10	3.86	10.09	0.95	9.63	1.36	12.79	3.32
90	22.92	8.29	15.72	2.20	11.90	4.25	10.17	1.09	10.40	1.24	13.84	4.44
100	19.12	3.14	17.14	5.02	11.79	4.39	10.41	1.78	11.03	3.52	14.03	3.04

Table D-6: Average contact pressures in the lateral condyle (MPa)

	Sigma FB		Sigma MB		CR-Flex		LPS-Flex		NKII UCP		NKII CP	
% DKB	*Mean*	*Std Dev*	*Mean*	*Std Dev*	*Mean*	*Std Dev*	*Mean*	*Std Dev*	*Mean*	*Std Dev*	*Mean*	*Std Dev*
0	2.92	0.72	2.43	1.01	2.86	1.57	2.86	1.02	1.90	1.04	2.62	0.49
10	2.47	0.52	2.75	1.39	2.93	0.96	3.10	0.66	2.53	0.63	3.39	1.12
20	3.00	1.41	2.05	0.51	3.17	0.95	3.41	0.82	2.92	0.49	3.78	0.92
30	4.15	1.60	4.26	2.24	3.37	0.96	3.59	0.93	3.41	0.93	4.19	1.11
40	4.84	1.61	4.53	3.69	3.56	0.85	3.79	0.89	3.54	0.74	5.20	0.97
50	5.35	1.82	4.70	2.18	4.05	1.05	4.04	1.02	3.33	0.83	5.64	1.17
60	6.71	2.94	8.51	4.98	4.67	1.50	4.28	1.07	4.05	1.56	5.76	1.47
70	5.69	1.67	5.86	2.81	5.25	1.74	4.66	1.41	4.40	1.03	5.96	1.39
80	6.95	2.21	7.60	4.53	5.58	1.96	5.08	1.77	4.61	0.25	6.28	1.18
90	8.73	1.19	8.14	2.30	5.85	2.63	5.57	2.05	5.01	0.47	6.62	1.52
100	12.24	2.33	12.56	2.61	5.13	1.50	6.34	2.33	5.26	0.61	6.52	1.31

Table D-7: Forces in the quadriceps muscle (BW)

	Sigma FB		Sigma MB		CR-Flex		LPS-Flex		NKII UCP		NKII CP	
% DKB	*Mean*	*Std Dev*	*Mean*	*Std Dev*	*Mean*	*Std Dev*	*Mean*	*Std Dev*	*Mean*	*Std Dev*	*Mean*	*Std Dev*
0	0.52	0.32	0.27	0.15	0.60	0.53	0.54	0.23	0.66	0.35	0.69	0.22
10	0.39	0.20	0.32	0.12	0.85	0.32	0.69	0.24	1.01	0.78	0.89	0.34
20	0.45	0.20	0.30	0.14	1.10	0.48	0.84	0.32	1.15	0.70	1.13	0.47
30	0.44	0.27	0.52	0.16	1.30	0.60	0.98	0.34	1.32	0.67	1.36	0.53
40	0.52	0.23	0.47	0.09	1.56	0.64	1.17	0.31	1.66	0.84	1.64	0.53
50	0.62	0.28	0.76	0.15	1.89	0.58	1.41	0.30	2.03	0.92	1.94	0.49
60	0.92	0.48	1.09	0.29	2.24	0.57	1.72	0.29	2.27	0.86	2.25	0.43
70	1.23	0.94	1.22	0.67	2.55	0.56	2.14	0.31	2.45	0.74	2.58	0.45
80	1.75	0.74	2.17	0.49	2.81	0.54	2.49	0.33	2.71	0.64	2.92	0.51
90	2.29	0.80	2.75	0.31	2.98	0.60	2.77	0.33	2.99	0.56	3.13	0.46
100	3.11	0.20	2.86	0.28	2.94	0.74	3.01	0.33	3.32	0.44	3.20	0.35

Table D-8: Forces in the patellar ligament (BW)

	Sigma FB		Sigma MB		CR-Flex		LPS-Flex		NKII UCP		NKII CP	
% DKB	*Mean*	*Std Dev*	*Mean*	*Std Dev*	*Mean*	*Std Dev*	*Mean*	*Std Dev*	*Mean*	*Std Dev*	*Mean*	*Std Dev*
0	0.50	0.42	0.28	0.02	0.54	0.08	0.56	0.21	0.54	0.28	0.79	0.07
10	0.32	0.40	0.31	0.06	0.66	0.17	0.67	0.17	0.69	0.24	0.84	0.12
20	0.33	0.32	0.26	0.16	0.77	0.22	0.77	0.17	0.81	0.26	0.89	0.18
30	0.32	0.29	0.38	0.29	0.86	0.22	0.84	0.16	0.86	0.26	0.95	0.19
40	0.33	0.22	0.29	0.13	0.97	0.21	0.92	0.15	0.91	0.26	1.05	0.19
50	0.36	0.50	0.46	0.06	1.07	0.20	0.99	0.15	0.96	0.27	1.16	0.19
60	0.49	0.18	0.61	0.10	1.15	0.20	1.08	0.19	1.06	0.24	1.26	0.19
70	0.63	0.18	0.66	0.10	1.21	0.21	1.18	0.22	1.17	0.22	1.35	0.18
80	0.85	0.12	1.03	0.10	1.27	0.22	1.25	0.23	1.24	0.21	1.43	0.18
90	1.02	0.13	1.26	0.09	1.31	0.23	1.31	0.21	1.31	0.21	1.49	0.21
100	1.32	0.04	1.24	0.03	1.36	0.22	1.37	0.19	1.40	0.21	1.56	0.23

Table D-9: Patellofemoral contact forces (BW)

	Sigma FB		Sigma MB		CR-Flex		LPS-Flex		NKII UCP		NKII CP	
% DKB	*Mean*	*Std Dev*	*Mean*	*Std Dev*	*Mean*	*Std Dev*	*Mean*	*Std Dev*	*Mean*	*Std Dev*	*Mean*	*Std Dev*
0	0.11	0.41	0.06	0.09	0.17	0.31	0.08	0.21	0.11	0.37	0.12	0.13
10	0.08	0.39	0.10	0.15	0.25	0.33	0.27	0.25	0.24	0.40	0.40	0.23
20	0.12	0.36	0.16	0.21	0.44	0.40	0.44	0.30	0.38	0.51	0.59	0.35
30	0.15	0.34	0.28	0.29	0.53	0.45	0.56	0.33	0.46	0.52	0.74	0.38
40	0.21	0.19	0.27	0.10	0.75	0.47	0.74	0.31	0.57	0.45	1.02	0.36
50	0.25	0.38	0.47	0.12	1.00	0.45	0.98	0.29	0.94	0.36	1.35	0.35
60	0.37	0.38	0.84	0.22	1.35	0.44	1.30	0.28	1.19	0.27	1.58	0.36
70	0.58	0.60	1.03	0.41	1.99	0.45	1.90	0.34	1.61	0.28	2.05	0.37
80	0.97	0.46	2.03	0.41	2.19	0.47	2.32	0.32	1.98	0.29	2.57	0.39
90	1.84	0.50	2.60	0.33	2.41	0.51	2.63	0.26	2.40	0.30	3.00	0.41
100	3.15	0.12	2.96	0.14	2.74	0.53	3.00	0.19	2.90	0.37	3.14	0.44

Table D-10: Total contact forces in the antero-posterior direction (BW)

	Sigma FB		Sigma MB		CR-Flex		LPS-Flex		NKII UCP		NKII CP	
% DKB	*Mean*	*Std Dev*	*Mean*	*Std Dev*	*Mean*	*Std Dev*	*Mean*	*Std Dev*	*Mean*	*Std Dev*	*Mean*	*Std Dev*
0	0.08	0.07	0.05	0.05	0.06	0.03	0.05	0.05	0.09	0.05	0.08	0.03
10	0.08	0.07	0.06	0.03	0.08	0.05	0.11	0.07	0.10	0.05	0.08	0.03
20	0.09	0.04	0.10	0.05	0.13	0.06	0.10	0.05	0.12	0.07	0.04	0.04
30	0.11	0.04	0.12	0.08	0.12	0.08	0.11	0.07	0.12	0.09	0.08	0.05
40	0.12	0.06	0.10	0.06	0.14	0.08	0.14	0.10	0.15	0.10	0.14	0.13
50	0.08	0.06	0.22	0.05	0.15	0.11	0.12	0.08	0.19	0.11	0.08	0.06
60	0.16	0.14	0.15	0.08	0.20	0.10	0.19	0.07	0.17	0.11	0.15	0.08
70	0.14	0.10	0.20	0.11	0.20	0.12	0.21	0.14	0.21	0.12	0.25	0.11
80	0.11	0.13	0.11	0.10	0.24	0.13	0.14	0.11	0.22	0.12	0.28	0.15
90	0.17	0.13	0.21	0.12	0.27	0.12	0.13	0.14	0.22	0.15	0.19	0.10
100	0.21	0.13	0.18	0.14	0.30	0.13	0.23	0.14	0.24	0.15	0.21	0.13

Table D-11: Total contact forces in the medio-lateral direction (BW)

	Sigma FB		Sigma MB		CR-Flex		LPS-Flex		NKII UCP		NKII CP	
% DKB	*Mean*	*Std Dev*	*Mean*	*Std Dev*	*Mean*	*Std Dev*	*Mean*	*Std Dev*	*Mean*	*Std Dev*	*Mean*	*Std Dev*
0	0.11	0.04	0.04	0.03	0.12	0.06	0.10	0.04	0.09	0.06	0.07	0.05
10	0.06	0.03	0.08	0.07	0.14	0.06	0.08	0.05	0.11	0.07	0.11	0.05
20	0.13	0.05	0.05	0.04	0.13	0.06	0.10	0.06	0.12	0.07	0.12	0.10
30	0.11	0.08	0.15	0.08	0.15	0.06	0.11	0.08	0.11	0.08	0.19	0.03
40	0.14	0.08	0.06	0.03	0.14	0.08	0.15	0.06	0.13	0.10	0.14	0.15
50	0.07	0.05	0.15	0.09	0.15	0.08	0.14	0.08	0.14	0.08	0.12	0.13
60	0.14	0.09	0.12	0.13	0.19	0.07	0.19	0.10	0.19	0.12	0.11	0.04
70	0.17	0.15	0.20	0.12	0.22	0.15	0.19	0.11	0.21	0.13	0.15	0.13
80	0.24	0.14	0.14	0.10	0.17	0.08	0.21	0.14	0.21	0.12	0.09	0.08
90	0.18	0.09	0.21	0.16	0.18	0.12	0.23	0.11	0.22	0.14	0.25	0.15
100	0.15	0.09	0.16	0.15	0.24	0.14	0.19	0.10	0.27	0.15	0.22	0.17

Table D-12: Total contact forces in the superior-inferior direction (BW)

	Sigma FB		Sigma MB		CR-Flex		LPS-Flex		NKII UCP		NKII CP	
% DKB	*Mean*	*Std Dev*	*Mean*	*Std Dev*	*Mean*	*Std Dev*	*Mean*	*Std Dev*	*Mean*	*Std Dev*	*Mean*	*Std Dev*
0	1.47	0.53	0.89	0.27	1.46	0.27	1.13	0.25	1.46	0.15	1.08	0.45
10	1.40	0.53	1.14	0.17	1.67	0.35	1.43	0.39	1.66	0.30	1.44	0.54
20	1.76	0.44	1.32	0.28	1.89	0.44	1.71	0.49	1.87	0.43	1.82	0.65
30	1.74	0.42	1.77	0.36	2.12	0.48	1.93	0.50	2.08	0.44	2.00	0.72
40	1.79	0.30	2.04	0.15	2.39	0.48	2.17	0.44	2.42	0.42	2.11	0.74
50	2.11	0.43	2.35	0.10	2.70	0.47	2.44	0.39	2.79	0.41	2.27	0.83
60	2.43	0.29	2.55	0.17	2.99	0.46	2.76	0.29	3.09	0.42	2.52	0.89
70	2.66	0.46	2.62	0.29	3.24	0.48	3.13	0.27	3.35	0.42	2.81	0.95
80	3.00	0.30	3.13	0.31	3.46	0.49	3.41	0.33	3.58	0.44	3.06	0.92
90	3.24	0.35	3.44	0.26	3.63	0.50	3.62	0.37	3.78	0.48	3.27	0.86
100	3.64	0.15	3.62	0.11	3.72	0.48	3.81	0.41	4.01	0.48	3.52	0.89

Vita

Adrija Sharma was born in Durgapur, a small city in India. His wanderlust, his interest in interacting with different people and cultures, and his love for the sea always motivated him to become a marine engineer. He pursued Bachelors of Mechanical Engineering, from Jadavpur University, Calcutta, India. During this time he was also the recipient of the coveted National Talent Search Scholarships. Not surprisingly enough, he joined the merchant navy after graduation. He worked for three years. However, influenced by the suffering of his beloved grandmothers due to arthritis, and with a vision to improve the quality of life of millions of people worldwide suffering from this disease, he started his post graduate studies in biomechanics and completed his PhD in Fall 2008.